# Investigations of Thermodynamics and Dynamics in Phase Separating Mixtures

A Thesis

Submitted for the Degree of

DOCTOR OF PHILOSOPHY

in the Faculty of Science

by

**Koyel Das**

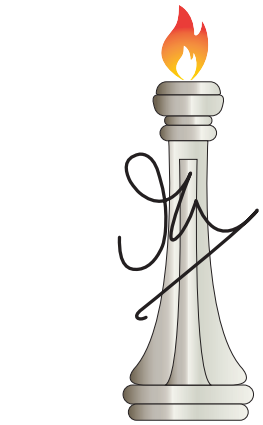


THEORETICAL SCIENCES UNIT
JAWAHARLAL NEHRU CENTRE FOR ADVANCED SCIENTIFIC RESEARCH
(A Deemed University)
Bangalore – 560 064

July 2022

*To my family and friends*

# DECLARATION

I hereby declare that the matter embodied in the thesis entitled "**Investigations of Thermodynamics and Dynamics in Phase Separating Mixtures**" is the result of investigations carried out by me at the Theoretical Sciences Unit, Jawaharlal Nehru Centre for Advanced Scientific Research, Bangalore, India under the supervision of **Prof. Subir K. Das**, and that it has not been submitted elsewhere for the award of any degree or diploma.

In keeping with the general practice in reporting scientific observations, due acknowledgment has been made whenever the work described is based on the findings of other investigators.

**Koyel Das**

# CERTIFICATE

I hereby certify that the matter embodied in this thesis entitled "**Investigations of Thermodynamics and Dynamics in Phase Separating Mixtures**" has been carried out by **Koyel Das** at the Theoretical Sciences Unit, Jawaharlal Nehru Centre for Advanced Scientific Research, Bangalore, India under my supervision and that it has not been submitted elsewhere for the award of any degree or diploma.

**Prof. Subir K. Das**
( Research Supervisor)

# Acknowledgements

I would like to expess my sincere gratitude to my Ph.D. supervisor Prof. Subir K. Das for his patience, guidance, and support. I have benefited greatly from his wealth of knowledge, encouragement with a perfect blend of insight and humor, as well as meticulous corrections. I am extremely grateful that he has allowed me to be a part of his research group, Soft Matter and Statistical Mechanics (SMSM), in the Theoretical Sciences Unit (TSU) of Jawaharlal Nehru Centre for Advanced Scientific Research (JNCASR).

I would also like to acknowledge the Graduate Student Advisory Committee (GSAC) members, Prof. Rajesh Ganapathy and Dr. Meher K. Prakash, for their timely evaluations of the progress of the thesis.

I would like to express my gratitude to all the course instructors, Prof. N.S. Vidhyadhiraja, Prof. Subir K. Das, Prof. Swapan K. Pati, Prof. Shobhana Narasimhan and Dr. Meher K. Prakash for the wonderful courses they offered.

I would like to acknowledge other faculty members of TSU.

My sincere thanks to my seniors from SMSM, Dr. Suman Majumder, Dr. Sutapa Roy, Dr. Jiarul Midya, Dr. Saikat Chakraborty, and Dr. Subhajit Paul. I am also thankful to all other past and short-term members of the group: Dr. Sunita, Dr. Sanat K. Singha, Arya for the cheerful times that we had. Special thanks to all the current members of the group - Nalina (for being best labmate one can ever have!), Arabinda, Soumik, Sohini, Dr. Tanay Paul, Purnendu and Anjaney for creating a vibrant ambience inside the lab.

I acknowledge University Grants Commission (UGC), India, and JNCASR for financial support.

I would also like to thank the Paramyukti National Supercomputing facility (NSM) at JNCASR for providing the computational facilities for carrying out some of the works.

I am grateful to all the staff members from Library, CompLab, Academic section, Administration, Accounts, Dhanvantari, Hostel office, Housekeeping department, Mess, and Dining hall for their kind services.

I am indebted to my school and college teachers.

Special thanks to all other friends Sharona, Subham, Biswanath, Arka, Moinak, Neha for making my stay enjoyable and Tarak for wonderful food he had prepared for us. A big thank to my longtime friend Poulomi for being helpful in the difficult times.

I owe my deepest gratitude to my parents, grandparents, brother, sister-in-law and Subhajit for their unconditional support and love.

# Synopsis

This thesis is based on investigations of a few structural and dynamical aspects in materials which undergo phase transitions of various types. Specifically we have considered phase separations in solid and liquid binary mixtures, following changes in relevant thermodynamic parameters. We have studied phenomena linked to equilibrium as well as nonequilibrium domains. In the nonequilibrium case our investigations focused on universality related to growth and/or aging during the above mentioned phase transitions. Our results in the equilibrium limit are by concerning descriptions of interfacial property with the variation of curvature and associated critical behavior. These are of much fundamental importance.

In **Chapter 1** we provide the theoretical background related to the works presented in the subsequent chapters. It includes the descriptions of scaling laws in growth dynamics and associated aging phenomena in nonequilibrium systems, as well as details of dependence of interfacial property on critical fluctuation, among other topics. The chapter also introduces various simulation techniques, viz., Monte Carlo and molecular dynamics, and discusses methodologies to analyze the simulation results. A brief overview of the subsequent chapters is provided in the following.

In **Chapters 2** and **3** we have presented results on aging dynamics during demixing transitions in symmetric solid (A+B) binary mixtures. We have followed a protocol where quenches of systems were performed to the ordered regions with initial configurations having long range spatial correlations, that were prepared at the demixing critical points. These results on kinetics are obtained via the Kawasaki exchange Monte Carlo simulations of the nearest neighbor Ising model, in space dimensions $d = 2$ and 3. The method preserves the value of system integrated order parameter that is necessary for the studies of phase separation kinetics. Using state-of-the-art technique we analyze results on the decay of the order-parameter autocorrelation function which is seen to exhibit power-law scaling with exponent $\lambda$. Via structural analysis we demonstrate that our estimated values of the exponent satisfy well known bounds in the considered dimensions. It transpires that the values of $\lambda$ for quenches from the correlated initial configurations are significantly different from those for the quenches from uncorrelated configurations. Discussion has been provided by comparing these results with those for nonconserved order-parameter dynamics, that applies to magnetic systems.

In **Chapter 4**, via hydrodynamics preserving molecular dynamics simulations, we study growth phenomena in a phase separating binary liquid mixture model with the

variation of composition, keeping the focus on off-critical compositions. We quench homogeneous configurations, prepared at temperatures much higher than the critical one, to state points inside the miscibility gap. For off-critical compositions, nucleated droplets of the minority species, in the background of the majority phase, are shown to grow via coalescence while pursuing Brownian motion. The value of the exponent, for the power-law growth, has been estimated. This nicely matches with a theoretical prediction. These results are compared with the growth that occurs via particle diffusion mechanism, in a non-hydrodynamic environment.

In **Chapters 5** and **6** we study the excess free energy contributions due to the presence of an interface between A-rich and B-rich phases in the coexistence scenario of binary liquid mixtures. We employ a semi-grand canonical Monte Carlo method that uses a successive umbrella sampling technique. With the variation of the composition, that the method allows, the shapes of the minority phase clusters change from spherical to cylindrical and finally, to slab-like structures, the latter having flat interfaces. We use a thermodynamic method to analyze the results. The procedure is capable of picking up information on shape and size of a nucleus or domain as well as corresponding interfacial tension. In **Chapter 5** we present and analyze results for spherical nucleus. Outcomes of our analysis are consistent with a form for the universal critical behavior for curvature dependent interfacial tension. Despite the form being universal, in terms of exponents, we show that there is a model dependent nonuniversal constant. We demonstrate that the latter strongly varies with the change of critical temperature in a monotonic fashion. In **Chapter 6** we analyze both spherical and cylindrical droplets. It is discussed how in complex situations the interfacial tension can be expressed as a function of the combination of the principal radii of curvature. Deviations from such descriptions are pointed out and discussed.

Finally, we summarize the results presented in the thesis. There we have provided discussions on future possibilities as well.

# Publications

- "Initial correlation dependence of aging in phase separating solid binary mixtures and ordering ferromagnets", Subir K. Das, **Koyel Das**, Nalina Vadakkayil, Saikat Chakraborty, and Subhajit Paul, Journal of Physics: Condensed Matter **32**, 184005 (2020).
- "Aging exponents for nonequilibrium dynamics following quenches from critical points", **Koyel Das**, Nalina Vadakkayil, and Subir K. Das, Physical Review E **101**, 062112 (2020).
- "Hydrodynamic Effects in Kinetics of Phase Separation in Binary Fluids: Critical versus off-critical compositions", **Koyel Das** and Subir K. Das, arXiv:2107.10698 (2021).
- "Critical Behavior of Curvature Dependent Interfacial Tension", **Koyel Das** and Subir K. Das, Manuscript under preparation.
- "Dependence of Interfacial Tension on Mean Radius of Curvature", **Koyel Das** and Subir K. Das, Manuscript under preparation.

# Table of contents

# List of figures

# List of tables

# Chapter 1

# Introduction

## 1.1 Phase Transition

Phases are states of matter characterized by macroscopic quantities like temperature ($T$), pressure ($P$), etc. Some common examples of such phases are solid, liquid, gas, etc. Change of phase, from one to another, occurs, when the above mentioned thermodynamic parameters are varied and is manifested by changes in the properties. Some other common examples are the transition from a paramagnetic phase to ferromagnetic one, demixing transition in a binary mixture, etc.

In Fig. 1.1 the phase behavior [1] corresponding to a normal chemical substance has been shown in the $P$ versus $T$ plane. With the variation in $T$ and $P$ the system can exist in solid, liquid or gas phases. Well-defined boundaries, which are known as the coexistence curves, divide the whole region into different sub-regions within which different phases are stable. Along the boundaries two phases can coexist with each other in equilibrium. If these phase boundaries are crossed, there occur jumps in derivatives of free energy at the first order, signalling transition of first order type [1–8]. The point at which all the three coexistence lines meet is known as the triple point. At this point three phases coexist. If one considers moving along the line of liquid-gas coexistence, the difference in densities between liquid and vapor phases vanishes at a point, referred to as the critical point ($T_c$, $P_c$). Beyond this it is possible to move continuously from liquid to vapor state without crossing a phase boundary. In this case the second derivatives exhibit interesting singularities [1–9]. The latter is referred to as second order or continuous transition. Transitions of various types can be probed via the change in appropriately defined order-parameter [1, 2, 8]. This quantity is non-zero in the ordered phase and has vanishing value in the disordered situation. E.g., in the

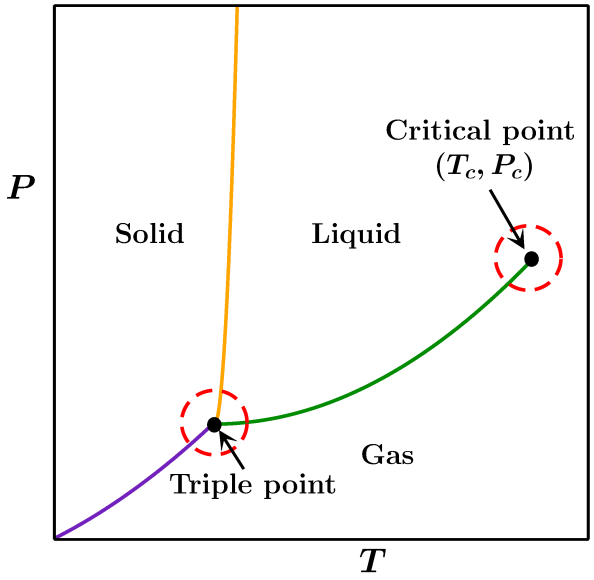


Fig. 1.1 Phase behavior of a typical chemical matter is shown in pressure ($P$) versus temperature ($T$) plane. It can be found in any of the three phases – solid, liquid, or gas. The solid curves denote lines of coexistence. Positions of the triple point and critical point $(T_c, P_c)$ have been marked.

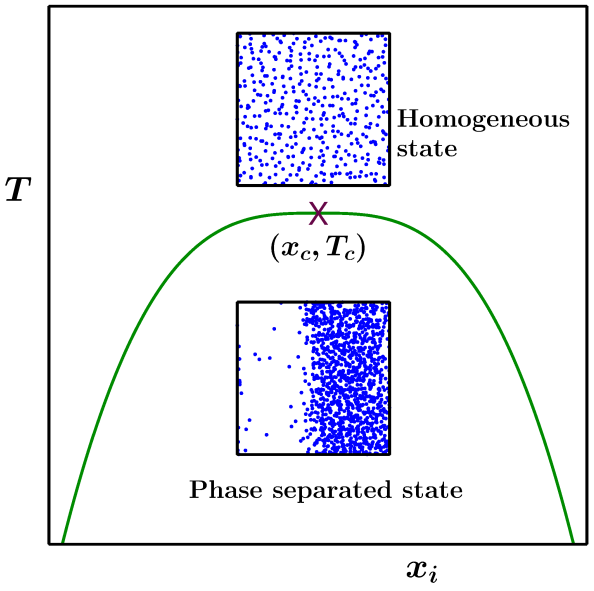


Fig. 1.2 Phase coexistence curve of a symmetric binary mixture is drawn schematically in the temperature ($T$) versus species concentration ($x_i$) plane. The continuous curve represents the binodal line and the cross marks corresponds to the critical point. Above the critical point the system is in homogeneous state, whereas, inside the coexistence curve system exhibits phase separation.

case of above mentioned magnetic transition system-integrated value of magnetization is the order-parameter. For a vapor-liquid transition, difference in densities between liquid and vapor phases, $\Delta\rho = \rho_l - \rho_v$, is the order-parameter. Analogously, composition or concentration difference, $\Delta x = x_A - x_B$, is the relevant order-parameter for phase separating binary (A+B) mixtures.

In Fig. 1.2 phase coexistence curve for a symmetric binary (A+B) mixture system has been plotted in temperature ($T$) versus concentration plane. Concentration of a species, $x_i$, is given by $x_i = \frac{N_i}{N}$, $N_i$ being the number of $i$-type particles, $i \in [A, B]$ and $N$ the total number of particles. Here the critical point is marked as $(x_c, T_c)$. Above $T_c$ the system is a uniform mixture of A and B particles and below $T_c$ the equilibrium situation is the coexistence of A-rich and B-rich phases, with the composition in different phases being represented by two branches of the coexisting curve as a function of temperature.

## 1.2 Critical Phenomena

Given that in Chapter 5 we will address question concerning critical behavior of curvature dependent interfacial tension, here we provide a brief discussion of critical phenomena. When a system is at or in the close proximity to the critical point there occur certain singularities [1, 4, 10–13], influenced by the order-parameter fluctuations [1, 4, 10]. This is referred to as the critical phenomena [1, 4, 10]. One can express these singularities as power-law functions of the reduced temperature $\epsilon$ $(= |T - T_c|/T_c)$. Below we define some of the critical exponents [1, 3, 8]:

$$\text{Order-parameter: } \psi \sim \epsilon^{\beta}, \tag{1.1}$$

$$\text{Susceptibility: } \chi \sim \epsilon^{-\gamma}, \tag{1.2}$$

$$\text{Heat capacity: } C \sim \epsilon^{-\alpha}, \tag{1.3}$$

$$\text{Correlation length: } \xi \sim \epsilon^{-\nu}. \tag{1.4}$$

The exponents $\alpha$, $\beta$, $\gamma$ and $\nu$ follow certain scaling relations [1, 3, 8]:

$$\text{Rushbrooke relation: } \alpha + 2\beta + \gamma = 2, \tag{1.5}$$

$$\text{Josephson relation: } \nu d = 2 - \alpha, \tag{1.6}$$

$$\text{Fisher relation: } \gamma = \nu(2 - \eta), \tag{1.7}$$

$$\text{Widom relation: } \gamma = \beta(\delta - 1). \tag{1.8}$$

In Eq. (1.6) $d$ is the system dimension, in Eq. (1.7) $\eta$ is an exponent associated with the spatial structure, and in Eq. (1.8) $\delta$ is the exponent associated, e.g., with magnetization ($m$) in a ferromagnetic system at $T = T_c$:

$$m \sim H^{1/\delta}, \tag{1.9}$$

where $H$ is the externally applied magnetic field. These exponents are universal in nature [1, 11]. This is in the sense that their values do not depend on the details of the interaction among the constituent particles. This is nicely captured within the Renormalization Group (RG) theory [3, 8]. Depending upon whether the interaction among the particles is short- or long-ranged, the scalar order-parameter there exist two universality classes [3, 8] for the above mentioned static properties, i.e., Ising universality class and the classical universality class. For 3D Ising class, the exponent values are [3, 8]

$$\alpha = 0.11,\ \beta = 0.325,\ \gamma = 1.239,\ \nu = 0.63. \tag{1.10}$$

This universality class includes systems with short range interactions. For the classical universality class one has

$$\alpha = 0,\ \beta = 1/2,\ \gamma = 1,\ \nu = 1/2. \tag{1.11}$$

Like the static quantities certain "equilibrium" dynamic properties also show universal behavior, although not as robust [11]. E.g., due to critical fluctuations the relaxation time diverges [11]. This phenomenon is known as critical slowing down, which gets reflected in the very slow dynamics in the system near criticality.

## 1.3 Phase ordering dynamics

When thermodynamic parameters are varied, a homogeneous system becomes unstable against the fluctuations and moves towards the new equilibrium which is inhomogeneous in nature, if the change is related to quench inside a miscibility gap [4–7]. E.g., if a homogeneous binary (A+B) mixture is suddenly cooled down from a high temperature isotropic configuration to a temperature below the miscibility gap, it will move towards the phase separated state via formation and growth of similar-particle-rich domains. This evolution [4–7] is a complex nonlinear process. During this one observes growth of

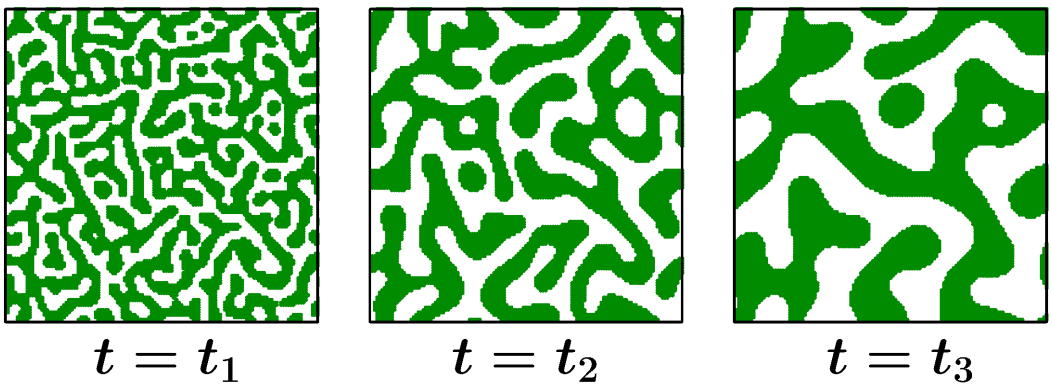


Fig. 1.3 Evolution snapshots following critical quench of a binary (A+B) mixture system. The green and white colors represent A and B particles, respectively. These results were obtained from the study of the well known Cahn-Hilliard equation [6, 7, 14, 15].

the characteristic lengths, $\ell(t)$, associated with domains, in a power-law manner, viz.,

$$\ell(t) \sim t^{\alpha}. \tag{1.12}$$

Values of the growth exponent $\alpha$ depend on various parameters like order parameter symmetry, its conservation, dimensionality, effects of hydrodynamics, etc [4–7]. In systems with conserved order-parameter dynamics, system integrated value remains constant with time. Depending upon the region of quench inside coexistence curve, the coarsening occurs via spinodal decomposition or nucleation and growth, which we discuss below. Note that Chapter 2, 3 and 4 deal with questions related to kinetics of phase separation.

### 1.3.1 Spinodal decomposition

Spinodal decomposition [4–7, 14, 15] is observed if a system is quenched with an overall density or composition around the critical value. Typical evolution snapshots are shown in Fig. 1.3, for a binary mixture model. In this case, the system becomes unstable against small length scale fluctuations which leads to phase separation. Here the evolving structures are essentially bicontinuous in nature. Note that the average domain length can be calculated as the average of the distances between two successive interfaces, as seen in Fig. 1.3, by scanning the systems in various directions. There exist other methods also to calculate this characteristic length scale in an evolving system. Outcomes of different methods are proportional to each other.

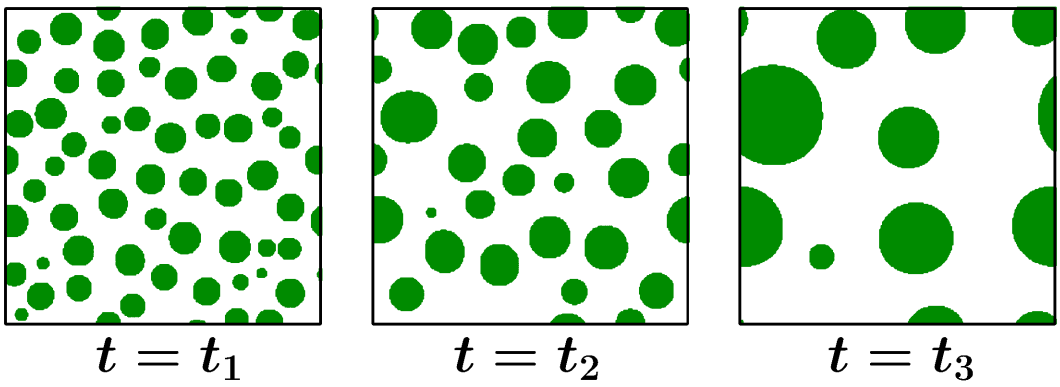


Fig. 1.4 Frames representing evolution following an off-critical quench of a binary (A+B) mixture system. The green and white colors correspond to A and B particles, respectively.

### 1.3.2 Nucleation and growth

If the region of quench is close enough to any branch of the coexistence curve then the phase-separation belongs to the so called nucleation and growth category [5, 6, 16, 17]. Fig. 1.4 demonstrates the representative evolution snapshots for offcritical binary fluid. In this case, the system is stable against fluctuations of small wavelength. However, long length scale rare fluctuations can produce instability in such systems, leading to formation of disconnected cluster or nuclei.

The creation of a nucleus introduces an interface between the two phases. Crucial facts related to this are of much interest in the equilibrium context. In Fig. 1.5(a) we have shown a nucleus of phase B of radius R, which is separated from the background phase A by an interface. The presence of the interfaces introduces a free energy barrier, $\Delta F$, which can be expressed as [5, 6]

$$\Delta F(R) = -\frac{4}{3}\pi R^3 f_v + 4\pi R^2 \gamma, \tag{1.13}$$

$f_v$ and $\gamma$ being the volume free energy density and surface tension, respectively. In Fig. 1.5(b) typical shape of $\Delta F$ is shown as a function of $R$. The stability of a nucleus is decided by the competition between the volume and surface terms. A nucleus is going to be stable only if its surface to volume ratio is low enough. At $R = R_c = 2\gamma/f_v$, the critical radius, $\Delta F_c$, the excess free energy, has its peak and is known as the activation energy. If the radius of a droplet is larger than $R_c$, it becomes a stable droplet as the total free energy lowers with the addition of new particles into it. These droplets can grow further with time, whereas nuclei smaller than the critical radius will shrink or

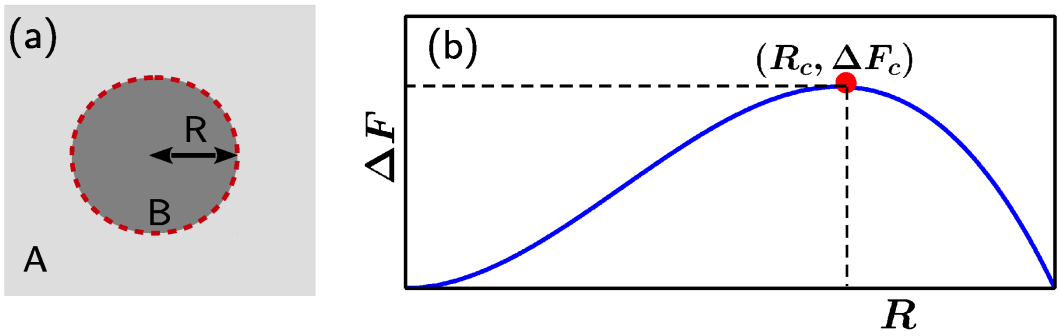


Fig. 1.5 (a) Schematic picture of a droplet of B particles is shown in the background consisting of A particles. The radius of the nucleus is $R$. The dashed circle highlights the position of the interface. (b) Excess free energy $\Delta F$ has been plotted as a function of $R$.

break. At a temperature $T$ the rate of formation of stable nuclei is proportional to $e^{-\frac{\Delta F_c}{k_B T}}$.

## 1.4 Growth in systems following conserved dynamics

For conserved order-parameter [6, 7], as mentioned earlier, the system integrated value of the order-parameter remains constant throughout the evolution. With the local order parameter $\psi(\vec{r}, t)$, one defines $\psi_{\text{tot}} = \int \psi(\vec{r}, t) dV$, as the global order parameter, $dV$ being a small volume element around $\vec{r}$. The constraint of $\psi_{\text{tot}}$ remaining constant with time, makes the dynamics much slower. To achieve adequately large length scales, and, thus, to comment on the growth and related behavior in the asymptotic limit, one requires to run simulations over real time scales that are extremely long even with modern computational facility. This is the reason why simulation studies remain challenging for this case. This is more true at low temperature for which metastability poses further serious problem. To avoid this we will stick to a reasonably high temperature, viz., $0.6T_c$, in both Chapter 2 and Chapter 3. We will discuss relevant growth laws for two cases belonging to this category, viz., solid and fluid binary mixtures.

### 1.4.1 Solid binary mixture

In this class of systems the growth occurs due to the diffusion of material following the gradient in chemical potential. The bigger domains or clusters grow larger at the cost of

the smaller ones. This phenomenon is known as Ostwald ripening, as it was described by German chemist Wilhelm Ostwald in 1896 [18, 19]. The corresponding growth can be described via the Lifshitz–Slyozov–Wagner (LSW) theory [20–23].

In this case the relevant space and time dependent order-parameter is defined as $\psi(\vec{r},t) = x_A(\vec{r},t) - x_B(\vec{r},t)$. For $\psi$, the evolution is expected to follow the continuity equation [6, 7]:

$$\frac{\partial\psi(\vec{r},t)}{\partial t} = -\vec{\nabla}\cdot\vec{J}(\vec{r},t), \tag{1.14}$$

where $\vec{J}(\vec{r},t)$ is the diffusion current,

$$\vec{J}(\vec{r},t) = -D\vec{\nabla}\mu(\vec{r},t), \tag{1.15}$$

$D$ and $\mu(\vec{r},t)$ being the diffusion coefficient and chemical potential, respectively. This leads to the construction of Cahn-Hilliard (CH) equation. Note that $\mu$, the chemical potential is defined through the first order derivative of the Ginzburg-Landau free energy functional with respect to $\psi$. One also associates the interface velocity with the gradient of chemical potential and writes [22]

$$\frac{d\ell(t)}{dt} \sim |\vec{\nabla}\mu| \sim \frac{\gamma}{\ell^2(t)}. \tag{1.16}$$

From Eq. (1.16) one gets

$$\ell(t) \sim t^{1/3}, \tag{1.17}$$

the Lifshitz–Slyozov–Wagner (LSW) law [20–22], which is typically valid for phase separation in solid mixtures at various dimensions. The demixing transition in solid binary mixtures can be studied numerically via the CH equation as well as via Kawasaki spin exchange Monte Carlo (MC) [24] simulations of the Ising model. The Ising Hamiltonian is

$$H = -J\sum_{<ij>} S_iS_j;\ S_i = \pm 1;\ J > 0. \tag{1.18}$$

Here an up spin $(+1)$ can be identified as one of the particle species (say A) and down spin $(-1)$ as the other one. In the MC simulations one selects a pair of nearest neighbor spins randomly and interchanges their positions. This trial is accepted or rejected via the Metropolis algorithm [24], which we will discuss later in the chapter.

### 1.4.2 Fluid system

In kinetics of phase separation in fluids, hydrodynamics does play an important role, which leads to faster growth. In this case the growth exponent depends upon morphology as well as dimensionality [16, 17, 25–48]. The domain coarsening in fluids will be discussed here in the context of liquid-liquid transition. For fluids, initially the growth occurs via diffusive mechanism as in solids [6, 7]. But as the domain size becomes considerably large, the system enters into the hydrodynamic regime.

For the quenches with compositions close to the critical value one observes formation of interconnected bicontinuous domains throughout the system. There advective transport of material through these channel-like domains occurs because of the pressure difference having connection with the interfacial tension [6, 7, 26–28, 42]. By balancing the surface energy density ($\frac{\gamma}{\ell}$) with the viscous stress ($6\pi\eta v_\ell/\ell$), $v_\ell$ and $\eta$ being the interface velocity and the shear viscosity, respectively, one writes

$$v_\ell = \frac{d\ell(t)}{dt} = \frac{\gamma}{6\pi\eta}. \tag{1.19}$$

This provides the viscous hydrodynamic growth [6, 7, 17, 26, 39, 42, 43]:

$$\ell(t) \sim t. \tag{1.20}$$

The crossover to this linear regime occurs when $\ell(t) >> \ell_{\rm vis} \sim (D\eta)^{1/2}$. At late time, when kinetic energy dominates over viscous stress, as $\ell$ becomes even larger, $\ell(t) >> \ell_{\rm in}(= \frac{\eta^2}{\rho\gamma})$, the growth law can be found by relating surface energy density ($\frac{\gamma}{\ell}$) with kinetic energy density ($\rho v_\ell^2$). Related dynamic equation is

$$\frac{d\ell(t)}{dt} = \sqrt{\frac{\gamma}{\rho\ell}}, \tag{1.21}$$

This provides

$$\ell(t) \sim t^{2/3}, \tag{1.22}$$

which is referred to as the inertial hydrodynamic growth [6, 7].

In the case of quenches close to the phase coexistence curve, disconnected droplets of the minority phase form. These may grow via diffusive motion and sticky collisions. This is known as diffusive coalescence mechanism [16, 17, 25, 26, 33–35, 37, 43, 48], that was proposed by Binder and Stauffer [16, 25, 26]. The droplet density ($n$), in this

mechanism, decays with time as

$$\frac{dn}{dt} = -CD\ell n^2, \tag{1.23}$$

$D$ being the diffusion constant and $C$ a proportionality constant. Since the droplets move in Brownian fashion, the Stoke-Einstein-Sutherland relation provides a constant value for $D\ell$ [49–51]. Incorporating this fact and using $n \sim 1/\ell^d$, that arises from conservation of material, in Eq. (1.23), one obtains

$$\frac{d\ell(t)}{dt} \sim \frac{1}{\ell^{d-1}}. \tag{1.24}$$

Solving Eq. (1.24) one gets $\ell(t) \sim t^{1/d}$. Therefore, in $d = 3$ the value of $\alpha$ is $1/3$, same as the LSW growth exponent, though the mechanisms are completely different. One can distinguish between these two by studying the growth amplitudes. Amplitude for BS growth will be higher than that of LS growth. The symbols $\eta$ and $\alpha$ here, as already clear, are different from the exponents that are defined in the critical phenomena context.

## 1.5 Structural aspect of nonequilibrium dynamics

During the coarsening process there appear different patterns which are self-similar in nature, i.e, the evolving structures at different times vary only by a change in the characteristic length $\ell(t)$ [2, 4–7]. To investigate this self-similarity one looks at certain functions that characterize the morphology of the system. Examples of such functions are the two-point equal-time correlation function $C(r,t)$, its Fourier transform, $S(k,t)$, the structure factor, etc. These functions exhibit scaling relations arising from the self-similar property, which we discuss below.

### 1.5.1 Two point equal-time correlation function

This function, $C(r,t)$, is calculated as [2, 7]

$$C(r,t) = \langle \psi(\vec{r},t)\psi(\vec{0},t)\rangle - \langle \psi(\vec{r},t)\rangle\langle \psi(\vec{0},t)\rangle, \tag{1.25}$$

where the angular brackets indicate statistical averaging. On the issue of averaging, we note that there are two sources of fluctuations, one arising from the differences

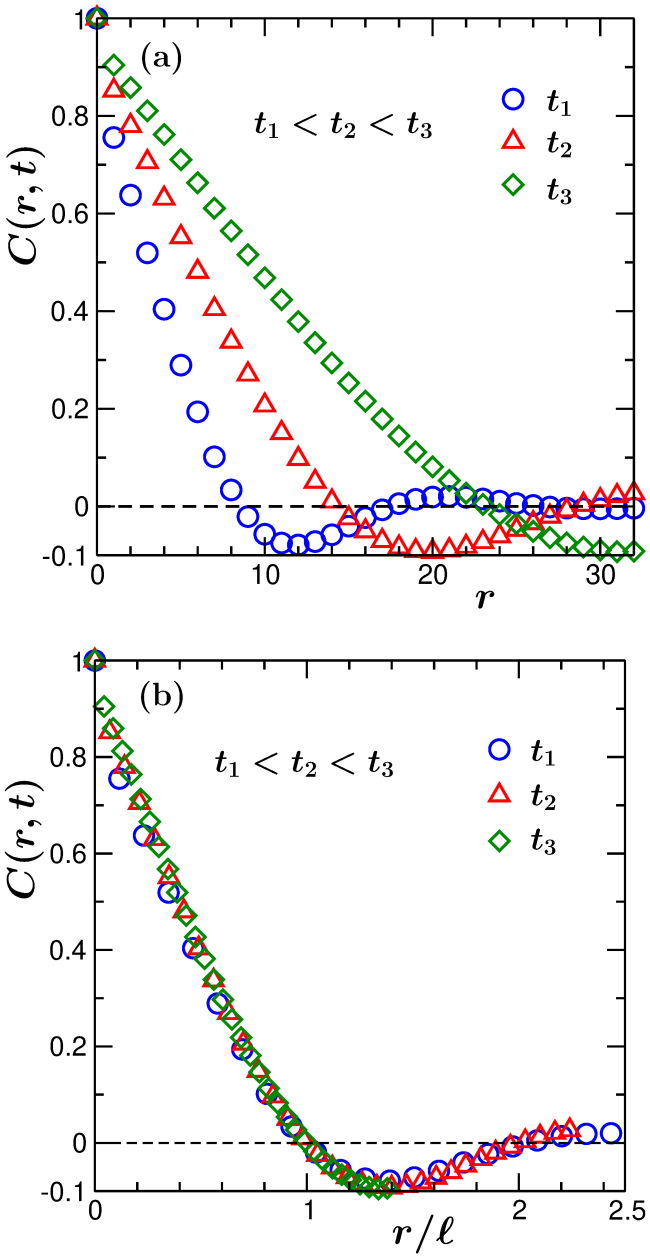


Fig. 1.6 (a) Two-point equal-time correlation functions, $C(r,t)$, are shown, from several times, versus the distance between two particles, $r$. (b) Plots of $C(r,t)$ with the variation of the scaled distance $r/\ell(t)$. These results are from one of the model systems we have used in the thesis, viz., the Ising model.

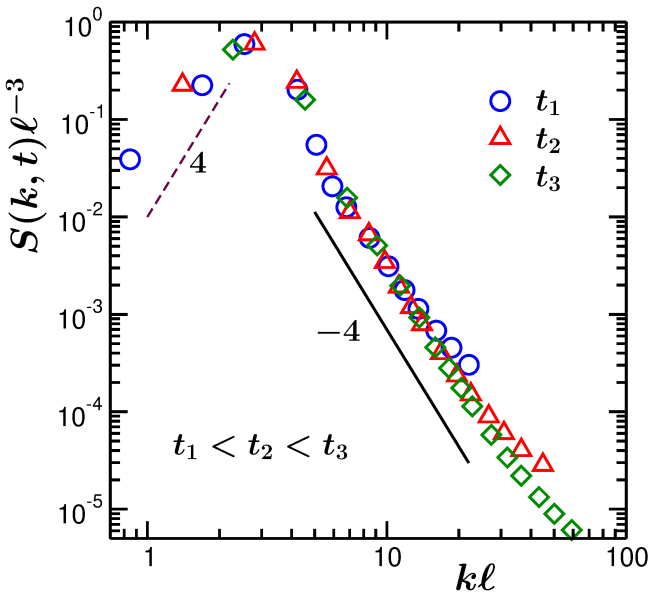


Fig. 1.7 Plots of the scaled structure factors, $S(k,t)\ell^{-3}$ ($k$ is the wave number), versus $k\ell$, for three different times. The solid line represents power-law decay with exponent $-4$ and is related to the Porod law. The dashed line corresponds to a power-law with exponent $\sigma$. These results are for the same model as in Fig. 1.6.

in the initial configurations and the other is the thermal effect. In general during a nonequilibrium process $C(r,t)$ at different times follow the scaling behavior [2, 7]

$$C(r,t) \equiv \tilde{C}(r/\ell(t)). \tag{1.26}$$

Here $\tilde{C}$ is a time independent master function. The domain length can also be measured from the decay of $C(r,t)$ as $C(r = \ell(t),t) = h$, $h$ being a constant. This scaling property of $C(r,t)$ validates power-law time dependence of growth of $\ell(t)$ [2, 7]. Fig. 1.6 demonstrates this scaling property. It can be noted from Eq. (1.25) that the correlation function depends only on the scalar separation between two space points. This arises from the expectation that the structure is spatially isotropic.

### 1.5.2 Structure factor

In experiments, instead of $C(r,t)$, the quantity which is commonly measured is the structure factor $S(k,t)$, where $k = |\vec{k}|$ is wave number. This is related to $C(r,t)$ as

$$S(k,t) = \int d\vec{r} e^{i\vec{k}\cdot\vec{r}} C(\vec{r},t). \tag{1.27}$$

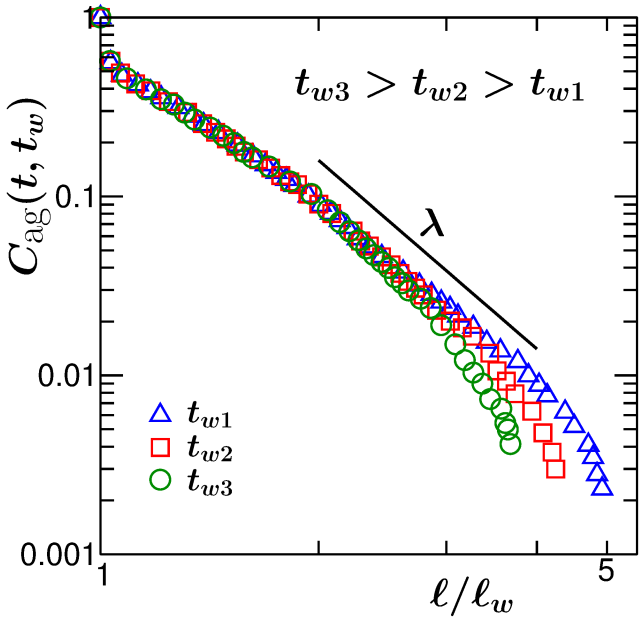


Fig. 1.8 Autocorrelation functions $C_{\rm ag}(t, t_w)$ for various $t_w$ values are plotted with the variation of $\ell/\ell_w$. The solid line denotes a power-law with the aging exponent $\lambda$. These results are from the same model system as in Fig. 1.6.

For a self-similar process, $S(k,t)$ exhibits the scaling property [2, 7]

$$S(k,t) \equiv \ell^d(t)\tilde{S}[k\ell(t)], \tag{1.28}$$

where $\tilde{S}$ is an analog of $\tilde{C}$. For large $k$, $S(k,t)$ decays in a power-law manner as $S(k,t) \sim k^{-(d+n_c)}$, $n_c$ representing order-parameter symmetry. This is known as the Porod law [52–54], which is nicely observed for sharp domain interfaces or defects. For $k \to 0$, $S(k,t)$ obeys the power-law behavior $S(k,t) \sim k^{\sigma}$ [55], in which the exponent $\sigma$ depends upon system dimensionality and the conservation of order-parameter. These are demonstrated in Fig. 1.7.

## 1.6 Aging in coarsening dynamics

Aging related properties [6, 56–58] form an interesting domain of nonequilibrium physics. This is related to the increase of relaxation time with the increase of age of the system. This says that an older system relaxes slower than a younger system. This is manifested in the behavior of two time quantities, e.g., the order-parameter autocorrelation function,

$C_{\rm ag}(t, t_w)$. The latter is defined as $(t > t_w)$ [6]

$$C_{\rm ag}(t, t_w) = \langle \psi(\vec{r}, t_w)\psi(\vec{r}, t)\rangle - \langle \psi(\vec{r}, t_w)\rangle\langle \psi(\vec{r}, t)\rangle. \tag{1.29}$$

Here $t$ and $t_w$ are, respectively, the observation and waiting times. The latter is also the age of the system. Note that in the definition of $C_{\rm ag}(t, t_w)$ we have set $r = 0$. Despite the fact that the decay rates depend on $t_w$, in various evolving systems $C_{\rm ag}(t, t_w)$ displays the scaling [6, 56] (see Fig. 1.8)

$$C_{\rm ag}(t, t_w) \sim (\ell/\ell_w)^{-\lambda}\,, \tag{1.30}$$

where $\ell$ and $\ell_w$ are the average domain lengths at $t$ and $t_w$, respectively, and $\lambda$ is the aging exponent, which satisfies certain bounds. These bounds were first proposed by Fisher and Huse (FH) [56]:

$$\lambda \geq \frac{d}{2}. \tag{1.31}$$

Yeung, Rao and Desai (YRD) [58] later formulated a more precise and generic bound:

$$\lambda \geq \frac{d+\sigma}{2}. \tag{1.32}$$

Chapters 2 and 3 in this thesis address questions concerning the influence of initial correlation on aging dynamics in coarsening systems. We have considered two particular cases, viz., we have quenched initial configurations with $\xi = 0$ and $\xi = \infty$ to temperatures below the critical points for Ising systems obeying order parameter conservation in $d = 2$ and 3. A more general study will, of course, consider initial configurations with continuously varying $\xi$. Note that $\xi = 0$ and $\xi = \infty$, as discussed in Sec. 1.2, correspond to preparations of initial equilibrium configurations at $T = \infty$ and $T = T_c$. We will see that in these two cases the aging exponents differ from each other drastically, in each of the considered space dimensions. Here, it is worth recalling that the renormalization group arguments suggest [59] that asymptotically the growth exponent $\alpha$ should be independent of the choice of $T$ or $\xi$ for the initial configurations. In light of the recent observation [60], however, of Mpemba effect in Ising model, it becomes necessary to verify whether the growth amplitude will also be independent of initial $\xi$. The theoretical expectation is similar for quenches to different temperatures below the critical point, as far as the exponent is concerned. In the latter case, the fact is expected

to hold for aging phenomena as well. The above expectations have connection with the convergences to fixed points related to $T = 0$ and $T = \infty$ upon renormalization [59, 61].

For an idea of the current status of the literature, on the value of $\lambda$, we have added a table here. We mention here that $C_{\rm ag}(t, t_w)$ in Eq. (1.29) can be decomposed into two

Table 1.1 List of numerically obtained values of $\lambda$ for the nearest neighbor Ising model. Here "Correlated" and "Uncorrelated" imply results for quenches from $T_s = T_c$ and $T_s = \infty$, respectively. The results for the correlated COP cases will be provided later.

| Model | $d = 2$ | | $d = 3$ | |
|---|---|---|---|---|
| | Correlated | Uncorrelated | Correlated | Uncorrelated |
| COP | – | 3.6±0.2 [62] | – | 7.5±0.4 [62] |
| NCOP | 0.14±0.02 [63] | 1.32±0.04 [64] | 0.57±0.07 [63] | 1.69±0.04 [64] |

parts, viz., a time translation invariant part and a time translation variant part. The first one is related to domain magnetization that behaves, even during pre-asymptotic period, like that in an equilibrium system. The second one is related to the global evolution and the scaling laws for aging are by concerning this.

## 1.7 Surface tension and its curvature dependence: An equilibrium property

From the perspective of thermodynamics, interfacial tension is an important quantity to calculate as it determines the energy barrier to overcome to form a stable cluster of a phase. This can be defined as the free energy per unit interfacial area. In the classical nucleation theory (CNT) curvature dependence of interfacial tension is typically ignored, even though related concepts exists since the time of Gibbs [65]. Tolman [66–68] proposed the corrections of the form [68]

$$\gamma(R) = \frac{\gamma(R = \infty)}{1 + \frac{(p-1)\delta}{R}}. \tag{1.33}$$

Here $\gamma(\infty)$ is the surface tension of a flat interface. The parameter $p$ equals 3 and 2, for spherical and cylindrical interfaces, respectively, and $\delta$, being separation between the equimolar surface and surface of tension [65, 69–71], has the dimension of length. This is referred to as the Tolman length.

For systems which are symmetric under the interchange of the two coexisting phases, $\delta$ vanishes [72]. There the curvature dependence of $\gamma$ can be written, to the leading

order, as [72, 73]

$$\gamma(R) = \frac{\gamma(\infty)}{1 + 2(\frac{\tilde{\ell}}{R})^2}, \tag{1.34}$$

where $\tilde{\ell}$ is the constant prefactor for the quadratic correction term. This is a function of bending rigidity ($\kappa$) and the rigidity constant ($\kappa'$) related to Gaussian curvature of the interface as [74, 75]

$$\tilde{\ell}^2 = -\frac{\kappa + \kappa'/2}{\gamma(\infty)}. \tag{1.35}$$

## 1.8 Methods

This thesis contains numerical studies of phase transitions in two different primary models of solid and liquid binary mixtures. For this purpose we have used Monte Carlo (MC) and molecular dynamics (MD) simulation methods.

### 1.8.1 Monte Carlo Simulation

To study different properties of phase separating systems we have employed various types of Monte Carlo simulations [24]. We have used Kawasaki spin-exchange MC simulations to study the aging dynamics in the conserved Ising model, mimicking growth in solid binary mixtures, and a semi-grandcanonical Monte Carlo (SGMC) technique to investigate the equilibrium interfacial properties in binary fluid mixtures. In solid binary mixtures, growth occurs via diffusive transport of matter as hydrodynamics does not play any role in the coarsening process. This process can be imitated nicely by MC simulation with order-parameter conserving Kawasaki dynamics. In this case, one starts with a lattice containing randomly located up and down spins. This corresponds to a homogeneous solid binary mixture at high temperature where the A and B species are perfectly mixed. Then the system is updated via trial moves. In this process exchange of spins between randomly selected neighboring sites is tried. These are accepted by following the well-known Metropolis algorithm. This algorithm [24] deals with the transition probability which depends on the energy deviation in the final state from the initial one.

$P_i(t)$, the probability to find a system in the $i$-th state at time $t$ follows the master equation

$$\frac{\partial P_i(t)}{\partial t} = -\sum_{i \neq j} [P_i(t)\Pi(i \to j) - P_j(t)\Pi(j \to i)], \tag{1.36}$$

where $\Pi(i \rightarrow j)$ is the rate for transition from the $i$-th state to the $j$-th state. At equilibrium, the left hand side of Eq. (1.36) should be zero, i.e., one has

$$P_i(t)\Pi(i \rightarrow j) = P_j(t)\Pi(j \rightarrow i). \tag{1.37}$$

This is known as the detailed balance equation. In the Metropolis algorithm [24]

$$\Pi(i \rightarrow j) = e^{-\frac{\Delta E}{k_B T}}, \qquad \Delta E > 0 \tag{1.38}$$

$$= 1, \qquad \Delta E \leq 0 \tag{1.39}$$

where $\Delta E = E_j - E_i$ and $k_B$ is the Boltzmann constant. This algorithm is implemented in numerical simulations by the following protocol [24].
(1) A particle or spin 's' is randomly selected from a configuration.
(2) Particle 's' undergoes a random displacement or exchanges its position with one of its randomly chosen nearest neighbors.
(3) The energy difference between the initial and final states is calculated.
(4) A random number $\Gamma$ is generated between 0 and 1.
(5) If $\Gamma < e^{-\frac{\Delta E}{k_B T}}$, then the trial move is accepted.

## Wolff Algorithm

Near the critical point $T_c$, large spatial correlations develop inside the system and the relaxation time ($\tau$) diverges as [4, 10]

$$\tau \sim \xi^z, \tag{1.40}$$

where $z$ is a dynamic critical exponent. Note that the correlation length $\xi$ diverges as in Eq. (1.4). We thus encounter a phenomenon called 'critical slowing down' [11]. In order to overcome this, Wolff algorithm [76] is useful. There, instead of attempting single spin-flip trials, one performs flipping of correlated clusters of spins having same sign. The algorithm is prescribed below [76].
(1) A particle or spin 'i' is randomly selected from a configuration.
(2) All nearest neighbors 'j' of this spin are added to a single cluster with a probability $1 - e^{-\frac{2J}{k_B T}}$, provided 'i' and 'j' are of similar type and the bond between them has not been considered before.
(3) Repeat the previous step for each connected spin and add it to the cluster accordingly, until no more bonds are left.

(4) Invert the whole cluster. This completes one Wolff step.
This is a rejection-free algorithm and thus, strongly suppresses dynamic slowing down near a critical point.

## Grand and Semi-grand Canonical Monte Carlo

The above discussion is for simulations in NVT or canonical ensemble. In case of grand canonical ensemble ($\mu$VT) [24], one considers fluctuations in the energy and number of particles at fixed volume and temperature. There, the acceptance probability will, in addition to $\Delta E$, depend also on the chemical potential $\mu$ of a particle.

The grandcanonical Monte Carlo is used for studying vapor-liquid transition. In the case of phase transition in a binary mixture (A+B), where the fluctuation in the concentration of a component ($x_A$ or $x_B$) is allowed by keeping the overall particle density constant, one can employ a semi-grandcanonical Monte Carlo (SGMC) technique [24]. In this technique other than the standard displacement moves one attempts to switch the species identity of a randomly selected particle (A $\rightarrow$ B $\rightarrow$ A). This is equivalent to placing one B particle at a vacant position which is being created by removing one A particle from that site. This is analogous to the Glauber dynamics [24] that is used to study kinetics of phase transition in magnetic systems.

With simple SGMC simulations [24], mainly at low temperatures ($T << T_c$), it is not always possible to sample the whole composition space because of the presence of high interfacial free energy barrier between the coexisting phases. There the system gets trapped in one side of the coexistence curve. To overcome such shortcomings, one can use more advanced simulation techniques such as the successive umbrella sampling method [77], where it is possible to control the composition in such a way that the whole range of the latter can be explored. Below we describe briefly the implementation of this technique.

Here, the relevant range of macrostates, defined by the concentration of a species, say A, i.e., $x_A$, is subdivided into $m$ number of overlapping windows of convenient width $\Delta x_A$. For each window, a separate SGMC simulation is done. In the $k$-th window, when, say, $N\Delta x_A = 1$, one has to start with $x_A : x_B = k : (N-k)$ and allow the system to change the value of $x_A$ only between $k$ and $k + N\Delta x_A$. If any SGMC move tries to bring the system out of this window, it will be rejected. If $H(k)$ counts how often $k$-th state is being visited by the system, one can formulate the probability distribution as [77]

$$\frac{P(k)}{P(0)} = \frac{H(1)}{H(0)} \cdot \frac{H(2)}{H(1)} \cdot \cdots \cdot \frac{H(k)}{H(k-1)}. \tag{1.41}$$

Once such a probability distribution is estimated, interfacial properties can be calculated via standard rules.

### 1.8.2 Molecular Dynamics Simulation

We have employed MD simulations [78] to study the nonequilibrium properties of liquid-liquid phase transition, for which the preservation of hydrodynamics is important. In these simulations, Newton's equations of motion are numerically solved for a large number of particles, interacting among themselves via a smooth potential, by using various algorithms. In this thesis we have used the Verlet velocity algorithm [78]. The position and velocity updates for the $x$-components of the $i$-th particle in this algorithm are given by

$$x(t+\Delta t) = x(t) + \dot{x}\Delta t + \ddot{x}\frac{\Delta t^2}{2}, \tag{1.42}$$

$$v_x(t+\Delta t) = v_x(t) + \frac{1}{2}\Delta t[\ddot{x}(t) + \ddot{x}(t+\Delta t)]. \tag{1.43}$$

This is the procedure of MD simulation in microcanonical (NVE) ensemble where the total energy remains constant. We have used MD simulations in canonical (NVT) ensemble. There, to keep the temperature of the system fixed, one needs to use a thermostat. In the literature there exists several thermostats that can control the temperature well. Some examples are Andersen thermostat [79], Nosé-Hoover thermostat [80–82], etc. In the Andersen thermostat [79] randomly selected particles are made to collide with an external heat reservoir. After a collision the new velocity of the particle is drawn from a Maxwell-Boltzmann distribution mimicking the desired temperature. Thus, this prescription builds a stochastic coupling of the system with an external heat bath of a constant temperature. The collision frequency or the strength of the coupling can be controlled by a parameter $\Omega$, which one has to choose wisely. As the value of $\Omega$ is increased, more collision events are going to happen, hence, there will be more and more deviation from the conservation of the local momentum, destroying the hydrodynamics. Therefore, this thermostat can not be used for replicating the real dynamics of a fluid system where preservation of hydrodynamics is important.

The Nosé-Hoover thermostat (NHT) [80–82], which is based on the efficient usage of the extended-Lagrangian approach, can be a very good choice if one needs to do deterministic MD simulation at a fixed temperature. Here the heat-bath is being considered as an intrinsic part of the system, which will be described by a position-like co-ordinate $s$, conjugate momentum $p_s$ and the "mass" $Q = p_s/\dot{s}$. The quantity $Q$ is considered as

the coupling constant between the reservoir and the real system. With this prescription one has the Hamiltonian of the system as

$$\mathcal{H} = \sum_{i=1}^{N} \frac{m_i}{2} s^2 \dot{r_i}^2 - U(\vec{r}) + \frac{Q}{2}\dot{s}^2 - (3N+1)k_B T \ln s \tag{1.44}$$

where $(3N+1)$ is the total number of degrees of freedom of the system and the logarithmic term is essential for proper time scaling. In the extended system time interval $\Delta t'$ does not equal the real time $\Delta t$, they are related as $\Delta t = s\Delta t'$. Another parameter $\zeta = \dot{s}/s$, known as the friction coefficient, is introduced. This quantity controls the particle velocities and, hence, the temperature of the system. The dynamical equations for the NHT are written as

$$m_i \dot{\vec{r}_i} = \vec{p}_i, \tag{1.45}$$

$$\dot{v}_i = -\frac{1}{m_i}\frac{\partial U(\vec{r})}{\partial \vec{r}} - \zeta \dot{\vec{v}}_i, \tag{1.46}$$

$$\dot{\zeta} = \frac{1}{Q}\left[\sum_{i=1}^{N} p_i^2/m_i - 3Nk_B T\right]. \tag{1.47}$$

As the difference between the desired temperature and the effective temperature (which is proportional to the kinetic energy of the constituent particles) increases, $\zeta$ fluctuates in such a way that the difference tends to decrease. The position and velocity update equations with NHT are

$$x_i(t+\Delta t) = x_i(t) + \dot{x}(t)\Delta t + [\ddot{x}(t) - \zeta \dot{x}(t)]\frac{\Delta t^2}{2}, \tag{1.48}$$

$$\begin{aligned} v_x(t+\Delta t) =& v_x(t) + \frac{\Delta t}{2}[\ddot{x}(t) + \ddot{x}(t+\Delta t) - 2\zeta \dot{x}(t)] \\ & - \frac{\Delta t^2}{2}\left[\frac{\zeta}{2}(\ddot{x}(t) + \ddot{x}(t+\Delta t) - 2\zeta \dot{x}(t)) \right. \\ & \left. + v_x(t)(\sum_{i=1}^{N} p_i^2/m_i - 3Nk_B T)/Q\right]. \end{aligned} \tag{1.49}$$

This thermostat can preserve hydrodynamics efficiently and, therefore, can be used for studying the dynamics in fluids.

## 1.9 Brief Overview of the thesis

In this thesis we have investigated various nonequilibrium and equilibrium aspects concerning phase separation in binary mixtures. In chapters 2 and 3 results for aging dynamics during demixing transitions in symmetric solid mixtures have been presented. These were obtained via MC simulations of the nearest neighbor Ising model in space dimensions $d = 2$ and 3. We have quantified the role of the long range correlation in the initial configuration on the dynamics. We have prepared the initial configurations at the demixing critical points and performed quenches to the ordered regions. The results were obtained via Kawasaki exchange Monte Carlo [24] simulations.

In chapter 4, we have presented results on the kinetics of demixing transition in binary fluids. This chapter deals with the identification of growth mechanism in the case of off-critical quench, for dense liquid mixtures, via hydrodynamics preserving molecular dynamics simulations [78].

In chapter 5 we study the excess free energy contribution due to the presence of the interface between two coexistence phases in a symmetric liquid mixture via semi-grand canonical Monte Carlo [24] simulations. By varying the composition, the shapes of the minority phase clusters change from spherical to cylindrical and finally, to slab-like structures with flat interfaces. Here we investigate the universality related to the critical behavior of the curvature dependent interfacial tension.

In chapter 6 it is discussed how in complex geometrical situations the interfacial tension can be expressed as a function of the combination of the principal radii of curvature. Deviations from such descriptions are pointed out and discussed.

# References


[1] H.E. Stanley, *Introduction to Phase Transitions and Critical Phenomena* (Clarendon Press, Oxford, 1971).

[2] K. Binder, in *Phase Transformation of Materials*, edited by R.W. Cahn, P. Haasen and E.J. Kramer (Wiley VCH, Weinheim, 1991).

[3] N. Goldenfeld, *Lectures on Phase Transitions and the Renormalization Group* (West View Press, 1992).

[4] A. Onuki, *Phase Transition Dynamics* (Cambridge University Press, Cambridge, UK, 2002).

[5] R.A.L. Jones, *Soft Condensed Matter* (Oxford University Press, Oxford, UK, 2002).

[6] *Kinetics of Phase transition*, edited by S. Puri and V. Wadhawan (CRC Press, Boca Raton, 2009).

[7] A.J. Bray, Adv. Phys. **51**, 481 (2002).

[8] M. Plischke and B. Bergersen, *Equilibrium Statistical Mechanics* (World Scientific, Singapore, 2006).

[9] M.E. Fisher, Rep. Prog. Phys. **30**, 615 (1967).

[10] M.E. Fisher, in *Critical Phenomena*, edited by M.S. Green (Academic, London, 1971).

[11] P.C. Hohenberg and B.I. Halperin, Rev. Mod. Phys. **49**, 435 (1977).

[12] V. Privman, P.C. Hohenberg, and A. Aharony, in *Phase Transitions and Critical Phenomena*, edited by C. Domb and J.L. Lebowitz (Academic Press, New York, 1991).

[13] M.A. Anisimov and J.V. Sengers, in *Equations of State for Fluids and Fluid Mixtures*, edited by J.V. Sengers, R.F. Kayser, C.J. Peters, and H.J. White (Elsevier, Amsterdam, 2000).

[14] J.W. Cahn, Trans. Metal. Soc. AIME **242**, 166 (1968).

[15] J.E. Hilliard, in *Phase Transformations*, edited by H.I. Aronson, (American Society for Metals, Metals Park, Ohio, 1970).

[16] K. Binder and D. Stauffer, Phys. Rev. Lett. **33**, 1006 (1974).

[17] S. Roy and S.K. Das, Phys. Rev. E **85**, 050602(R) (2012).

[18] W. Ostwald, *Lehrbuch der allgemeinen chemie* (University of California Libraries, 1896).

[19] W. Ostwald, Zeitschrift für Physikalische Chemie. **22**, 289 (1897).

[20] I.M. Lifshitz and V.V. Slyozov, J. Phys. Chem. Solids **19**, 35 (1961).

[21] C. Wagner, Z. Electrochem. **65**, 581 (1961).

[22] D.A. Huse, Phys. Rev. B **34**, 7845 (1986).

[23] J.G. Amar, F.E. Sullivan, and R.D. Mountain, Phys. Rev. B **37**, 196 (1988).

[24] D.P. Landau and K. Binder, *A Guide to Mote Carlo Simulations in Statistical Physics* (Cambridge University Press, Cambridge, 2009).

[25] K. Binder, Phys. Rev. B **15**, 4425 (1977).

[26] E.D. Siggia, Phys. Rev. A **20**, 595 (1979).

[27] H. Furukawa, Phys. Rev. A **31**, 1103 (1985).

[28] H. Furukawa, Phys. Rev. A **36**, 2288 (1987).

[29] M. San Miguel, M. Grant, and J.D. Gunton, Phys. Rev. A **31**, 1001 (1985).

[30] J.E. Farrell and O.T. Valls, Phys. Rev. B **43**, 630 (1991).

[31] A. Shinozaki and Y. Oono, Phy. Rev. E **48**, 2622 (1993).

[32] T. Koga and K. Kawasaki, Physica A **196**, 389 (1993).

[33] H. Tanaka, Phys. Rev. Lett. **72**, 1702 (1994).

[34] H. Tanaka, J. Chem. Phys. **103**, 2361 (1995).

[35] H. Tanaka, J. Chem. Phys. **105**, 10099 (1996).

[36] M. Laradji, S Toxvaerd, and O.G. Mouritsen, Phys. Rev. Lett. **77**, 2253 (1996).

[37] H. Tanaka, J. Chem. Phys. **107**, 3734 (1997).

[38] S. Bastea and J. Lebowitz, Phys. Rev. Lett. **78**, 3499 (1997).

[39] V.M. Kendon, M.E. Cates, I. Pagonabarraga, J.C. Desplat, and P. Blandon, J. Fluid Mech. **440**, 147 (2001).

[40] C. Datt, S.P. Thampi, and R. Govindarajan, Phys. Rev. E **91**, 010101(R) (2015).

[41] S. Majumder and S.K. Das, Europhys. Lett. **95**, 46002 (2011).

[42] S. Ahmad, S.K. Das, and S. Puri, Phys. Rev. E **85**, 031140 (2012).

[43] S. Roy and S.K. Das, Soft Matter **9**, 4178 (2013).

[44] R. Shimizu and H Tanaka, Nat. Commun. **6**, 7407 (2015).

[45] A.K. Thakre, W.K. den Otter and W.J. Briels, Phys. Rev. E **77**, 011503 (2008).

[46] H. Kabrede and R. Hentschke, Physica A **361**, 485 (2006).

[47] S.W. Koch, R.C. Desai, and F.F. Abraham, Phys. Rev. A **27**, 2152 (1983).

[48] V. Kumaran, J. Chem. Phys. **109**, 7644 (1998).

[49] J.-P. Hansen and I.R. McDonald, *Theory of Simple Liquids* (Academic Press, London, 2008).

[50] S.K. Das, J.V. Sengers and M.E. Fisher, J. Chem. Phys. **127**, 144506 (2007).

[51] T.M. Squires and J.F. Brady, Phys. Fluids **17**, 073101 (2005).

[52] G. Porod, *Small-Angle X-Ray Scattering*, edited by O. Glatter and O. Kratky (Academic Press, New York, 1982).

[53] Y. Oono and S. Puri, Mod. Phys. Lett. B **2**, 861 (1988).

[54] A.J. Bray and S. Puri, Phys. Rev. Lett. **67**, 2670 (1991).

[55] C. Yeung, Phys. Rev. Lett. **61**, 1135 (1988).

[56] D.S. Fisher and D.A. Huse, Phys. Rev. B **38**, 373 (1988).

[57] F. Liu and G.F. Mazenko, Phys. Rev. B **44**, 9185 (1991).

[58] C. Yeung, M. Rao and R.C. Desai, Phys. Rev. E **53**, 3073 (1996).

[59] K. Humayun and A. J. Bray, J. Phys. A: Math. Gen. **24**, 1915 (1991).

[60] N. Vadakkayil and S.K. Das, Phys. Chem. Chem. Phys. **23**, 11186 (2021).

[61] M.E. Fisher, Rev. Mod. Phys. **70**, 653 (1998).

[62] J. Midya, S. Majumder and S.K. Das, Phys. Rev. E **92**, 022124 (2015).

[63] K. Das, N. Vadakkayil, and S.K. Das, Phys. Rev. E **101**, 062112 (2020).

[64] J. Midya, S. Majumder and S.K. Das, J. Phys. Condens. Matter **26**, 452202 (2014).

[65] J. Willard Gibbs, *Collected Works* (Longmans Green and Company, New York, 1928).

[66] R.C. Tolman, J. Chem. Phys. **16**, 758 (1948).

[67] R.C. Tolman, J. Chem. Phys. **17**, 118 (1949).

[68] R.C. Tolman, J. Chem. Phys. **17**, 333 (1949).

[69] J.S. Rowlinson and B. Widom, *Molecular Theory of Capillarity* (Clarendon, Oxford, 1982).

[70] J.S. Henderson, in *Fluid Interfacial Phenomena*, edited by C.A. Croxton (Wiley, New York, 1986).

[71] J.S. Rowlinson, J. Phys. Condens. Matter **6**, A1 (1994).

[72] M.P.A. Fisher and M. Wortis, Phys. Rev. B **29**, 652 (1984).

[73] B.J. Block, S.K. Das, M. Oettel, P. Virnau, and K. Binder, J. Chem. Phys. **133**, 154702 (2010).

[74] E.M. Blokhuis and D. Dedeaux, Mol. Phys. **80**, 705 (1993).

[75] A.E. van Giessen, E.M. Blokhuis, and D.J. Bukman, J. Chem. Phys. **108**, 1148 (1998).

[76] U. Wolff, Phys. Rev. Lett. **62**, 361 (1989).

[77] P. Virnau and M. Müller, J. Chem. Phys. **120**, 10925 (2004).

[78] D. Frenkel and B. Smit, *Understanding Molecular Simulations: From Algorithms to Applications* (Academic Press, San Diego, 2002).

[79] H.C. Andersen, J. Chem. Phys. **72**, 2384 (1980).

[80] S. Nosé, J. Chem. Phys. **81**, 511 (1984).

[81] W.G. Hoover, Phys. Rev. A **31**, 1695 (1985).

[82] W.G. Hoover, *Studies in Modern Thermodynamics*, (Elsevier, 1991).

# Chapter 2

# Initial Correlation Dependence of Aging in Phase Separating 2D Solid Binary Mixtures

## 2.1 Introduction

When a homogeneous mixture is quenched from a high starting temperature ($T_s$) to a final temperature ($T_f$) inside the miscibility gap, the system falls unstable against the fluctuations and moves towards a new equilibrium state via formation of domains rich in particles of similar type [1–5]. Understanding of this nonequilibrium process is crucial from scientific as well as technological point of views. The relaxation of such systems are often investigated via the two-time auto-correlation function. This is defined as [6]

$$C_{\rm ag}(t,t_w) = \langle \psi(\vec{r},t)\psi(\vec{r},t_w)\rangle - \langle \psi(\vec{r},t)\rangle\langle \psi(\vec{r},t_w)\rangle, \tag{2.1}$$

where $\psi$ is a space ($\vec{r}$) and time dependent scalar order parameter. Here $t$ and $t_w$ ($\leq t$) are the observation and waiting times, respectively. Note that $t_w$ is also known as the age of the system.

In nonequilibrium systems the time-translation invariance is not obeyed. This implies that if one starts from different $t_w$ values, the relaxation rates differ. Nevertheless $C_{\rm ag}(t,t_w)$ exhibits certain scaling property [6–22]:

$$C_{\rm ag}(t,t_w) \sim (\ell/\ell_w)^{-\lambda}, \tag{2.2}$$

$\ell$ and $\ell_w$ being the average domain sizes at times $t$ and $t_w$, respectively. The exponent $\lambda$ is referred to as the aging exponent. In phase ordering systems $\ell$ grows with time in a power-law fashion [1–4, 6]

$$\ell \sim t^{\alpha}, \tag{2.3}$$

where $\alpha$ is the growth exponent. For the complete understanding of nonequilibrium universality classes [2, 19] quantification of these exponents is important.

For the quench from $T_s = \infty$, corresponding to random initial configurations, the values of the above mentioned exponents are well studied [13, 14, 18–20, 23]. Another relevant case can be the quench from the critical temperature $T_c$ [19, 20, 24–26]. At $T_c$ for a thermodynamically large system size, the correlation length, $\xi$, diverges, i.e., $\xi = \infty$ [2, 3, 27]. This large correlation length in the initial structure influences the evolution of a system, when quenched from $T_s = T_c$. So the corresponding universality class differs from the case of $T_s = \infty$. This aspect of universality has been demonstrated already in the case of ordering ferromagnets [19, 20]. The value of the growth exponent is reported to be same whereas there are differences in the other structural and dynamic quantities [19, 20, 24–26] for quenches from $T_s = \infty$ and $T_s = T_c$.

In contrast to the magnetic case, for which there is no constraint on the conservation of system integrated order parameter during evolution [2], the task of understanding of coarsening phenomena is known to be significantly more difficult, at least theoretically and computationally, for conserved order parameter dynamics that applies to kinetics of phase separation in multi-component mixtures [2]. Computational difficulty [23, 28, 29], to a certain extent, arises from the significantly slower dynamics in the latter case. Note that for the nonconserved case [2, 30] $\alpha = 1/2$, whereas for the conserved case [2, 31, 32] $\alpha = 1/3$. Furthermore, irrespective of the type of dynamics, conserved or nonconserved, quantitative understanding of aging behavior, even for simple models, still remains difficult, convergence in the settlement of issues being rather slow [7–20, 33–37], despite the availability of huge computational resources.

Nevertheless, there exists studies on systems that follow conserved order parameter dynamics where methods like finite size scaling techniques [14, 38] have been adopted for the analyses. One of such studies is on phase separating binary (A+B) mixture, where the quantification of $\lambda$ has been done via finite-size scaling method [14] for the quench from $T_s = \infty$. Here and in a number of previous studies [14, 16, 17] it is shown that $\lambda$ obeys certain bound, given by Yeung, Rao and Desai (YRD) [9]:

$$\lambda \geq \frac{d+\beta}{2}, \tag{2.4}$$

where $d$ is the system dimensionality and $\beta$ is the power-law exponent of structure factor [39] in the limit $k \to 0$, with $k$ being the wave number. This can be written as

$$S(k \to 0, t_w) \sim k^{\beta}. \tag{2.5}$$

For nonconserved order-parameter dynamics the structural scaling for $T_s = T_c$ is reported to be different from that of $T_s = \infty$ [19, 20]. This points towards the fact that the value of $\lambda$ differs in the two cases leading to different universality classes. One can expect this to be true for the case of conserved order-parameter dynamics as well.

In this chapter we focus on the conserved case, i.e., we take up the task of estimating $\lambda$ for solid binary (A+B) mixtures with $T_s = T_c$. Note that nonequilibrium universality classes are also decided [2] by the space dimension, order-parameter symmetry and presence of hydrodynamics. Here we focus on $d = 2$ and scalar order parameter, in absence of hydrodynamics, i.e., in our model system coarsening occurs due to simple diffusive transport, as expected in solid mixtures.

We have also shown that the estimated value of $\lambda$ is consistent with the lower bound given by YRD. These numbers are discussed with reference to the corresponding numbers [14] for $T_s = \infty$. It transpires that for conserved order parameter also $\lambda$ for $T_s = T_c$ is hugely different from that for $T_s = \infty$.

## 2.2 Models and Methods

We study nonequilibrium dynamics in solid binary mixtures via Kawasaki exchange [40] Monte Carlo method [41–43], using the Ising model [27] in space dimension 2. The Ising Hamiltonian is given by [27, 42]

$$H = -J \sum_{<ij>} S_i S_j;\ S_i = \pm 1;\ J > 0, \tag{2.6}$$

where the values $+1$ and $-1$, of $S_i$ or $S_j$, correspond to particles of types A and B, respectively. We considered a square lattice, with periodic boundary conditions [42] in both the directions. The value of critical temperature for this model [27, 42] in $d = 2$ is $\simeq 2.269 J/k_B$. Here $J$ and $k_B$ are the interaction strength and Boltzmann constant, respectively.

A trial move in the Kawasaki exchange Ising model (KIM) is the interchange of particles between randomly selected nearest neighbor sites. The probability of acceptance

of trial moves is given by [41–43]

$$P(i \to j) = \min(1, \exp(-(E_j - E_i)/k_B T_f)), \tag{2.7}$$

where $E_{i(j)}$ is the energy of the state $i(j)$. One Monte Carlo step (MCS) consists of $L^2$ trial moves, where $L$ is the linear dimension of a square box, in units of the lattice constant $a$. Time in our simulation is measured in units of MCS. Throughout the chapter, we set the quantities $J$, $k_B$ and $a$ to unity.

We present results mainly from the quenches of the systems from $T_s = T_c^L$, where $T_c^L$ is the system-size dependent critical temperature [38, 44]. The final temperature is kept fixed at $T_f = 0.6T_c$. This choice of temperature is to avoid metastability as discussed in the previous chapter. For the purpose of comparison we have performed quenches from $T_s = \infty$ also. Here note that the asymptotic growth exponent $\alpha$ are said to be same [20] for both $T_s = \infty$ and $T_s = T_c$ for quenches to $T_f < T_c$.

In the vicinity of the critical point one encounters critical slowing down [45], making the simulations time taking. In order to avoid this, for obtaining the equilibrium configurations at $T_c^L$, we have used the Wolff algorithm [46–48]. There a cluster of similar particles is identified and flipped randomly. This, to a good extent, ease the simulation at $T_c^L$.

The average domain lengths within a system can be calculated from the domain size distribution function, $P(\ell_d, t)$, as [23, 29]

$$\ell(t) = \int P(\ell_d, t)\ell_d d\ell_d, \tag{2.8}$$

where $\ell_d$ corresponds to the separation between two successive interfaces along any Cartesian direction. In the calculation of the autocorrelation functions [see Eq. (2.1)], the order parameter $\psi$ is the spin value in Eq. (2.6) at a lattice site. All the results presented here are averaged over a large number of independent initial realizations. Depending upon the system size this number ranges between 100 and 500.

## 2.3 Results

In Fig. 2.1 snapshots during the evolutions for different $T_s$ values are presented. The upper frames are for $T_s = \infty$ and the lower ones are for $T_s = T_c^L$. All the pictures are for $L = 128$. In the early time there are differences in the evolving structures for the two starting temperatures, which is visible from the presented snapshots. For the quench

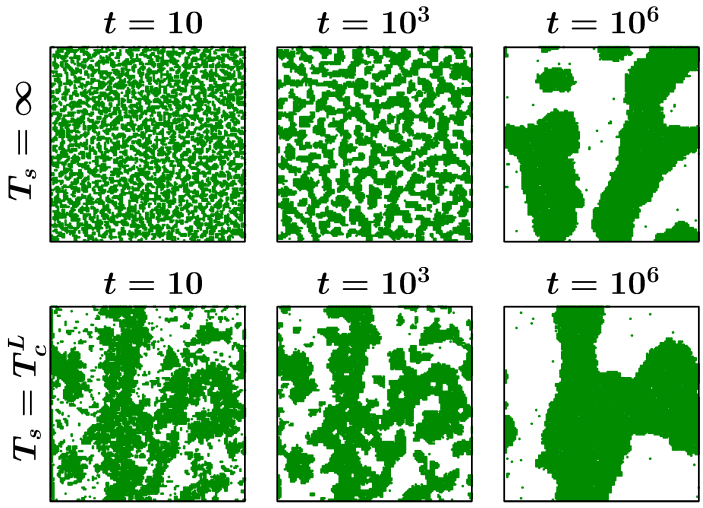


Fig. 2.1 Snapshots for the Kawasaki Ising model during evolutions following quenches from $T_s = \infty$ (upper frames) and $T_s = T_c^L$ (lower frames), with $L = 128$. For both the cases snapshots from three different times are shown. The dots represent A particles and the rest of the space is occupied by B particles. Here and in other places all results are from quenches to $T_f = 0.6T_c$. This figure is from reference [46].

from $T_s = \infty$ one encounters the standard finite-size effect [23, 29, 38, 42, 49] when $\ell$ approaches $L$ at late time. But in the case of $T_s = T_c^L$ in addition to this nonequilibrium finite-size effect, finite-length correlations [38, 42] in the starting configurations lead to equilibrium finite-size effect. In the close proximity of $T_c$, the correlation length behaves as [27],

$$\xi \sim \epsilon^{-\nu}; \epsilon = \frac{T_s - T_c}{T_c}, \tag{2.9}$$

where $\nu$ is a static critical exponent. For thermodynamically large systems, $\xi = \infty$ at the critical point. Since one can handle only finite systems, $L < \infty$, in computer simulations $\xi$ is always finite. The maximum value, that $\xi$ can attain is the system size, $L$. This fact, in one way, makes the evolution process different from that of $T_s = \infty$. The systems quickly deviate from the desired [19, 20] scaling form than the quenches from $T_s = \infty$ when the quench is being done from $T_s = T_c^L$. This can be appreciated from the snapshots corresponding to $T_s = T_c^L$ in Fig. 2.1, where the changing fractality in structures during evolution is visible. This additional finite-size effect makes the computation difficult. Nevertheless we have adopted appropriate extrapolation exercise of the size-affected quantitative data, to overcome this issue. This needs knowledge of $T_c^L$ for various values of $L$. Below we present the results of the latter before going to the main discussion on aging. A plot of $T_c^L$ versus $1/L$ is shown in Fig. 2.2 (taken from [46, 47]).

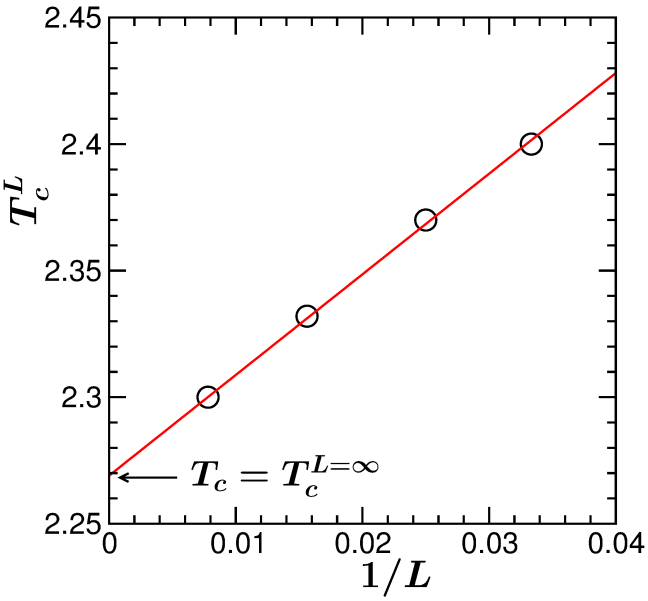


Fig. 2.2 Finite-size critical temperatures $T_c^L$ are plotted as a function of $1/L$, obtained for Glauber Ising Model. The continuous line corresponds to the scaling form in Eq. (2.10), where $T_c$ and $\nu$ are fixed to their 2D Ising values. This figure has been taken from references [46, 47].

These results were obtained from Glauber Ising Model [50]. The protocol that we have followed for this is the following [46, 47]. Via Monte Carlo simulations, which provide the fluctuations in the magnetization, in equilibrium scenario, we obtained order-parameter distributions for various temperatures as well as system sizes. As is well known, below $T_c$ the distributions, constructed from such fluctuations, are double-peaked, positions of the peaks corresponding to the points on the coexistence curve. Whereas, above $T_c$ distributions are single-peaked. The temperature, at which the transition from double-to-single peak occurs, has been identified as the system-size dependent critical temperature, $T_c^L$ [46, 47].

Given that static critical universality is very robust, we will use the same data for the study of nonequilibrium phenomena in Kawasaki dynamics. The $T_c^L$ exhibits the scaling form [42, 44, 51, 52]

$$T_c^L - T_c \sim L^{-1/\nu}, \tag{2.10}$$

which can be constructed from Eq. (2.9). For the 2D Ising universality class $\nu = 1$. The data set containing $T_c^L$ for various $L$ obeys this scaling relation, represented by the continuous line in Fig. 2.2 by fixing $\nu$ and $T_c$ to the 2D Ising values. In the limit $L \to \infty$ it tends towards the thermodynamic $T_c$ ($\simeq 2.269$).

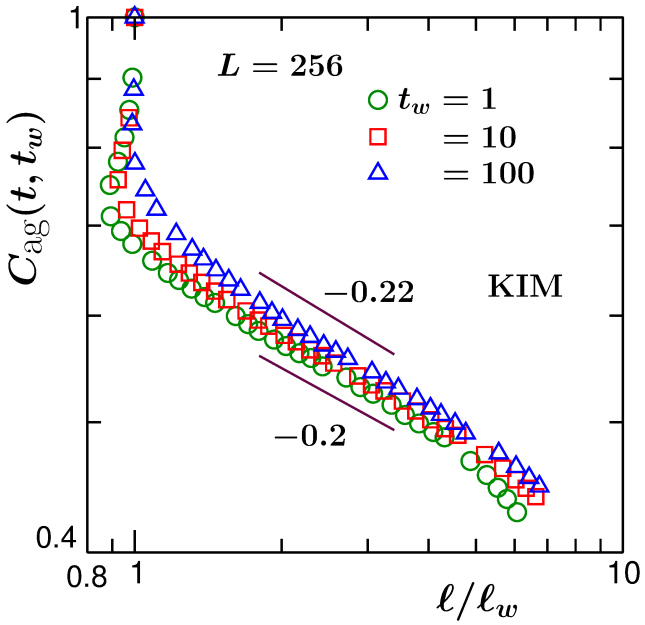


Fig. 2.3 Log-log plots of autocorrelation function, $C_{ag}(t, t_w)$ versus $\ell/\ell_w$. Data for a few different $t_w$ are shown. Results are for $L = 256$. The solid lines represent power laws. The values of the exponents are mentioned next to the lines. This figure is from reference [46].

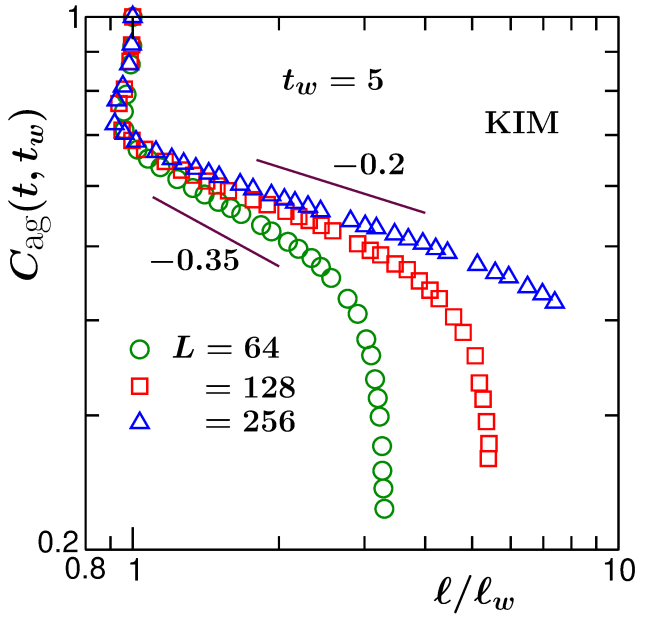


Fig. 2.4 Same as Fig. 2.3 but here we have fixed $t_w$ to 5 and presented results for a few values of $L$. This figure is from reference [46].

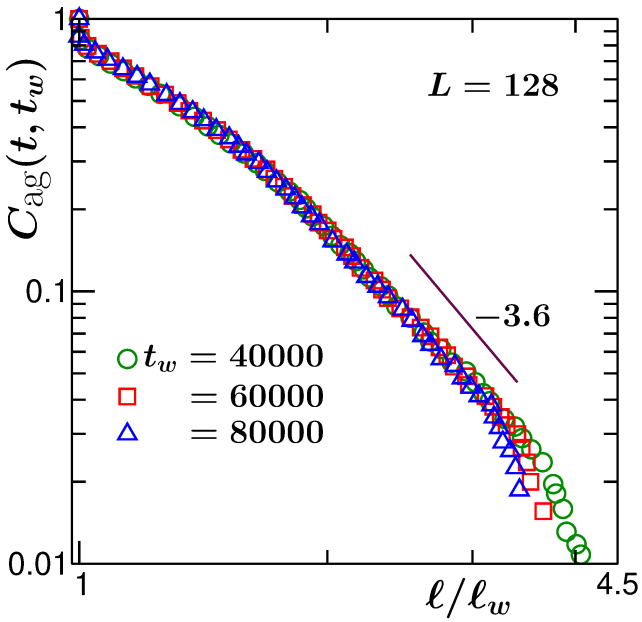


Fig. 2.5 Log-log plots of autocorrelation function, $C_{\rm ag}(t, t_w)$ versus $\ell/\ell_w$ for the quench from $T_s = \infty$. Data for a few different $t_w$ are shown. Results are for $L = 128$. The solid line represents power law. The value of the exponent is mentioned next to the line.

In Fig. 2.3 we present results for $C_{\rm ag}(t, t_w)$, versus $\ell/\ell_w$. We fix the system size and include data from few different $t_w$ values. In Fig. 2.4 we show the similar plots. But here $t_w$ is fixed and $L$ is varied. In none of the cases collapse of data is observed. This should be contrasted with the available literature [13, 14] for quenches from $T_s = \infty$. A representative picture for this is shown in Fig. 2.5. Such non-scaling behavior for quenches from the critical point is because of the fact that for $L < \infty$, the structure, during evolution, quickly starts deviating from the desired scaling, as already mentioned. To overcome this problem we will perform an appropriate extrapolation exercise to obtain the value of $\lambda$ in the $L = \infty$ limit.

Note that very early-time structural change brings artificial non-monotonicity in the length. This is reflected in the plots of Fig. 2.3 for smaller values of $t_w$. During this period, we believe, the system is trying to arrive at the scaling structure, giving rise to an unavoidable inconsistency in the measurement of domain length, but only for a brief early time period. Thus, this non-monotonicity in the domain length should not be taken seriously. On the other hand, with the increase of time departure from this scaling structure occurs, earlier for smaller systems.

In both Fig. 2.3 and 2.4, a common feature is the following. Each of the data sets tend to stabilize to a power-law decay over a certain range of $\ell/\ell_w$, but deviates from

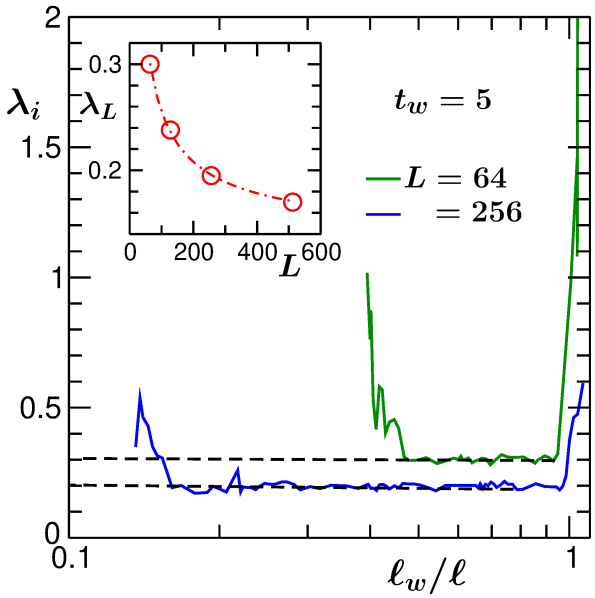


Fig. 2.6 Plots of instantaneous exponents $\lambda_i$ versus $\ell/\ell_w$ for two different values of $L$ on a semi-log scale for a fixed value of $t_w$ $(= 5)$. We estimated the $L$-dependent value, $\lambda_L$, from the flat regions of these plots. The data set of this figure is from reference [46]. In the inset we have shown the behavior of $\lambda_L$, as a function of $L$, for $t_w = 5$. The dot-dashed line corresponds to a fit to a power-law form.

it when $\ell$ approaches $L$, i.e., $\xi$. These stabilized exponent values are, however, different from each other in Fig. 2.3 as well as in Fig. 2.4. In Fig. 2.3, this is because of the fact that the structure for each $t_w$ is different. Recall, we have already mentioned above that this is a nonequilibrium feature related to finite system of any particular size. On the other hand, even though in the case of Fig. 2.4 $t_w$ is fixed, here one has different finite-size effects for different $L$ to start with, owing to different initial $\xi$ for different $L$. Nevertheless, the exponents stay stable for longer ranges with the increase in system size for a fixed $t_w$. Moreover, the rate of change of the exponent keeps decreasing with the increase of $L$. Therefore to obtain the value of $\lambda$ in the thermodynamic limit $(L = \infty)$, one needs to consider larger and larger system sizes which is computationally expensive. Instead of that we adopt an intelligent extrapolation method using relatively smaller systems. An advantage of using smaller systems is that one can acquire better statistics by simulating many independent initial configurations. This can be achieved by using the same computational power that one needs to run single large system. Note that reduction of error is not directly proportional to the system size [29, 49]. It is also worth mentioning that the faster decay of $C_{\rm ag}(t, t_w)$ for large $\ell/\ell_w$, because of the finiteness of the system, is unavoidable in a computer simulation. Only for $L = \infty$ it will decay

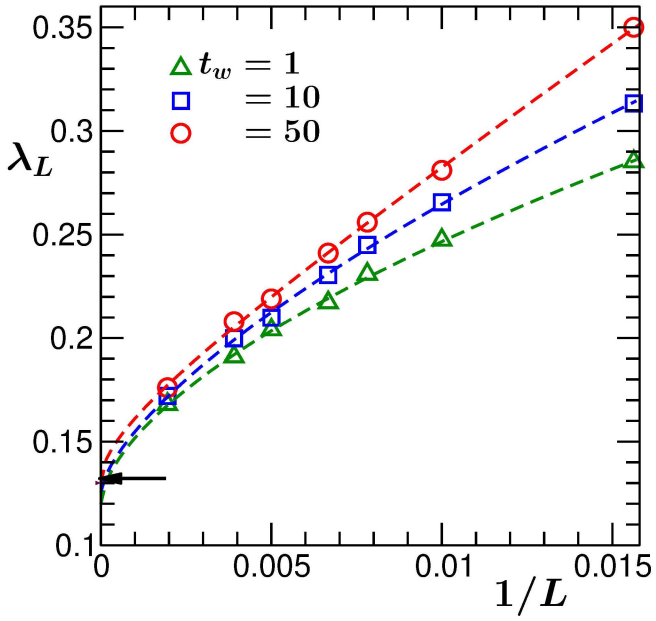


Fig. 2.7 We have plotted $\lambda_L$ as a function of $1/L$. Results for a few values of $t_w$ are included. The lines are power-law fits for extracting $\lambda = \lambda_{L=\infty}$, value of which is marked by an arrow-headed line. This figure is from reference [54].

indefinitely with a unique exponent. Next we will move to the extrapolation exercise to estimate the thermodynamic aging exponent.

For the purpose of extrapolation, we need to gather the exponents corresponding to the stabilized regions in Fig. 2.3. One can evaluate accurately the system-size dependent aging exponents, $\lambda_L$, from the flat regions of the instantaneous exponent [32], $\lambda_i$, versus $\ell_w/\ell$ plots. Here $\lambda_i$ is defined as [14, 28, 32]

$$\lambda_i = -\frac{d \ln C_{\rm ag}(t, t_w)}{d \ln x}; \; x = \frac{\ell}{\ell_w}. \tag{2.11}$$

In Fig. 2.6, as illustration, we plot this quantity as a function of $x$ for two values of $L$ by fixing $t_w$ to 5. One can justify this by taking a closer look at the behavior of $C_{\rm ag}(t, t_w)$ in Fig. 2.3. In the inset of Fig. 2.6, we have shown a plot of $\lambda_L$, as a function of $L$, for $t_w = 5$. This data set is consistent with a power-law behavior. See the dot-dashed line and further discussion below. A fit provides $\lambda = 0.13$. For all values of $t_w$ one can expect that $\lambda_L$ will have same convergence in the limit $L = \infty$. The reason for such a statement is the following. In the limit $L = \infty$ the evolving structures obey certain self-similarity throughout the evolution [19, 20]. This means that there the value of $\lambda$ should be independent of the choice of $t_w$. For finite $L$, as being observed, situation

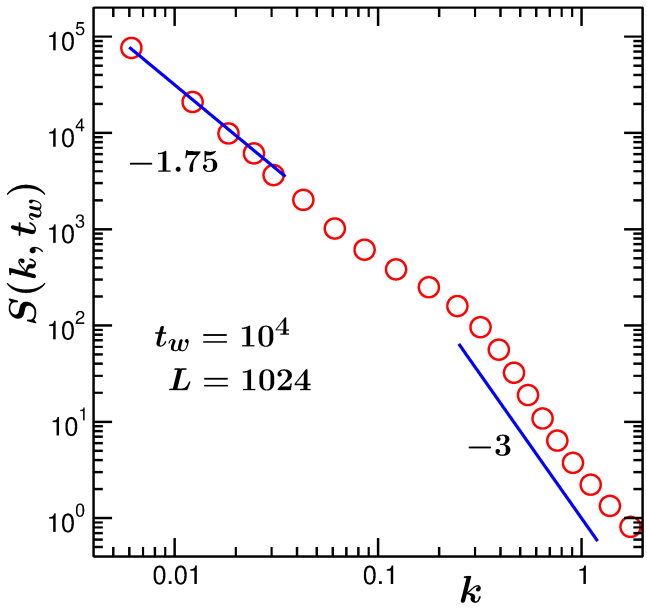


Fig. 2.8 Plot of equal-time structure factor, $S(k, t_w)$, as a function of wave number $k$, on a log-log scale for $L = 1024$ and $t_w = 10^4$. The solid line in the small $k$ limit is a power-law with exponent $\beta = -1.75$ and the one in the large $k$ regime corresponds to the Porod law [2]. This figure is from reference [54].

is different. However, the extrapolation exercise for different $t_w$ values is expected to provide us the thermodynamic limit $\lambda$. If the value of $\lambda$, estimated from this method, is different from that for $T_s = \infty$, it should give indirect evidence that there exist different structural scalings in the conserved case for $T_s = \infty$ and $T_s = T_c$, which is being already reported in the nonconserved case in $d = 2$ [19, 20].

Finally, to obtain the thermodynamic limit value, in Fig. 2.7 we have plotted $\lambda_L$, as a function of $1/L$, for a few values of $t_w$. The dashed lines there are fits to the form

$$\lambda_L = \lambda + AL^{-b}, \tag{2.12}$$

where $A$ and $b$ are constants. These multiple plots provide a good sense of convergence. From this exercise we quote

$$\lambda = \lambda_{L=\infty} = 0.13 \pm 0.02. \tag{2.13}$$

This number we compare with [14] $\lambda$ when $T_s = \infty$ in $d = 2$, viz.,

$$\lambda \simeq 3.6. \tag{2.14}$$

There exists huge difference between the quoted values in Eqs. (2.13) and (2.14). Next our objective is to check whether these numbers satisfy the YRD bound or not. For that purpose, in Fig. 2.8 we have plotted $S(k, t_w)$ as a function of $k$, on a log-log scale, for large enough values of $L$ and $t_w$, since scaling (overlap of data from different $t_w$) is observed starting from large $t_w$. In this case $\beta$ assumes a negative value, viz., $\beta \simeq -1.75$. Thus, the corresponding lower bound is below the above quoted value, i.e., $\lambda \simeq 0.13 \pm 0.02$. It is worth mentioning here that the value of $\beta$ for a thermodynamically large critical system is same as the number quoted above. For $L = \infty$, at criticality $\beta = -7/4$ in $d = 2$. This can be appreciated from the fact that the exponent for the power-law decay of $C(r)$ at criticality is $p = d - 2 + \eta$ or $2\beta/\nu$, where $\eta$, $\beta$ and $\nu$ are various critical exponents [3] ($\beta = 1/8$, $\nu = 1$, $\eta = 1/4$). Our system size is large enough to almost realize this value.

## 2.4 Conclusion

In this chapter we have studied the aging phenomena in 2D nearest neighbor Ising model via the Monte carlo simulations for quenches from $T_s = T_c$. Our focus was on kinetics of phase separation in solid binary mixtures. For this we have used the Kawasaki exchange kinetics [40]. We have probed aging via the order-parameter autocorrelation function [7] $C_{\rm ag}(t, t_w)$ and estimated the aging exponent $\lambda$ which corresponds to the power-law decay of the same. For $T_s = T_c$ the initial configurations have long-range correlations [27]. This provides a different universality class than the case of $T_s = \infty$ [19, 20].

For quenches from the critical point, despite having multiple sources of finite-size effects, we have appropriately analyzed the out-of-equilibrium data by devising an extrapolation method. We believe that this method provides us quite accurate results, valid for thermodynamically large systems.

It appears that for phase separating binary mixtures, the value of $\lambda$ for $T_s = T_c$ is significantly smaller than that for the universality class corresponding [8, 13, 14] to $T_s = \infty$. Nevertheless the obtained value for $T_s = T_c$ satisfies the lower bounds predicted by Yeung, Rao and Desai [9]. To the best of our knowledge, these are the first results for solid mixtures, as far as quenches from $T_c$ is concerned.

Other important exponent that can be calculated for the binary mixture with both $T_s = \infty$ and $T_s = T_c$ is the one related to the decay of persistence probability [34]. For this exponent, however, due to certain technical reasons [53] quenches to very low temperature becomes necessary. In that case, for conserved dynamics, there exists se-

vere problem with metastability. This makes the problem rather challenging, which, nevertheless, we intend to pursue in future.

## Copyright and Permission

The results of this chapter have been published in:
Subir K. Das, **Koyel Das**, Nalina Vadakkayil, Saikat Chakraborty, and Subhajit Paul, "Initial correlation dependence of aging in phase separating solid binary mixtures and ordering ferromagnets", J. Phys.: Condens. Matter **32**, 184005 (2020). DOI https://doi.org/10.1088/1361-648X/ab6d10.


There possibly exists minor text overlap with the thesis "N. Vadakkayil, *Structure and Dynamics Away from Equilibrium: Scaling results from a few condensed matter systems*, Ph. D. thesis, Jawaharlal Nehru Centre for Advanced Scientific Research, India, (2021)" in which results for the nonconserved dynamics are incorporated from the same source mentioned above.

# References


[1] K. Binder, in *Phase Transformation of Materials*, edited by R.W. Cahn, P. Haasen and E.J. Kramer (Wiley VCH, Weinheim, 1991), vol. 5. p. 405.

[2] A.J. Bray, Adv. Phys. **51**, 481 (2002).

[3] A. Onuki, *Phase Transition Dynamics* (Cambridge University Press, Cambridge, UK, 2002).

[4] R.A.L. Jones, *Soft Condensed Matter* (Oxford University Press, Oxford, UK, 2002).

[5] J.D. Gunton, R. Toral, and A. Chakrabarti, Physica Scripta. **T33**, 12 (1990).

[6] M. Zennetti, in *Kinetics of Phase Transitions*, edited by S. Puri and V. Wardhawan (CRC Press, Boca Raton, 2009).

[7] D.S. Fisher and D.A. Huse, Phys. Rev. B **38**, 373 (1988).

[8] F. Liu and G.F. Mazenko, Phys. Rev. B **44**, 9185 (1991).

[9] C. Yeung, M. Rao and R.C. Desai, Phys. Rev. E **53**, 3073 (1996).

[10] M. Henkel, A. Picone and M. Pleimling, Europhys. Lett. **68**, 191 (2004).

[11] F. Corberi, E. Lippiello and M. Zannetti, Phys. Rev. E **74**, 041106 (2006).

[12] E. Lorenz and W. Janke, Europhys. Lett. **77**, 10003 (2007).

[13] J. Midya, S. Majumder and S.K. Das, J. Phys. Condens. Matter **26**, 452202 (2014).

[14] J. Midya, S. Majumder and S.K. Das, Phys. Rev. E **92**, 022124 (2015).

[15] N. Vadakkayil, S. Chakraborty, and S.K. Das, J. Chem. Phys. **150**, 054702 (2019).

[16] S. Paul and S.K. Das, Phys. Rev. E **96**, 012105 (2017).

[17] S. Roy, A. Bera, S. Majumder and S.K. Das, Soft Matter **15**, 4743 (2019).

[18] F. Corberi and R. Villavicencio-Sanchez, Phys. Rev. E **93**, 052105 (2016).

[19] K. Humayun and A.J. Bray, J. Phys. A: Math. Gen. **24**, 1915 (1991).

[20] A.J. Bray, K. Humayun and T.J. Newman, Phys. Rev. B **43**, 3699 (1991).

[21] S.B. Dutta, J. Phys. A: Math. Theor. **41**, 395002 (2008).

[22] S. Puri and D. Kumar, Phys. Rev. Lett. **93**, 025701 (2004).

[23] S. Majumder and S.K. Das, Phys. Rev. E **84**, 021110 (2011).

[24] S. Chakraborty and S.K. Das, Eur. Phys. J. B **88**, 160 (2015).

[25] S. Chakraborty and S.K. Das, Phys. Rev. E **93**, 032139 (2016).

[26] T. Blanchard, L.F. Cugliandolo and M. Picco, J. Stat. Mech.: Theor. Expt. P12021 (2014).

[27] M.E. Fisher, Rep. Prog. Phys. **30**, 615 (1967).

[28] J.G. Amar, F.E. Sullivan and R.D. Mountain, Phys. Rev. B **37**, 196 (1988).

[29] S. Majumder and S.K. Das, Phys. Rev. E **81**, 050102 (2010).

[30] S.M. Allen and J.W. Cahn, Acta Metall. **27**, 1085 (1979).

[31] I.M. Lifshitz and V.V. Slyozov, J. Phys. Chem. Solids **19**, 35(1961).

[32] D.A. Huse, Phys. Rev. B **34**, 7845 (1986).

[33] J.F. Marko and G.T. Barkema, Phys. Rev. E **52**, 2522 (1995).

[34] A.J. Bray, S.N. Majumdar and G. Schehr, Adv. Phys. **62**, 225 (2013).

[35] S. Majumder and S.K. Das, Phys. Rev. Lett. **111**, 055503 (2013).

[36] S. Ahmad, F. Corberi, S.K. Das, E. Lippiello, S. Puri, and M. Zannetti, Phys. Rev. E **86**, 061129 (2012).

[37] C. Yeung and D. Jasnow, Phys. Rev. B **42**, 10523 (1990).

[38] M.E. Fisher and M.N. Barber, Phys. Rev. Lett. **28**, 1516 (1972).

[39] C. Yeung, Phys. Rev. Lett. **61**, 1135 (1988).

[40] K. Kawasaki, in *Phase Transition and Critical Phenomena*, edited by C. Domb and M.S. Green (Academic, New York, 1972), Vol. 2, p. 443.

[41] K. Binder and D.W. Heermann, *Monte Carlo Simulations in Statistical Physics* (Springer, Switzerland, 2019).

[42] D.P. Landau and K. Binder, *A Guide to Mote Carlo Simulations in Statistical Physics* (Cambridge University Press, Cambridge, 2009).

[43] D. Frenkel and B. Smit, *Understanding Molecular Simulations: From Algorithms to Applications* (Academic Press, San Diego, 2002).

[44] E. Luijiten, M.E. Fisher and A.Z. Panagiotopoulos, Phys. Rev. Lett. **88**, 185701 (2002).

[45] P.C. Hohenberg and B.I. Halperin, Rev. Mod. Phys. **49**, 435 (1977).

[46] S.K. Das, K. Das, N. Vadakkayil, S. Chakraborty and S. Paul, J. Phys. Condens. Matter **32**, 184005 (2020).

[47] N. Vadakkayil, *Structure and Dynamics Away from Equilibrium: Scaling results from a few condensed matter systems*, Ph. D. thesis, Jawaharlal Nehru Centre for Advanced Scientific Research, India, (2021).

[48] U. Wolff, Phys. Rev. Lett. **62**, 361 (1989).

[49] D.W. Heermann, L. Yixue and K. Binder, Physica A **230**, 132 (1996).

[50] R.J. Glauber, J. Math. Phys. **4**, 294 (1963).

[51] S. Roy and S.K. Das, Europhys. Lett. **94**, 36001 (2011).

[52] J. Midya and S.K. Das, J. Chem. Phys. **146**, 044503 (2017).

[53] B. Derrida, Phys. Rev. E **55**, 3705 (1997).

[54] K. Das, N. Vadakkayil, and S.K. Das, Phys. Rev. E **101**, 062112 (2020).

# Chapter 3

# Initial Correlation Dependence of Aging in Phase Separating 3D Solid Binary Mixtures

## 3.1 Introduction

Inspired by the interesting observation in the previous chapter, our objective here is to estimate the aging exponent $\lambda$ for initial configurations with $\xi = \infty$ in the case of the three-dimensional ($d = 3$) phase separating solid binary ($A + B$) mixtures [1, 2]. The basic scaling picture is already described. Below we stress upon the difficulty associated with the study.

Here also we consider the nearest neighbor ferromagnetic Ising model. Even for such simple model and technically easier case of $\xi = 0$, estimation of $\lambda$ remained difficult [3, 4]. In $d = 3$, it is, of course, significantly more challenging. For quenches from the critical point, additional difficulty is expected in computer simulations. In computational studies there will exist two sources of finite-size effects [5]. First one is due to non-accessibility of $\xi = \infty$ in the initial correlation [5] and the second is related to the fact [6, 7] that the domain length $\ell < \infty$, always. Nevertheless, via appropriate method of analysis [8], we estimate the value of $\lambda$ quite accurately. It transpires, like in $d = 2$, that the obtained value is drastically different from that [9] for $\xi = 0$. This is despite the fact that the growth exponent $\alpha$ does not depend upon the choice of initial $\xi$.

## 3.2 Model and Methods

As mentioned, for this study we have used the ferromagnetic Ising model [10, 11]. Monte Carlo (MC) simulations [10–12] are performed by employing Kawasaki exchange kinetics [13] on a simple cubic lattice of linear dimension $L$, with periodic boundary condition in all directions. In our simulations, one Monte Carlo step (MCS), the chosen unit of time, is equivalent to $L^3$ trial moves.

For this system the value [11] of critical temperature is $T_c \simeq 4.51 J/k_B$, $k_B$ being the Boltzmann constant. Given that in computer simulations the thermodynamic critical point is not accessible, as stated in the previous chapter, we have quenched the systems from $T_s = T_c^L$, the finite-size critical temperature for a system of linear dimension $L$ [5, 8]. The final temperature was set to $T_f = 0.6T_c$ and composition was fixed at 50% up and 50% down spins.

For faster generation of the equilibrium configurations at $T_c^L$, Wolff algorithm [14] has been used, similar to the previous chapter.

Quantitative results are presented after averaging over a minimum of 100 independent initial configurations. To facilitate extrapolation of the results for aging in the thermodynamically large size limit, we have performed simulations with different system sizes. In the present case the value of $L$ varies between 24 and 128. We have presented the structural data for $L = 512$. Details on the statistics and the system sizes for the calculations of $T_c^L$ can be found in the next section.

## 3.3 Results

As already mentioned, in computer simulations finite-size effects lead to severe difficulties in studies of phenomena associated with phase transitions. In kinetics of phase transitions, $\ell$ never reaches $\infty$, due to the restriction in the system size [6, 7]. This is analogous to the fact that in critical phenomena [5] one always has $\xi < \infty$. There, of course, exist scaling methods to overcome the problems in both equilibrium and nonequilibrium contexts [5–9, 11, 15, 16]. For studies of coarsening phenomena starting from the critical point [8, 17–19], difficulties due to both types of effects are encountered. Nevertheless, via construction of appropriate extrapolation method [8] we will arrive at quite accurate conclusions. In critical phenomena the true value of $T_c$ cannot be realized for $L < \infty$. In such a situation, for reaching conclusions in the $L = \infty$ limit, one defines $T_c^L$, pseudo critical temperature for a finite system, and relies on appropriate scaling

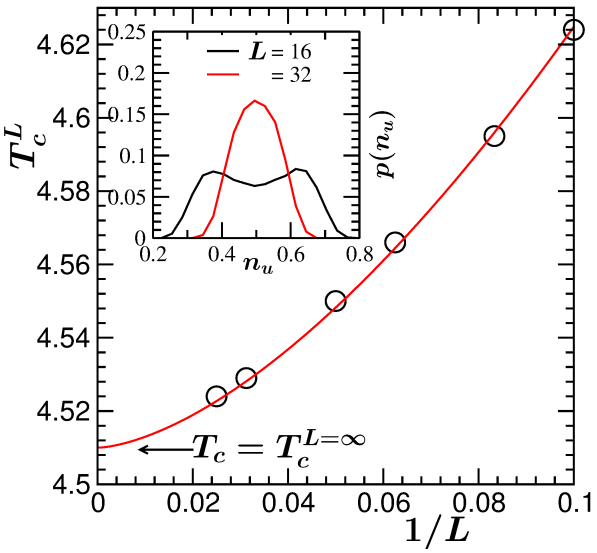


Fig. 3.1 Finite-size critical temperature, $T_c^L$, for the 3D Ising model, is plotted as a function of $1/L$. The solid line is a fit to the expected critical behavior [see Eq. (3.1)], by fixing $\nu$ and $T_c$ to 0.63 and 4.51, respectively. The simulation results were obtained via Glauber as well as Wolff algorithms. Inset: Order-parameter distributions, $p$, for two system sizes at the same temperature ($T = 4.54$), are plotted versus the concentration ($n_u$) of up spins. These results are taken from Refs. [26, 27].

relations [20–23]. $T_c^L$ is expected to exhibit the behavior [20–24]

$$T_c^L - T_c \sim L^{-1/\nu}, \tag{3.1}$$

where $\nu$ is the critical exponent corresponding to the divergence [24, 25] of $\xi$ at $T_c$. In Fig. 3.1 the results for $T_c^L$ are shown, as a function of $1/L$ [26, 27]. The solid line there is a fit to the scaling form in Eq. (3.1) by fixing [11, 24, 25] $\nu$ and $T_c$ to the 3D Ising values ($\simeq 0.63$ and $\simeq 4.51$, respectively). The quality of fit confirms the validity of Eq. (3.1) as well as the accuracy of the estimations. The amplitude ($\simeq 4.4$) is obtained from the fit to extract $T_c^L$ for $L$ larger than the presented ones.

The results in Fig. 3.1 were obtained by using the Glauber as well as the Wolff algorithms [11, 14, 28], by using temperature dependent probability distributions for the corresponding order parameter. These distribution functions are double-peaked in the ordered region [8, 11]. On the other hand, above criticality one observes single peak character. The temperature at which the crossover from double to single peak shape occurs is taken as the $T_c^L$ for a particular choice of $L$. In the inset of Fig. 3.1 the distributions, $p(n_u)$, from two different system sizes at same temperature have been shown. It

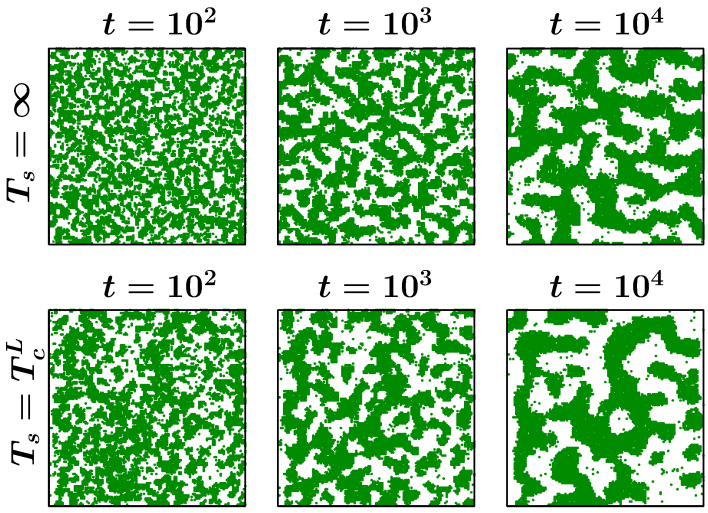


Fig. 3.2 Two-dimensional sections of the evolution snapshots, recorded during the Monte Carlo simulations of the conserved Ising model in $d = 3$, are presented for quenches to $T_f = 0.6T_c$. At the top of each of the frames we have mentioned the corresponding time. The upper panels correspond to the evolution for quench from $T_s = \infty$ and the lower ones are for quenches from finite-size critical temperature $T_c^L$ with $L = 128$. For both the cases the quench temperature is $T_f = 0.6T_c$. In all the frames the down spins (or $B$ particles) are left unmarked.

is seen that for the larger value of $L$ there is only one peak while the distribution for the smaller system has two peaks. This is expected in the present set up and is consistent with Eq. (3.1). The probability distribution close to $T_c^L$ were shown, for each $L$, after averaging over a minimum of 500 independent runs.

To facilitate appropriate analysis of the autocorrelation data we will perform quenches from $T_c^L$ for different values of $L$. For each $L$, value of $\lambda$, to be referred to as $\lambda_L$, will be estimated. Finally, the thermodynamic limit number will be obtained from the convergence of $\lambda_L$ in the $L = \infty$ limit. In addition to the $L$-dependence, there will be other effects as well. These we will discuss in appropriate places. In Fig. 3.2 we present two-dimensional cross-sections of the snapshots, taken during the evolutions, for quenches from $T_s = \infty$ (upper panel) as well from $T_s = T_c^L$ (lower panel). For the sake of completeness we have compared the snapshots for the critical starting temperature with the ones for quenches with $\xi = 0$, i.e., from $T_s = \infty$. The structure for quenches from the critical point appears different from that for $T_s = \infty$. Note that all the presented pictures are from simulations with $L = 128$ and the results for the critical point correspond to quenches from $T_c^L$, as mentioned above. The behavior of the equal time structure

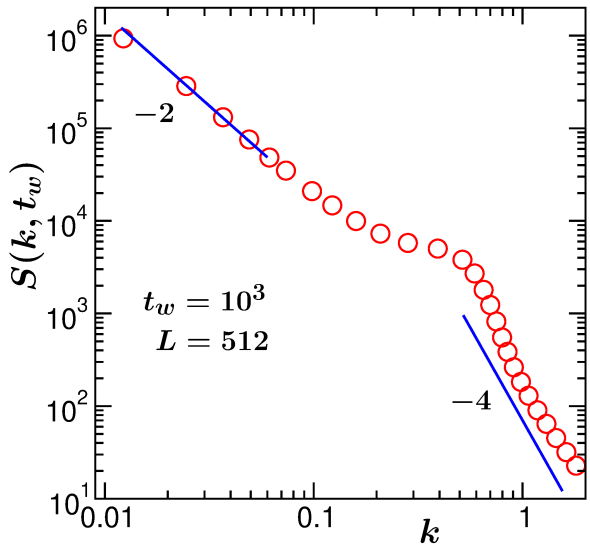


Fig. 3.3 Log-log plot of structure factor versus wave number. The solid lines are power-laws with exponent values noted in the figure. The values of $t_w$ and $L$ are also mentioned.

factor, for a thermodynamically large system, at criticality is expected to be [11, 24, 25]

$$S(k, 0) \sim k^{-2}, \tag{3.2}$$

given that the critical exponent $\eta$ ($\simeq 0.036$ for $d = 3$), the Fisher exponent, that characterizes the power-law factor of the critical correlation as $r^{-(d-2+\eta)}$, has a small value. Typically in most of the coarsening systems scaling in the decay of autocorrelation function [cf. Eq. ( 2.2 )] starts from a reasonably large value of $t_w$. By then the structure is expected to have changed from that at the beginning. Thus, the exponent '$-2$' in Eq. (3.2) should be verified before being taken as the value of $\beta$ in the YRD bound, that is discussed in the previous chapter, for understanding of results following quenches from $T_c$. Furthermore, for $T_s = T_c$, one may even ask about the validity of a stable $\beta$. This is related to the question whether there exists a scaling regime or the structure is continuously changing. Keeping this in mind, in Fig. 3.3 we present plot of $S(k, t_w)$ versus $k$ for large enough value of $L$ and $t_w$. It appears that $\beta$ is stable at '$-2$', noting that $t_w$ is rather large, even though character of structure changes at large $k$, e.g., an appearance of the Porod law [1] ($S(k) \sim k^{-4}$) is clearly visible that corresponds to the existence of domain boundaries. This value of $\beta$, i.e., $-2$, will be used later for verifying the YRD bound.

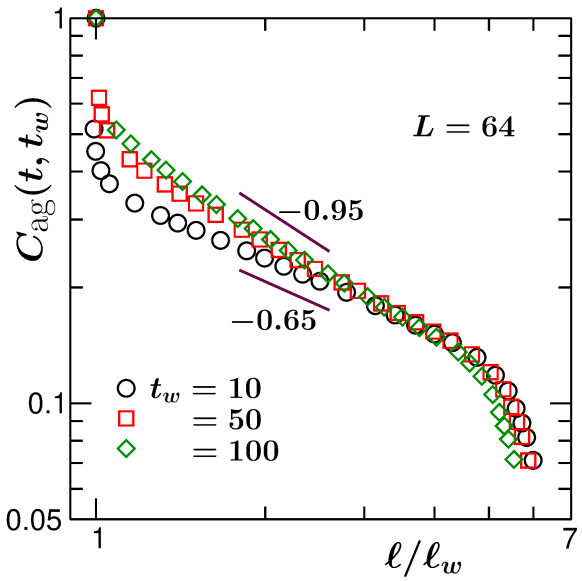


Fig. 3.4 Log-log plots of the order-parameter autocorrelation function, $C_{\rm ag}(t, t_w)$, versus $\ell/\ell_w$. Data for a few different values of $t_w$ are included. These results are from simulations with $L = 64$. The solid lines represent power-laws, the exponents being mentioned in appropriate places.

Note here that in Fig. 3.3 we have presented representative results with appropriate understanding of finite-size effects and onset of scaling in the structure as well as in aging. Even though the results in Fig. 3.3 are from $L = 512$, simulating this size for long enough time, a necessity in studies of aging phenomena, in $d = 3$ is very time consuming. So, for aging the presented data are from smaller values of $L$ and the conclusions in the thermodynamic limit is drawn via appropriate extrapolations.

First results for $C_{\rm ag}(t, t_w)$ are presented in Fig. 3.4, versus $\ell/\ell_w$, on a log-log scale by fixing the system size, for a few different values of $t_w$. The observations are the following.

There exist clear non-scaling behaviors of the data sets. In the small $\ell/\ell_w$ region the collapse of the data set for $t_w = 10$ with those for the larger $t_w$ values is rather poor. This, we believe, is due to the fact that in the scaling regime the structure is different [29] from the initial configuration [8]. (Also note that the scaling structure for $T_s = T_c$ is different from that for $T_s = \infty$.) During this switch-over to the scaling behavior the extraction of $\ell$ is also ambiguous, due to continuous change in the structure that, thus, lacks the scaling of correlation function. Given the complexity of finite-size and other effects, further analysis is required, to come to a conclusion about the value of the aging exponent.

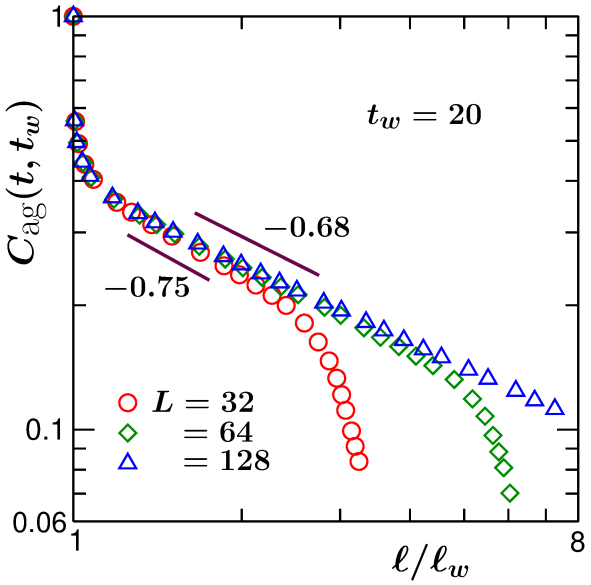


Fig. 3.5 Log-log plots of $C_{\rm ag}(t, t_w)$ versus $\ell/\ell_w$, for $t_w = 20$ and different values of the linear dimension of the simulation box. The solid lines represent power-laws.

Here one gets an impression that the exponent has a tendency to increase with the increase of $t_w$. The phenomenon of convergence, however, is more complex and requires systematic study involving both $t_w$ and $L$. This we will perform in the rest of the chapter.

Next we examine the effects of system size on the "scaling" regime. We remind the reader that in addition to the standard growth related one, there exists another type of finite-size effect related to $\xi < \infty$. Due to this, with changing system size the exponent will differ in "the scaling regime" as well. Related results are presented in Fig. 3.5.

In Fig. 3.5 we show $C_{\rm ag}(t, t_w)$, for different values of $L$, versus $\ell/\ell_w$, on a log-log scale, by fixing $t_w$ to 20. In addition to the delayed appearance of late time finite-size effects, with the increase of system size the decay exponent shows the tendency of shifting towards smaller value [8]. To pick the stable power-law regime appropriately, by discarding the finite-size affected and early transient regimes, in Fig. 3.6 we plot the instantaneous exponent [7, 9, 15, 30, 31]

$$\lambda_i = -\frac{d \ln C_{\rm ag}(t, t_w)}{d \ln x}; \; x = \frac{\ell}{\ell_w}, \tag{3.3}$$

as a function of $\ell_w/\ell$, for two values of $L$ with $t_w = 20$. From the flat parts we extract $L$-dependent exponent $\lambda_L$. We have performed this exercise for multiple values of $t_w$.

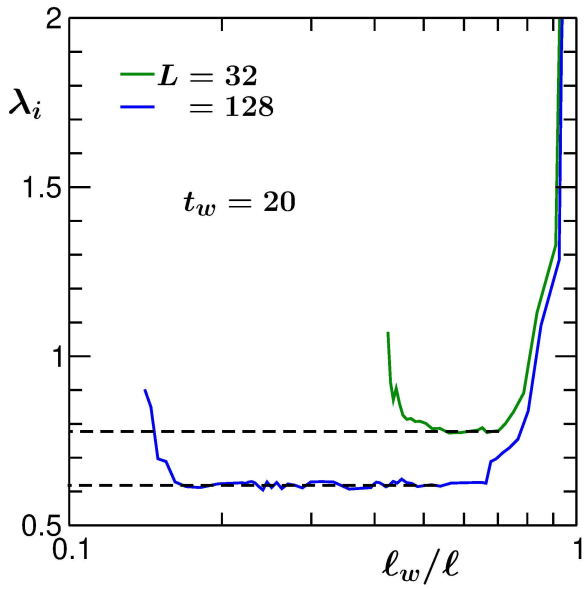


Fig. 3.6 Plots of the instantaneous exponents, $\lambda_i$, versus $\ell_w/\ell$, for $t_w = 20$ and two values of $L$. The dashed horizontal lines represent the estimated values of $\lambda_L$, the $L$-dependent aging exponent.

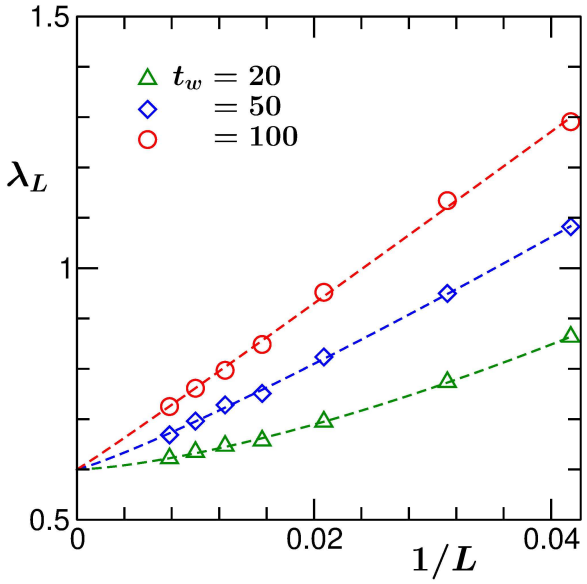


Fig. 3.7 Plots of $\lambda_L$ versus $1/L$, for the conserved Ising model. Data from a few different values of $t_w$ are shown. The dashed lines are power-law fits to the simulation data sets.

The above mentioned flat behavior in the intermediate regime confirms that there exists power-law relationship between $C_{\rm ag}(t, t_w)$ and $\ell/\ell_w$.

Data for $\lambda_L$, when plotted versus $1/L$, for multiple values of $t_w$, should provide a good sense of convergence [8]. Corresponding number should be the value of $\lambda$ for a thermodynamically large system. This exercise has been shown in Fig. 3.7. The dashed lines there are fits to the form

$$\lambda_L = \lambda + AL^{-b}, \tag{3.4}$$

where $A$ and $b$ are constants. The estimated values of $\lambda$, obtained after averaging over the convergences of the fittings, by considering different numbers of data points for each $t_w$, along with those for uncorrelated initial configurations [9, 15, 32], are quoted in table 3.1.

All numbers in this table are from simulation studies. For the comparison of these numbers with the YRD bound, in table 3.2 we have quoted the values of $\beta$ for 50 : 50 composition of up and down spins (see caption for more details) [8, 29]. For the uncorrelated case it is clear that the structures are different. Finally in the table 3.3

Table 3.1 List of values of $\lambda$ for the nearest neighbor conserved Ising model. Here "Correlated" and "Uncorrelated" imply results for quenches from $T_s = T_c$ and $T_s = \infty$, respectively. For the values of the lower bounds [3] please see Table 3.2.

| $d = 2$ | | $d = 3$ | |
|---|---|---|---|
| Correlated | Uncorrelated | Correlated | Uncorrelated |
| 0.13±0.02 | 3.6±0.2 | 0.64±0.05 | 7.5±0.4 |

we have shown a comparison of $\lambda$ values for the conserved case with those for the nonconserved dynamics. Interestingly, even though the results for the $T_s = \infty$ case differ significantly, the numbers for $T_s = T_c$ are in striking agreement.

Table 3.2 List of $\beta$ values for the conserved nearest neighbor Ising model. Validity of YRD bound can be checked by putting these numbers in Eq. (2.4) and comparing the outcome with the results quoted in table 3.1. While preparing this table, $\eta$ in $d = 3$ has been set to zero. For the sake of convenience, we have put the values of the bounds [3] inside the parentheses.

| $d = 2$ | | $d = 3$ | |
|---|---|---|---|
| Correlated | Uncorrelated | Correlated | Uncorrelated |
| -1.75 (0.125) | 4 (3) | -2 (0.5) | 4 (3.5) |

Table 3.3 List of values of $\lambda$ from $d = 2$ and 3, by comparing the results for conserved Ising model with those from the nonconserved case.

| Model | $d = 2$ | | $d = 3$ | |
|---|---|---|---|---|
| | Correlated | Uncorrelated | Correlated | Uncorrelated |
| KIM | 0.13±0.02 | 3.6±0.2 | 0.64±0.05 | 7.5±0.4 |
| GIM | 0.14±0.02 | 1.32±0.04 | 0.57±0.07 | 1.69±0.04 |

## 3.4 Conclusion

Universality in kinetics of phase transition [1] is less robust compared to that in equilibrium critical phenomena [11, 24, 25]. In kinetics, the classes are decided [1] by transport mechanism, space dimension, order-parameter symmetry and its conservation, etc. In each of these cases there can be further division into universality classes [8, 17–19, 33] based on the range of spatial correlation in the initial configurations. In this chapter we have examined the influence of long range correlation on the decay of order-parameter autocorrelation function, a key quantity for the study of aging phenomena [34, 35] in out-of-equilibrium systems, by quenching the three-dimensional conserved nearest neighbor Ising model [24, 25] from the critical point to the ordered region.

The conserved dynamics here is related to the kinetics of phase separation in solid binary mixtures. Despite difficulty due to multiple sources of finite-size effects, we have estimated the exponent for the power-law fall of the autocorrelation function rather accurately. We observe that the decay is significantly slower than that for the quench from perfectly random initial configurations [9, 15, 32, 34, 35].

In the literature of aging phenomena there exist lower bounds [3, 35] for the values of $\lambda$. Our obtained exponent value is consistent with one of these bounds. This we have checked via the analysis of structure, a property that is embedded in the construction of the bound. For quenches with $\xi = 0$ the values of $\lambda$ differ significantly between the conserved and nonconserved dynamics. This is an interesting fact.

This work, combined with a few others [8, 9, 15, 17–19, 33], provides a near-complete information on the universality in coarsening dynamics in Ising model, involving "realistic" space dimensions, conservation property of the order parameter and spatial correlations in the initial configurations. Analogous studies in other systems should be carried out, by employing the methods used here, to obtain more complete understanding, e.g. of the influences of hydrodynamics on relaxation in out-of-equilibrium systems with long range initial correlations.

## Copyright and Permission

The results of this chapter have been published in:
**Koyel Das**, Nalina Vadakkayil, and Subir K. Das, Phys. Rev. E **101**, 062112 (2020). DOI https://doi.org/10.1103/PhysRevE.101.062112.


There exists possibility of minor text overlap with the thesis "N. Vadakkayil, *Structure and Dynamics Away from Equilibrium: Scaling results from a few condensed matter systems*, Ph. D. thesis, Jawaharlal Nehru Centre for Advanced Scientific Research, India, (2021)" in which results for the nonconserved dynamics are incorporated from the same source mentioned above.

# References


[1] A.J. Bray, Adv. Phys. **51**, 481 (2002).

[2] K. Binder, in *Phase Transformation of Materials*, edited by R.W. Cahn, P. Haasen and E.J. Kramer (Wiley VCH, Weinheim, 1991), vol. 5. p. 405.

[3] C. Yeung, M. Rao and R.C. Desai, Phys. Rev. E **53**, 3073 (1996).

[4] J.F. Marko and G.T. Barkema, Phys. Rev. E **52**, 2522 (1995).

[5] M.E. Fisher and M.N. Barber, Phys. Rev. Lett. **28**, 1516 (1972).

[6] D.W. Heermann, L. Yixue and K. Binder, Physica A **230**, 132 (1996).

[7] S. Majumder and S.K. Das, Phys. Rev. E **84**, 021110 (2011).

[8] S.K. Das, K. Das, N. Vadakkayil, S. Chakraborty and S. Paul, J. Phys. Condens. Matter **32**, 184005 (2020).

[9] J. Midya, S. Majumder and S.K. Das, Phys. Rev. E **92**, 022124 (2015).

[10] K. Binder and D.W. Heermann, *Monte Carlo Simulations in Statistical Physics* (Springer, Switzerland, 2019).

[11] D.P. Landau and K. Binder, *A Guide to Mote Carlo Simulations in Statistical Physics* (Cambridge University Press, Cambridge, 2009).

[12] D. Frenkel and B. Smit, *Understanding Molecular Simulations: From Algorithms to Applications* (Academic Press, San Diego, 2002).

[13] K. Kawasaki, in *Phase Transition and Critical Phenomena*, edited by C. Domb and M.S. Green (Academic, New York, 1972), Vol. 2, p. 443.

[14] U. Wolff, Phys. Rev. Lett. **62**, 361 (1989).

[15] J. Midya, S. Majumder and S.K. Das, J. Phys. Condens. Matter **26**, 452202 (2014).

[16] S.K. Das, S. Roy, S. Majumder and S. Ahmad, Europhy. Lett. **97**, 66006 (2012).

[17] T. Blanchard, L.F. Cugliandolo and M. Picco, J. Stat. Mech.: Theor. Expt. P12021 (2014).

[18] S. Chakraborty and S.K. Das, Eur. Phys. J. B **88**, 160 (2015).

[19] S. Chakraborty and S.K. Das, Phys. Rev. E **93**, 032139 (2016).

[20] E. Luijiten, M.E. Fisher and A.Z. Panagiotopoulos, Phys. Rev. Lett. **88**, 185701 (2002).

[21] S.K. Das, Y.C. Kim and M.E. Fisher, Phys. Rev. Lett. **107**, 215701 (2011).

[22] S. Roy and S.K. Das, Europhys. Lett. **94**, 36001 (2011).

[23] J. Midya and S.K. Das, J. Chem. Phys. **146**, 044503 (2017).

[24] M. Plischke and B. Bergersen, *Equilibrium Statistical Physics* (World Scientific, London, 2005).

[25] M.E. Fisher, Rep. Prog. Phys. **30**, 615 (1967).

[26] K. Das, N. Vadakkayil, and S.K. Das, Phys. Rev. E **101**, 062112 (2020).

[27] N. Vadakkayil, *Structure and Dynamics Away from Equilibrium: Scaling results from a few condensed matter systems*, Ph. D. thesis, Jawaharlal Nehru Centre for Advanced Scientific Research, India, (2021).

[28] R.J. Glauber, J. Math. Phys. **4**, 294 (1963).

[29] C. Yeung, Phys. Rev. Lett. **61**, 1135 (1988).

[30] D.A. Huse, Phys. Rev. B **34**, 7845 (1986).

[31] J.G. Amar, F.E. Sullivan and R.D. Mountain, Phys. Rev. B **37**, 196 (1988).

[32] F. Liu and G.F. Mazenko, Phys. Rev. B **44**, 9185 (1991).

[33] A.J. Bray, K. Humayun and T.J. Newman, Phys. Rev. B **43**, 3699 (1991).

[34] M. Zennetti, in *Kinetics of Phase Transitions*, edited by S. Puri and V. Wardhawan (CRC Press, Boca Raton, 2009).

[35] D.S. Fisher and D.A. Huse, Phys. Rev. B **38**, 373 (1988).

# Chapter 4

# Hydrodynamic Effects in Kinetics of Phase Separation in Binary Fluids: Critical versus off-critical compositions

## 4.1 Introduction

In this chapter we discuss results on kinetics of phase separation in a binary (A+B) fluid mixture. Here our focus is on growth of average domain size $\ell$. For self-similar growth, corresponding scaling picture is already discussed by defining structural quantities like the two-point equal time order-parameter correlation function. Note that a time dependent local order parameter can be defined as the concentration difference between the two species.

Typically $\ell$ grows in a power-law fashion as [1–5]

$$\ell \sim t^{\alpha}. \tag{4.1}$$

The growth exponent $\alpha$ depends upon several parameters [1, 5]. In non-hydrodynamic environment, one expects $\alpha = 1/3$. This is referred to as the Lifshitz-Slyozov (LS) growth law [6–14] and is a result of diffusive transport of particles, via chemical potential gradient. The LS picture applies to phase separating solid mixtures and remains valid for critical as well as off-critical compositions [6, 7], for the entire growth period. In fluids, however, hydrodynamics is important. There the mechanisms and exponents are

different for the above two situations that give rise, respectively, to bicontinuous and disconnected droplet morphologies [15–39]. This is true for vapor-liquid as well as liquid-liquid transitions, in the former case density playing the role of composition. Below we briefly describe these in the liquid-liquid context.

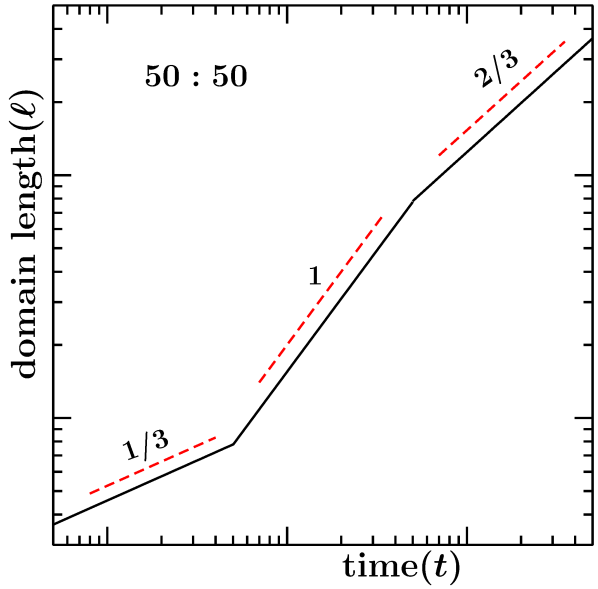


Fig. 4.1 Schematic diagram of the behavior $\ell$, as a function of $t$, for 50 : 50 mixture. Three different regimes of growth with exponents $\alpha = 1/3$, 1 and 2/3 have been shown here in hydrodynamic situation.

In the case of a composition close to the critical value, say, a 50 : 50 proportion of A and B particles for a symmetric model of mixture, growth occurs via transport of material through tube-like structure [4, 5, 17–19, 40]. Overall growth in this situation is not described by a single exponent. At very early time LS picture remains valid [4, 5]. Following this hydrodynamics becomes important, leading to a crossover of the exponent to $\alpha = 1$, in space dimension $d = 3$, which is referred to as the viscous hydrodynamic growth [4, 5, 17, 30, 33, 34, 40]. At an even later time a further crossover occurs to a smaller value, viz., $\alpha = 2/3$, known as the inertial hydrodynamic exponent [4, 5]. Please see Fig. 4.1 for a schematic depiction. For a composition close to any of the branches of the coexistence curve, on the other hand, the late time growth, in a hydrodynamic environment, may occur via coalescence of disconnected droplets that consist primarily of particles of the minority phase [15–17, 24–26, 28, 33, 34, 39]. This we discuss below.

For diffusive motion of the droplets, between collisions, expected for liquid mixtures, because of high density background phase, a theory for growth was proposed by Binder

and Stauffer (BS) [15–17]. In this case, solution of the dynamical equation [15]

$$\frac{\mathrm{d}n}{\mathrm{d}t} = -D\ell n^2, \tag{4.2}$$

for droplet density $n\,(\propto 1/\ell^d)$, provides $\alpha = 1/d$. In Eq. (4.2), $D$ is a diffusion coefficient, having dependence upon $\ell$. It is expected that $D\ell$ will remain a constant, during the growth period, in accordance with the generalized Stokes-Einstein-Sutherland [41–43] relation. In $d = 3$, the BS value is same as the LS exponent. The difference in the mechanisms is expected to be captured in the amplitudes of growth, this being larger for the BS case. The ratio of the amplitudes for the two mechanisms is supposed to follow the relation [28, 33]

$$\frac{A_{BS}}{A_{LS}} = K\phi^{1/3}, \tag{4.3}$$

where $K$ is a constant ($\simeq 6$) and $\phi$ is the volume fraction of the minority species in the mixture.

In this work, while presenting results for a wide range of compositions, we primarily address the issue of growth via diffusive coalescence in a phase separating binary fluid mixture. We have performed molecular dynamics [44, 45] (MD) simulations. In our canonical ensemble simulations the temperature is controlled via the Nosé-Hoover thermostat (NHT) [44, 46–48]. The latter is known to preserve hydrodynamics. The obtained results were analyzed via various advanced methods to arrive at conclusions on the growth and mechanism.

Even though the original theoretical picture is for binary fluids, confirmation of this, via simulations of atomistic models, exists only for vapor-liquid transition [33, 34, 49]. To the best of our knowledge, this is the first such study for a liquid-liquid transition.

## 4.2 Model and Methods

In our model system, two particles, located at $\vec{r}_i$ and $\vec{r}_j$, with $r = |\vec{r}_i - \vec{r}_j|$, interact via the potential [45]:

$$U(r) = V(r) - V(r_c) - (r - r_c)\left[\frac{dV(r)}{dr}\right]_{r=r_c}, \tag{4.4}$$

for $r < r_c$, the latter being a cut-off distance. In Eq. (4.4), $V(r)$ is the standard Lennard-Jones (LJ) potential [45]

$$V(r) = 4\epsilon_{\alpha\beta}\left[\left(\frac{\sigma_{\alpha\beta}}{r}\right)^{12} - \left(\frac{\sigma_{\alpha\beta}}{r}\right)^{6}\right]. \tag{4.5}$$

The cut and shift, implemented via the second term on the right hand side of Eq. (4.4), for the sake of computational convenience, leaves the force at $r = r_c$ discontinuous. This was corrected via the introduction of the last term [45] in the same equation. In Eq. (4.5), $\epsilon_{\alpha\beta}$ and $\sigma_{\alpha\beta}$, $\alpha, \beta \in$ [A,B], represent the interaction strengths and diameters, respectively, for various combinations of particles. In this work we have chosen [50, 51]

$$\sigma_{AA} = \sigma_{BB} = \sigma_{AB} = \sigma, \tag{4.6}$$

and

$$\epsilon_{AA} = \epsilon_{BB} = 2\epsilon_{AB} = \epsilon. \tag{4.7}$$

The factor 2 implies that the like particle interactions are twice as strong as the unlike particle interactions. Thus, one expects a phase separation between A and B species. We have set mass ($m$) of all the particles to be the same.

For this *symmetric* model, the phase diagram, in $d = 3$, is accurately known for (number) density of particles $\rho = 1$. It is, of course, expected [50–52] that the critical concentration, for any of the species, will be $x_\alpha^c = 1/2$, because of the symmetry. The critical temperature, $T_c$, was estimated to be $\simeq 1.421\epsilon/k_B$, where $k_B$ is the Boltzmann constant [50–52]. In the following we set $\sigma$, $\epsilon$, $m$ and $k_B$ to unity. In this work we study the kinetics by quenching homogeneous configurations, prepared at a high temperature, to the temperature $T = 1$. The compositions are chosen in such a way that the final state points fall inside the miscibility gap [50–52].

We have performed MD simulations [44] in periodic cubic boxes of linear dimension $L$, the latter being measured in units of $\sigma$. As already stated, the temperature was controlled via the application of a NHT [44, 46–48] that is known to preserve hydrodynamics well. For comparative purpose, towards the end, we have also presented results that were obtained via the application of a stochastic thermostat, viz., the Andersen thermostat (AT) [44, 53].

In our MD method we have used the Verlet velocity integration scheme [44, 45], with time discretization step $\Delta t = 0.001\tau$. Here $\tau$ $(= \sqrt{m\sigma^2/\epsilon})$ is our LJ unit of time, which is unity because of the above mentioned choices of $\epsilon$, $\sigma$ and $m$. All our quantitative

results are obtained after averaging over runs with a minimum of 50 independent initial configurations. Unless otherwise mentioned, all the simulations were performed with $L = 64$ and NHT. We have used used LAMMPS package [54, 55] for this purpose.

There exist reports by stating deficiencies of NHT as a hydrodynamics preserving thermostat [56, 57]. On the other hand, many works report results, by using NHT, that produce key expectations for hydrodynamic behavior in kinetics of phase separation. In this connection, we draw attention to Ref. [57]. In this work, in the equilibrium context, results on various transport properties in fluids were compared from the calculations in canonical (with NHT) and microcanonical ensembles. Note that in the latter ensemble hydrodynamics is perfectly satisfied. It was observed that other than bulk viscosity, results on other transport coefficients were in good agreement from the two ensembles. Given that we are dealing with a nearly incompressible fluid, bulk viscosity is less relevant. Thus, application of NHT is rather safe here.

We have calculated lengths from the decay of the correlation function as

$$C(r = \ell, t) = c, \tag{4.8}$$

by fixing $c$ to the first zero of the correlation function. It is worth mentioning here, for conserved order-parameter dynamics, the class to which the present problem belongs, $C$ exhibits damped oscillation around zero. This we will see in the next section. For the calculation of $C(r, t)$ we have mapped the continuum configurations to the ones on a simple cubic lattice [6]. The length was also obtained by direct identification of the droplets [58] and counting numbers of particles within those [49]. The latter, of course provides volume, from which average length can be trivially obtained following calculation of the average volume via the first moment of a distribution. Results from different methods are essentially proportional to each other, differing by constant factors.

For disconnected morphology, the droplet identification [58] is important for the purpose of confirmation of the mechanism as well, e.g., via the calculation of mean-squared-displacement (MSD) of the centres of mass (CM) of the droplets. Note that for $N_p$ particles belonging to a particular droplet the centre of mass is calculated as [41]

$$\vec{R}_{CM}(t) = \frac{1}{N_p} \sum_{i=1}^{N_p} \vec{r}_i(t). \tag{4.9}$$

The MSD is then obtained from the formula [41]

$$\text{MSD} = \langle (\vec{R}_{CM}(t') - \vec{R}_{CM}(0))^2 \rangle. \tag{4.10}$$

Here $t'$ is a time that is shifted with respect to the time at the beginning of an observation.

## 4.3 Results

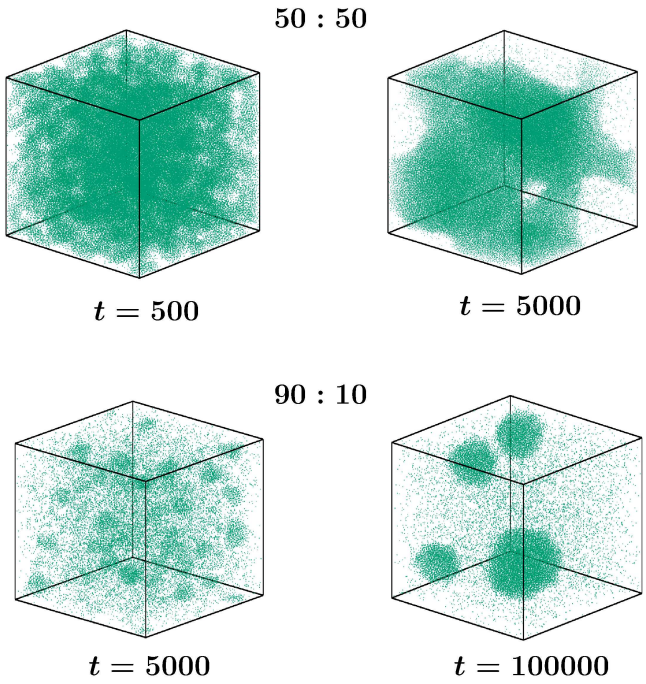


Fig. 4.2 Snapshots, that were recorded during the molecular dynamics simulations, following quenches of high temperature homogeneous configurations to $T = 1$, are shown for $50 : 50$ (upper frames) and $90 : 10$ (lower frames) compositions of A and B particles. Only the locations of the B particles are marked. For each of the compositions, frames from two different times are included.

In Fig. 4.2 we show snapshots taken during the evolutions of two typical homogeneously mixed configurations towards respective equilibriums, following quenches inside the coexistence curve. For $50 : 50$ composition, it is appreciable that the morphology consists of interconnected tube-like domains. For the asymmetric composition, disconnected droplet morphology is clearly identifiable. In the latter case the growth seems to be much slower. Our objective here is to provide a composition dependent quanti-

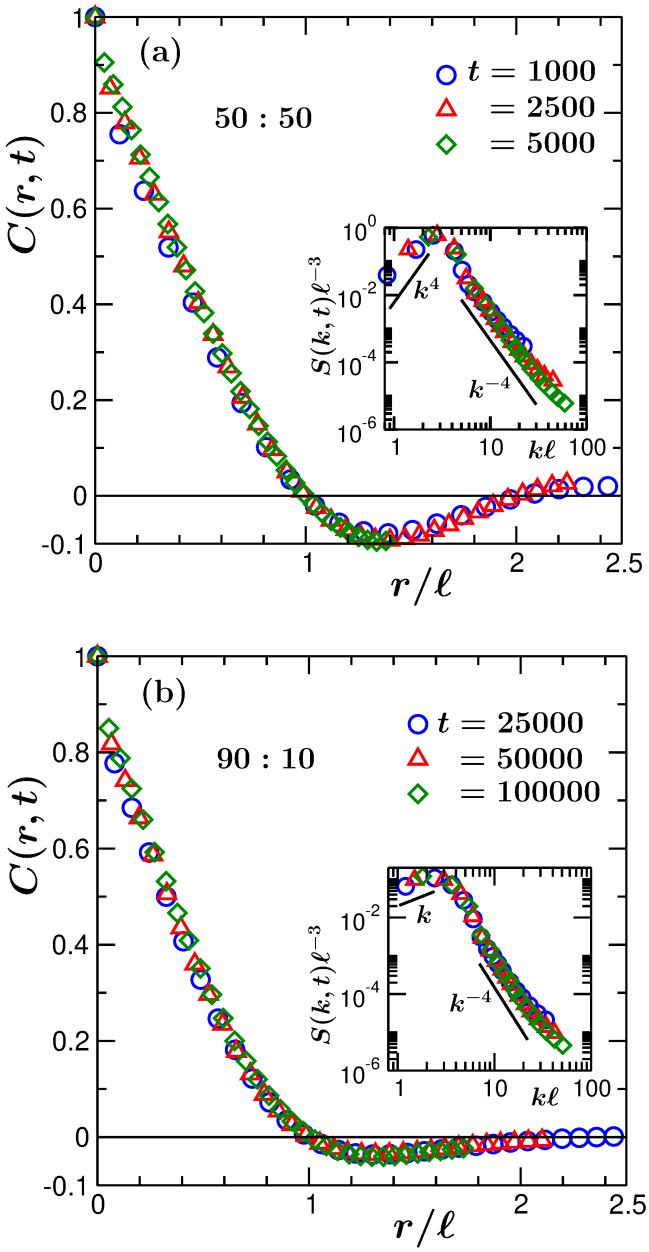


Fig. 4.3 (a) Two-point equal time correlation functions, $C(r,t)$, are shown, from a few different times, versus the scaled distance $r/\ell(t)$, for 50 : 50 composition. In the inset we show the analogous scaling plots for the structure factor, $S(k,t)$, $k$ being the wave number. The solid lines represent power laws. (b) Same as (a) but here the composition is 90 : 10.

tative picture and obtain an understanding on the pathway to the equilibrium for the disconnected case.

In Fig. 4.3 we show scaling exercise [4] for the correlation function. There $C(r,t)$ is plotted versus $r/\ell$. Results from a few different times, for two compositions, have been included. Part (a) contains results for the symmetric composition and the results for 90 : 10 composition are included in part (b). Nice collapse of the data sets imply self-similarity of growth in both the cases. For conserved order-parameter dynamics one expects damped oscillation of $C(r,t)$ around zero. This is clearly visible here. In the asymmetric composition case the minimum is expectedly quite shallower compared to the symmetric or critical (50 : 50) composition case [7, 59, 60].

In the insets of Fig. 4.3 we have shown the scaling plots of $S(k,t)$, the structure factor, a quantity that is of direct experimental relevance [4]. This is the Fourier transform of $C(r,t)$. The expected scaling form for this quantity is [4]

$$S(k,t) \equiv \ell^d \tilde{S}(k\ell), \tag{4.11}$$

where $\tilde{S}(y)$ is another time independent master function. Clearly, good collapse of data from different times is visible. The small $k$ behavior is consistent with [40, 60] $k^4$, for the symmetric case, referred to as the Yeung's law [61]. The result for the asymmetric case, however, is at deviation [60] with the Yeung's law. The large $k$ behavior is consistent with a power-law having an exponent $-4$, in both the cases. This is the expected Porod law [62–64] in $d = 3$, for a scalar order-parameter, and is an outcome of scattering from sharp interfaces. The deviations that are observed can be due to the interfacial roughness that is appreciable from the noise that is noticed in the snapshots of Fig. 4.2. Such noise can be gotten rid of via choices of lower quench temperatures. This will, however, lead to slower dynamics, preventing us from accessing the desired growth regimes over appreciable periods of time. Even crystallization is a possibility. In our study, for the purpose of analysis, this noise was largely eliminated via the application of a majority rule [6]. Before moving to the discussion on growth, we mention that $\ell$ can be estimated from the first moment of $S(k,t)$ as well [4].

In Fig. 4.4 (a) we have shown $\ell$ versus $t$ plots for several different compositions. For compositions at or close to the symmetric value, intermediate time behavior, over long periods, is linear, consistent with the expectation for viscous hydrodynamic growth. The saturations at late times are due to finite size of the systems. Late time behavior, for compositions far away from the critical value, is consistent with $\alpha = 1/3$. This is expected for the BS [15–17] mechanism, in $d = 3$. For a more convincing confirmation, of the values of the exponent, we have calculated the instantaneous exponent [6, 11, 12],

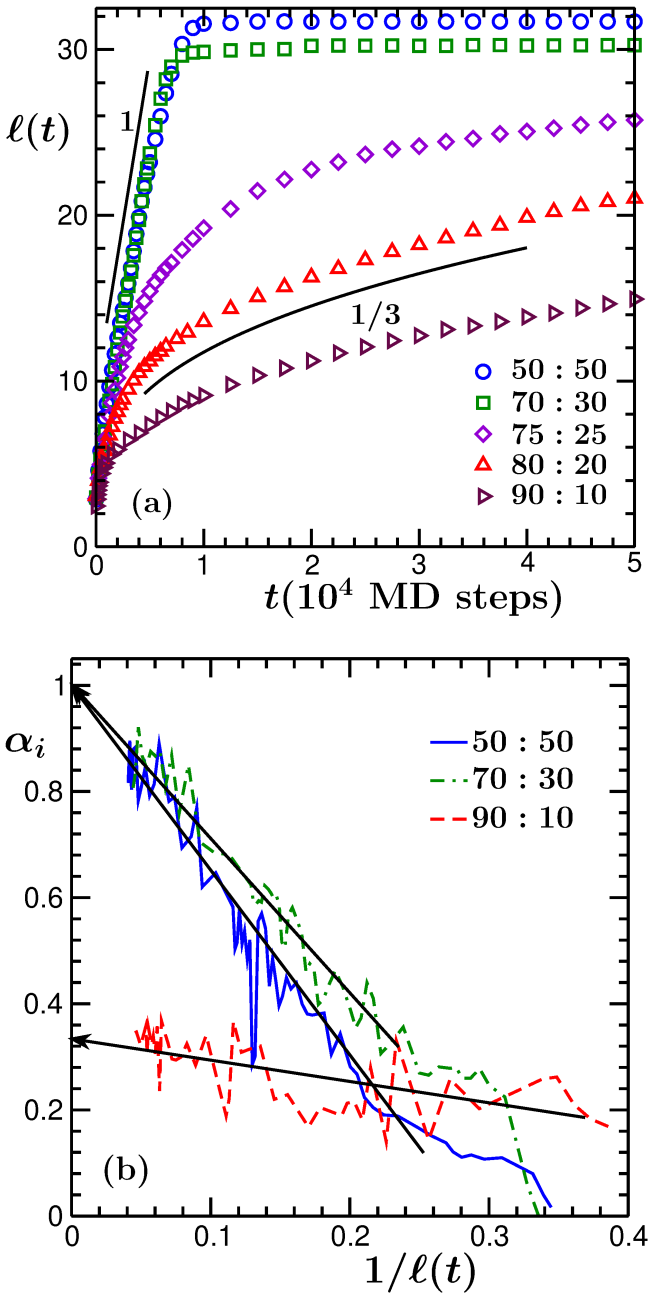


Fig. 4.4 (a) Average domain lengths, $\ell(t)$, are shown with the variation of time, for quenched systems having different compositions of A and B particles. The solid lines represent power-laws with mentioned exponents. (b) Instantaneous exponents are shown as a function of $1/\ell$, for the compositions 50 : 50, 70 : 30 and 90 : 10. The arrow-headed lines there are guides to the eyes.

$\alpha_i = d\ln\ell/d\ln t$. This quantity is shown in Fig. 4.4(b), as a function of $1/\ell$. The convergences, in the $\ell \to \infty$ limit, to $\alpha = 1$ and $\alpha = 1/3$, can be appreciated. For

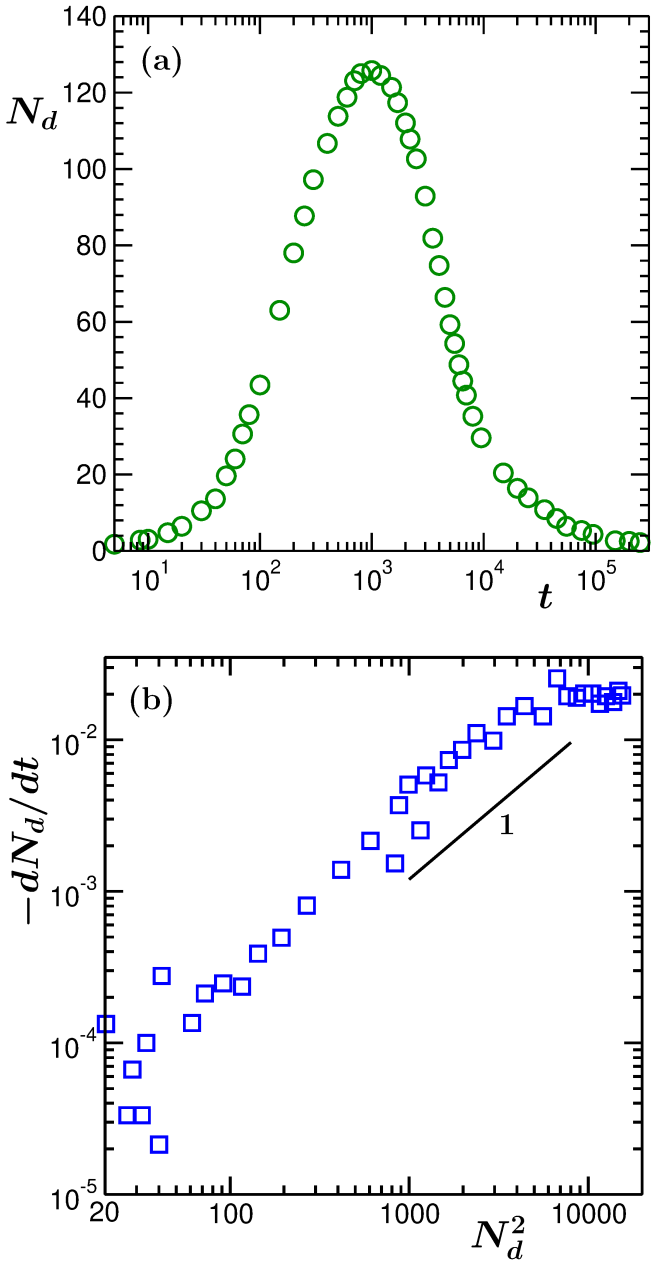


Fig. 4.5 (a) Here we have plotted the number of droplets, consisting primarily of the particles of the minority phase, as a function of time, on a semi-log scale, for 90 : 10 composition. (b) A plot of $-\mathrm{d}N_d/\mathrm{d}t$ versus ${N_d}^2$, on a log-log scale, corresponding to the plot in (a). The solid line is a power-law with exponent 1.

$\ell < \infty$, smaller values of $\alpha_i$, compared to the expected ones, can be attributed to the presence of non-zero offsets at the beginning of a scaling regime. If such initial length

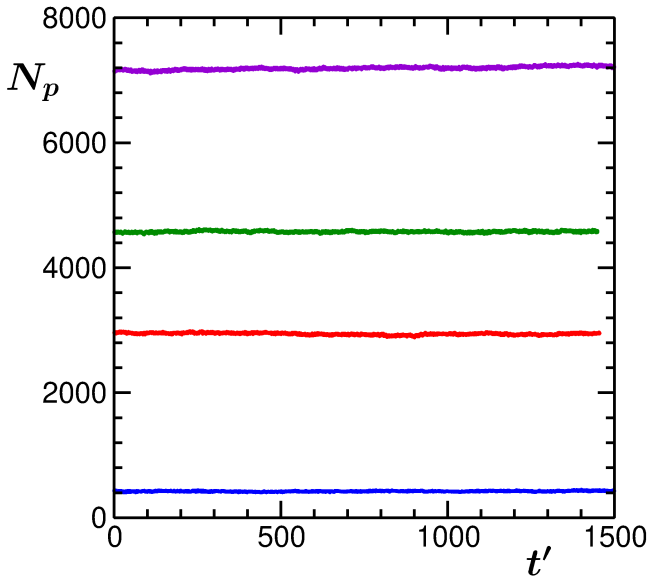


Fig. 4.6 Numbers of particles, $N_p$, in a few droplets, are shown as a function of the translated time $t' = t - t_0$, $t_0$ being the beginning of an observation. These results are for the composition 90 : 10 and $L = 48$. During the presented periods the considered droplets did not undergo collision with other droplets.

has a value $\ell_0$, $\alpha_i$ is expected to exhibit the behavior [6, 12]

$$\alpha_i = \alpha \left[1 - \frac{\ell_0}{\ell}\right]. \tag{4.12}$$

Clearly, for all the compositions, data in Fig 4.4 (b) are consistent with Eq. (4.12). In the rest of the paper we focus only on the discontinuous morphology unless otherwise mentioned, for the representative case of 90 : 10 composition. Having identified the exponent for the power-law growth, in the following we present results that will ascertain that the growth indeed occurs via diffusive coalescence mechanism, when hydrodynamics is preserved.

In Fig. 4.5 (a) we present a plot for the number of droplets as a function of time. The early part is dominated by nucleation. The late time decay is due to growth. In part (b) of this figure we have shown a plot of $-dN_d/dt$ versus ${N_d}^2$. There the focus is on the late time growth part. Thus, we have shown data from $t = 5000$ onward. The linear behavior on a double-log scale indicates a power-law. We expect [34] an exponent 1 for diffusive coalescence — see Eq. (4.2) and related discussion. That indeed is observed. This also indirectly validates the Stokes-Einstein-Sutherland [41–43] relation in this extended context.

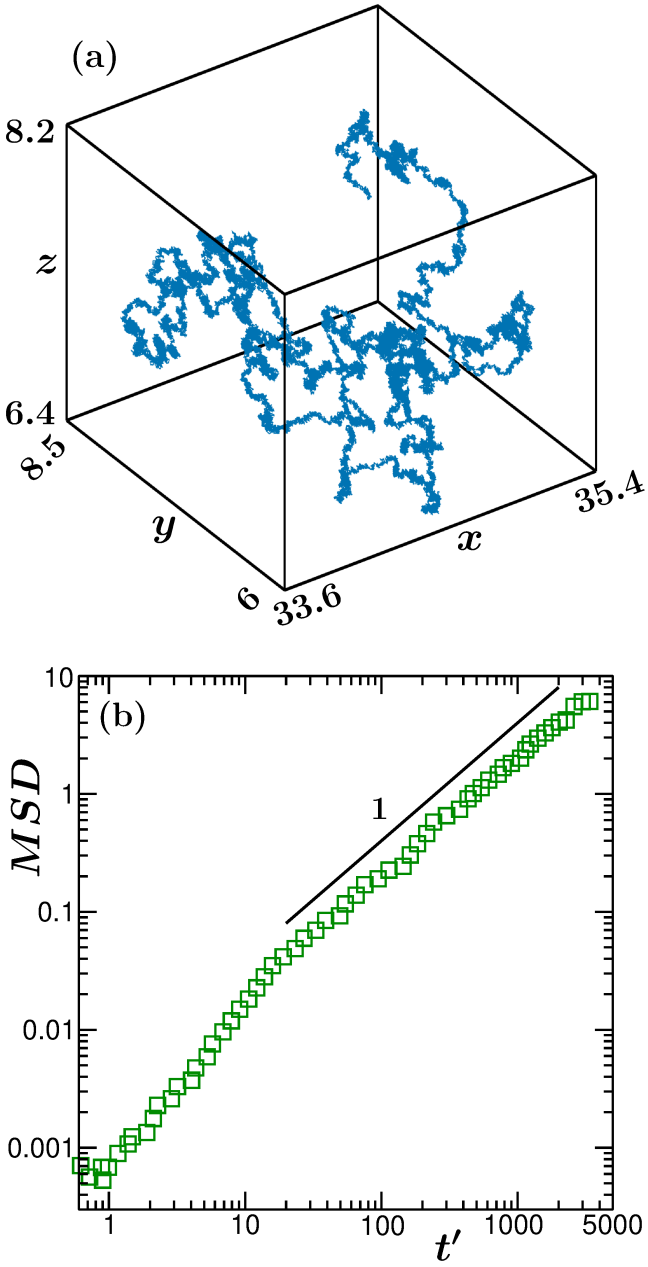


Fig. 4.7 (a) Here we show the trajectory of the centre of mass of a typical droplet. (b) Log–log plot of the mean-squared-displacement (MSD) of a droplet, as a function of the shifted time $t'$. During this period the droplet did not encounter any collision with other droplets. The solid line represents the diffusive displacement. These results are for the composition 90 : 10.

In Fig. 4.6 we show numbers of particles in several droplets, with the variation of time $t'$ that is calculated from the beginning of an observation. During the presented periods these droplets did not collide with any other droplets. In each of the cases

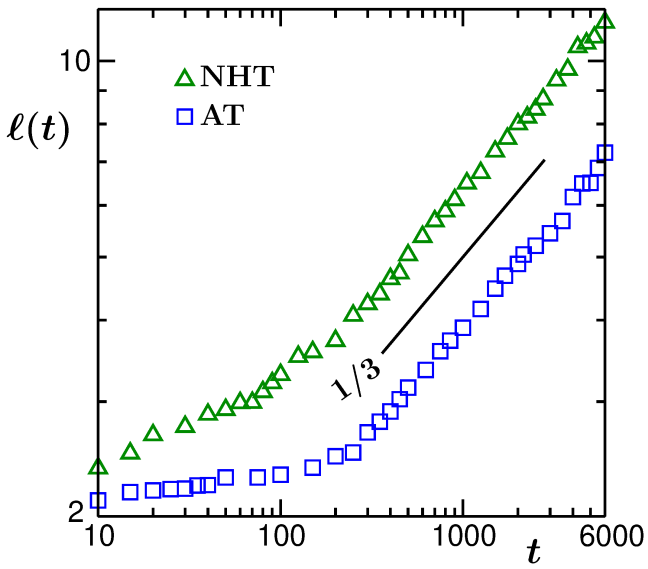


Fig. 4.8 Plots of $\ell$ versus time, on a log-log scale. Here we have compared the results obtained via the applications of NHT with those gathered by using AT. These results are for the composition 80 : 20. The solid line is a power-law with exponent 1/3.

the value of $N_p$ remains practically constant. This again suggests that LS-like particle diffusion mechanism [8] is playing negligible role in the growth. The number of droplets is decreasing, as seen in Fig. 4.5, due to coalescence.

In Fig. 4.7 we have shown results related to the motion of the centres of mass of the droplets. In part (a) a trajectory of the CM of a typical droplet is seen. Random motion of the droplet is visible. In part (b) we have shown MSD versus time plot for such a droplet. Clearly diffusive displacement is visible, at late times.

The above results suggest that the growth is occurring via the diffusive coalescence mechanism. In Fig. 4.8 we provide further information. There we have compared growth plots obtained for NHT and AT. Hydrodynamic effect is not expected for AT. Thus, NHT should provide faster evolution, even though the exponent in both the cases should be the same. Plots of Fig. 4.8 are consistent with this picture. Certainly $A_{BS}/A_{LS}$ is $> 1$. However, a proper match with the theoretically expected number is not obtained [33]. This is due to the fact that even though NHT provides hydrodynamics, a perfect match of transport with natural system can not be expected, unless various thermostat parameters are appropriately tuned.

## 4.4 Conclusion

We have studied kinetics of phase separation in a high density symmetric binary (A+B) fluid model [45, 50–52]. We have considered mixture compositions symmetric as well as close to one of the branches of the coexistence curve. While around the symmetric composition a bicontinuous nonequilibrium domain morphology is obtained, for compositions close to a coexistence curve the domain morphology consists of disconnected droplets of the minority phase in the background of a sea consisting of particles of the majority species. The symmetric case is much studied and in agreement with the previous studies [17–19, 40] we observe linear viscous hydrodynamic evolution within the achievable simulation length and time scales.

We have performed molecular dynamics simulations for our study. To capture hydrodynamics, in our canonical ensemble simulations, we have used a thermostat that is known for its capability of conservation [44] of local momentum, etc. Main focus is on the disconnected morphology. These results were compared with those obtained via the application of a stochastic thermostat [44].

We observe that the droplets are not static in hydrodynamic environment. Via the calculation of mean-squared-displacements of the centres of mass, we show that these exhibit diffusive motion. Due to sticky collisions among these droplets, the number density of these objects in the system decreases, thereby the characteristic length scale increases. For this diffusive coalescence mechanism we have accurately estimated the exponent for the power-law growth. This in good agreement with a theoretical expectation [15–17].

The picture described above is different from that is provided by the results obtained in a stochastic situation. In this case the droplets are practically static and growth occurs via particle diffusion, as in solid mixtures [6–8, 11, 12]. However, the exponent remains same in both the cases. We have estimated the ratio of the growth amplitudes in the two cases. This suggests that the hydrodynamic growth is faster.

In future it will be interesting to study the aging properties [65] of such off-critical binary mixtures. It will be important to compare the results obtained with and without hydrodynamics. There exist crucial open question concerning the inertial hydrodynamic growth [4, 30, 66] as well, for bicontinuous structure. Note that for the latter type of morphology, to access the behavior at very late time, by avoiding finite-size effects, one requires to simulate much larger systems over very long time. This was difficult to achieve with the resources that are available to us.

This material has been submitted to arXiv. The arXiv link is https://arxiv.org/abs/2107.10698.

# References


[1] K. Binder, *Phase Transformation of Materials*, edited by R.W. Cahn, P. Haasen and E.J. Kramer (Wiley VCH, Weinheim, 1991), vol. 5. p. 405.

[2] R.A.L. Jones, *Soft Condensed Matter* (Oxford University Press, Oxford, UK, 2002).

[3] A. Onuki, *Phase Transition Dynamics* (Cambridge University Press, Cambridge, UK, 2002).

[4] A.J. Bray, Adv. Phys. **51**, 481 (2002).

[5] S. Puri and V. Wadhawan (eds.), *Kinetics of Phase Transitions* (CRC Press, Boca Raton, FL, 2009).

[6] S. Majumder and S.K. Das, Phys. Rev. E **84**, 021110 (2011).

[7] S. Majumder and S.K. Das, Phys. Chem. Chem. Phys. **15**, 13209 (2013).

[8] I.M. Lifshitz and V.V. Slyozov, J. Phys. Chem. Solids **19**, 35(1961).

[9] C. Wagner, Z. Electrochem. **65**, 581 (1961).

[10] P. Voorhees, Ann. Rev. Mater. Sci. **22**, 197 (1992).

[11] D.A. Huse, Phys. Rev. B **34**, 7845 (1986).

[12] J.G. Amar, F.E. Sullivan, and R.D. Mountain, Phys. Rev. B **37**, 196 (1988).

[13] J.F. Marko and G.T. Barkema, Phys. Rev. E **52**, 2522 (1995).

[14] D.W. Heermann, L. Yixue, and K. Binder, Physica A, **230**, 132 (1996).

[15] K. Binder and D. Stauffer, Phys. Rev. Lett. **33**, 1006 (1974).

[16] K. Binder, Phys. Rev. B **15**, 4425 (1977).

[17] E.D. Siggia, Phys. Rev. A **20**, 595 (1979).

[18] H. Furukawa, Phys. Rev. A **31**, 1103 (1985).

[19] H. Furukawa, Phys. Rev. A **36**, 2288 (1987).

[20] M. San Miguel, M. Grant, and J.D. Gunton, Phys. Rev. A **31**, 1001 (1985).

[21] J.E. Farrell and O.T. Valls, Phys. Rev. B **43**, 630 (1991).

[22] A. Shinozaki and Y. Oono, Phy. Rev. E **48**, 2622 (1993).

[23] T. Koga and K. Kawasaki, Physica A **196**, 389 (1993).

[24] H. Tanaka, Phys. Rev. Lett. **72**, 1702 (1994).

[25] H. Tanaka, J. Chem. Phys. **103**, 2361 (1995).

[26] H. Tanaka, J. Chem. Phys. **105**, 10099 (1996).

[27] M. Laradji, S Toxvaerd, and O.G. Mouritsen, Phys. Rev. Lett. **77**, 2253 (1996).

[28] H. Tanaka, J. Chem. Phys. **107**, 3734 (1997).

[29] S. Bastea and J. Lebowitz, Phys. Rev. Lett. **78**, 3499 (1997).

[30] V.M. Kendon, M.E. Cates, I. Pagonabarraga, J.C. Desplat, and P. Blandon, J. Fluid Mech. **440**, 147 (2001).

[31] C. Datt, S.P. Thampi, and R. Govindarajan, Phys. Rev. E **91**, 010101(R) (2015).

[32] S. Majumder and S.K. Das, Europhys. Lett. **95**, 46002 (2011).

[33] S. Roy and S.K. Das, Phys. Rev. E **85**, 050602(R) (2012).

[34] S. Roy and S.K. Das, Soft Matter **9**, 4178 (2013).

[35] R. Shimizu and H Tanaka, Nat. Commun. **6**, 7407 (2015).

[36] A.K. Thakre, W.K. den Otter and W.J. Briels, Phys. Rev. E **77**, 011503 (2008).

[37] H. Kabrede and R. Hentschke, Physica A **361** 485 (2006).

[38] S.W. Koch, R.C. Desai, and F.F. Abraham, Phys. Rev. A **27**, 2152 (1983).

[39] V. Kumaran, J. Chem. Phys. **109**, 7644 (1998).

[40] S. Ahmad, S.K. Das, and S. Puri, Phys. Rev. E **85**, 031140 (2012).

[41] J.-P. Hansen and I.R. McDonald,*Theory of Simple Liquids* (Academic Press, London, 2008).

[42] S.K. Das, J.V. Sengers and M.E. Fisher, J. Chem. Phys. **127**, 144506 (2007).

[43] T.M. Squires and J.F. Brady, Phys. Fluids **17**, 073101 (2005).

[44] D. Frenkel and B. Smit, *Understanding Molecular Simulations: From Algorithms to Applications* (Academic Press, San Diego, 2002).

[45] M.P. Allen and D.J. Tildesly, *Computer Simulations of Liquids* (Clarendon, Oxford, 1987).

[46] S. Nosé, J. Chem. Phys. **81**, 511 (1984).

[47] W.G. Hoover, Phys. Rev. A **31**, 1695 (1985).

[48] W.G. Hoover, *Studies in Modern Thermodynamics*, (Elsevier, 1991).

[49] S. Roy and S.K. Das, J. Chem. Phys. **139**, 044911 (2013).

[50] S.K. Das, M.E. Fisher, J.V. Sengers, J. Horbach, and K. Binder, Phys. Rev. Lett. **97**, 025702 (2006).

[51] S.K. Das, J. Horbach, K. Binder, M.E. Fisher, and J.V. Sengers, J. Chem. Phys. **125**, 024506 (2006).

[52] S. Roy and S.K. Das, Europhys. Lett. **94**, 36001 (2011).

[53] H.C. Andersen, J. Chem. Phys. **72**, 2384 (1980).

[54] S. Plimpton, J. Comp. Phys. **117**, 1 (1995).

[55] http://lammps.sandia.gov.

[56] M.P. Allen and F. Schmid, Mol. Simul. **33**, 21 (2007).

[57] S. Roy and S.K. Das, Euro. Phys. J. E **38**, 132 (2015).

[58] J. Hoshen and R. Kopelman, Phys.Rev.B **14**, 3438 (1976).

[59] S.K. Das and S. Puri, Phys. Rev. E **65**, 026141 (2002).

[60] S. Paul and S.K. Das, Phys. Rev. E **96**, 012105 (2017).

[61] C. Yeung, Phys. Rev. Lett. **61**, 1135 (1988).

[62] G. Porod, *Small-Angle X-Ray Scattering*, edited by O. Glatter and O. Kratky (Academic Press, New York, 1982).

[63] Y. Oono and S. Puri, Mod. Phys. Lett. B **2**, 861 (1988).

[64] A.J. Bray and S. Puri, Phys. Rev. Lett. **67**, 2670 (1991).

[65] D.S. Fisher and D.A. Huse, Phys. Rev. B **38**, 373 (1988).

[66] V.M. Kendon, J.C. Desplat, P. Bladon and M.E. Cates, Phys. Rev. Lett. **83**, 576 (1999).

# Chapter 5

# Critical Behavior of Curvature Dependent Interfacial Tension

## 5.1 Introduction

Nucleation of a new phase and subsequent transition process, following variation in different thermodynamic parameters, in a system remains one of the important topics of research since long [1–16]. When a homogeneous binary (A+B) mixture, say, in a cubic box, is suddenly quenched inside the coexistence region, based on the composition the interface between the two coexisting phases can have different geometrical shapes [13, 14]. Close to the critical composition and for extreme off-critical quenches one observes the formations of flat and spherical interfaces, respectively. In a range between these two cases cylindrical interface appears. Formations of such curved boundaries can as well be observed when a phase-separating system is placed between walls [17–20]. Understanding thermodynamics associated with such interfaces has fundamental as well as technological importance, having strong bearing with structure and dynamics in porous media [21, 22].

The excess free energy contribution for the interface creation is [1–3]

$$\Delta F = -\frac{4}{3}\pi R^3 f_v + 4\pi R^2 \gamma, \tag{5.1}$$

where $f_v$ and $\gamma$ denote the bulk free energy density and surface tension, respectively. Here the nucleating phase is considered to be a sphere of radius $R$. Typically in the classical nucleation theory [1–8, 23–27] the interface is assumed to be flat which is not true at small length scales.

Corrections to flat interfacial tension have found mentions from the time of Gibbs [28] and discussed in details by Tolman [29–31]. The latter wrote the form with the leading order correction as

$$\gamma(R) = \frac{\gamma(\infty)}{1 + 2(\frac{\delta}{R})}, \tag{5.2}$$

$\delta$ being the Tolman length. Interpretation of $\delta$ is still debated. Its dependence on temperature is a matter of current research [32–34]. For systems which are symmetric under interchange of the two coexisting phases, $\delta$ is expected to vanish [35] identically, possibly because the interchange of particle identities alters the sign of the curvature keeping the thermodynamics same. For a symmetric model [14, 36, 37] the curvature dependence of $\gamma(R)$ can be written, to the leading order, as

$$\gamma(R) = \frac{\gamma(\infty)}{1 + 2(\frac{\ell}{R})^2}, \tag{5.3}$$

where $\ell$, another length, is discussed in the literature to be a function of bending rigidity and rigidity constant related to the Gaussian curvature [38, 39].

At critical points, various quantities show power-law singularities [40–46]. The critical behaviors of correlation length ($\xi$), susceptibility ($\xi$) and flat interfacial tension ($\gamma(\infty)$) can be described as

$$\xi \approx \xi_0^{\pm} \tau^{-\nu}, \tag{5.4}$$

$$\chi \approx \chi_0^{\pm} \tau^{-\gamma} \tag{5.5}$$

and

$$\gamma(\infty) = \gamma \approx \gamma_0 \tau^{(d-1)\nu}. \tag{5.6}$$

Here $\tau = |T - T_c|/T_c$, $T$ and $T_c$ being respectively the temperature and its critical value, $d$ is the spatial dimension and $\nu$, $\gamma$ are two critical exponents. These exponents are universal in nature and for the three dimensional (3D) Ising class [45, 46] the values are [40]

$$\nu \simeq 0.63, \quad \gamma \simeq 1.239. \tag{5.7}$$

Although the critical amplitudes are not universal, there exist universality in certain ratios containing these.

Recently it is observed that the critical character of $\ell$ is same as the correlation length $\xi$ [14, 37], namely,

$$\ell \approx \ell_0 \tau^{-\nu}. \tag{5.8}$$

Given that previously it was reported [32] that $\delta \sim \tau^{-(\nu-\beta)}$, where $\beta$, the exponent related to the critical behavior of order-parameter, has value 0.326 for 3D Ising universality [40], Eq. (5.8), with the aid of Eq. (5.3), *practically* makes critical scaling of curvature dependent surface tension as [14, 37]

$$\gamma(R)\xi^2 = \frac{C_1}{1 + C_2(\frac{\xi}{R})^2}. \tag{5.9}$$

Here $C_1 = \gamma_0(\xi_0^-)^2$ is a universal constant with value $\simeq 0.089$ [47, 48]. Character of the other constant $C_2$ needs investigation. The form in Eq. (5.9) should be valid for asymmetric model as well, at the critical proximity. This is because, as already evident from the above discussion, $\delta$ has a milder critical divergence [32].

Here we study the critical property of surface tension for symmetric binary mixtures and aim to quantify the behavior of $C_2$. We consider different models for which critical temperatures vary significantly.

## 5.2 Models and Methods

We have considered an A+B mixture of $N$ $(= N_A + N_B)$ particles, $N_A$ and $N_B$ being the numbers for species A and B, each of mass $m$. Like in chapter 4, any two constituent particles sitting at $\vec{r}_i$ and $\vec{r}_j$ interact following the Lennard-Jones (LJ) potential [49] $(r = |\vec{r}_i - \vec{r}_j|)$,

$$V(r) = 4\epsilon_{\alpha\beta}\left[\left(\frac{\sigma_{\alpha\beta}}{r}\right)^{12} - \left(\frac{\sigma_{\alpha\beta}}{r}\right)^{6}\right], \quad \alpha, \beta \in [\text{A,B}]. \tag{5.10}$$

The choices of $\epsilon_{\alpha\beta}$ and $\sigma_{\alpha\beta}$ remain same as in the previous chapter. Therefore the mixture parameters are perfectly symmetric which will lead to demixing transition with critical concentration $x_A = N_A/N = 0.5$ [50, 51]. Appropriate order-parameter in this case is

$$m = x_A - 1/2. \tag{5.11}$$

This will be negative and positive in the B-rich and A-rich phases, respectively.

For faster computation two different variants [52, 53] of the LJ potential have been used, which are detailed below.

(i) Truncated and shifted LJ (tsLJ) potential [52, 53]:

$$\begin{aligned} U(r) &= V(r) - V(r_c), \quad && r < r_c \\ &= 0, && r > r_c, \end{aligned} \tag{5.12}$$

(ii) Truncated, shifted and force-corrected LJ (tsfLJ) potential [52]:

$$\begin{aligned} U(r) &= V(r) - V(r_c) - (r - r_c)\left[\frac{dV}{dr}\right]_{r=r_c}, \quad && r < r_c \\ &= 0, && r > r_c. \end{aligned} \tag{5.13}$$

Here $r_c$ is a cut-off distance. The value of $r_c$ is chosen as $2.5\sigma$. For each of the varieties (i) and (ii) we have considered different overall densities that lead to the studies of a total of five different models. The densities are chosen in such a way that an overlap of a liquid-liquid transition with a vapor-liquid transition does not occur. In table 5.1 we have described the details of different models.

Table 5.1 Details of different models. Results for model III is borrowed from Refs. [14, 37].

| Interaction potential | Overall density ($N/L^3$) | Name of the model |
|---|---|---|
| tsLJ | 1.0 | Model I |
| | 0.7 | Model II |
| tsfLJ | 1.0 [14, 37] | Model III |
| | 0.7 | Model IV |
| | 0.65 | Model V |

All the presented results, except for those in Fig. 5.1, are averaged over 60 or more independent initial realizations. For Fig. 5.1 this number is 10.

For the estimation of phase behavior Monte Carlo (MC) simulations have been performed in a semi-grand canonical ensemble (SGMC) [49]. In this SGMC method, in a cubic box of length $L$ the total number of particles $N$ is held fixed. However, the compositions $x_A$ $(= N_A/N)$ and $x_B$ $(= N_B/N)$ are allowed to change.

The method [49] incorporates two different trial moves: displacements of particles and switch $(A \rightarrow B \rightarrow A)$ of their identities. These are accepted by following the standard Metropolis criterion [49], where the Boltzmann factor contains the change in energy $\Delta E$ as well as the difference in chemical potentials between the two species $\Delta\mu = \mu_A - \mu_B$. However $\Delta\mu$ is zero for symmetric situation. This basic SGMC method

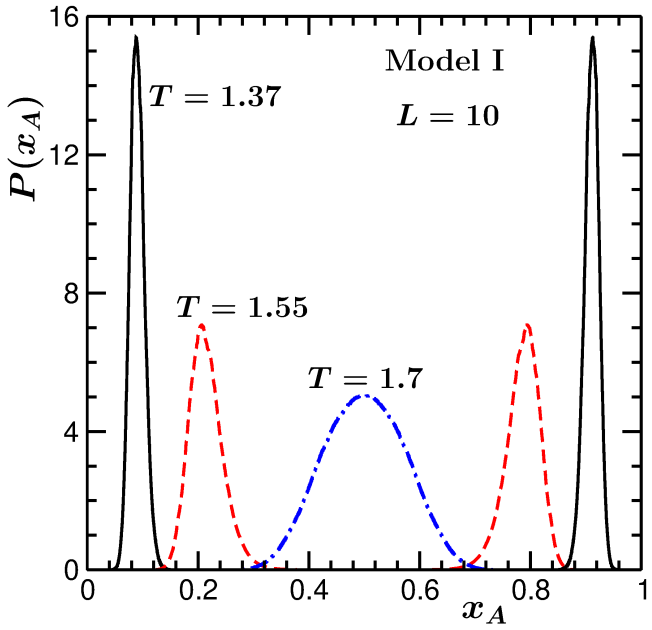


Fig. 5.1 Plots of probability distributions, $P(x_A)$, versus concentration, $x_A$, of A-type particles, from various temperatures with system size $L = 10$. These results were obtained via SGMC simulation of Model I.

has certain drawback. This will be discussed and an advanced method will be used later – see discussion at the end of the next section.

## 5.3 Results from Basic Semi-grand Canonical Monte Carlo Simulations

The SGMC technique allows one to note the fluctuating value, say, $N_A$, of $A$ particles, thus, providing the probability distribution $P(x_A)$ for $x_A$. Symmetry of the models states

$$P(x_A) = P(1 - x_A). \tag{5.14}$$

At temperatures lower than $T_c$, $P(x_A)$ has a double-peak structure with peaks located at $x_A^{\text{coex}}$ and $= 1 - x_A^{\text{coex}}$, corresponding to the A-rich and B-rich phases. Above $T_C$, distribution has a single peak with the position of the peak located at $\langle x_A \rangle = \langle x_B \rangle = \frac{1}{2}$, the critical composition. In Fig. 5.1 we show $P(x_A)$ from a few temperatures above and below the critical point of Model I. From these one estimates the concentration susceptibility as

$$k_B T \chi = N(\langle x_A^2 \rangle - \langle x_A \rangle^2), \tag{5.15}$$

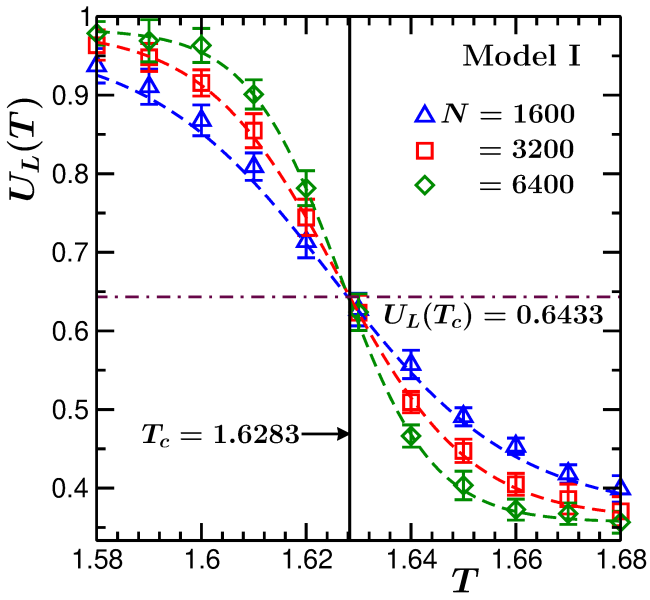


Fig. 5.2 Plots of the Binder cumulant $U_L(T)$ versus $T$, from several system sizes, for Model I. The dashed lines are fits to $y = a_0 \tanh(a_1 x - a_2) - a_3$, where $a_0$, $a_1$, $a_2$ and $a_3$ are constants. The dot-dashed horizontal line and the solid vertical line indicate the values $U_L(T_c) = 0.6433$ and $T_c = 1.628$, respectively. $U_L(T_c)$ appears consistent with the 3D Ising value 0.6236.

where $\langle x_A \rangle = 1/2$ and $\langle x_A^2 \rangle = \int_0^1 x_A^2 P(x_A) dx_A$ above $T_c$. Below $T_c$, from the two-peak structures one can obtain $\langle x_A \rangle = 2 \int_{1/2}^1 x_A P(x_A) dx_A$ and $\langle x_A^2 \rangle = 2 \int_{1/2}^1 x_A^2 P(x_A) dx_A$, the factor '2' at the beginning has connection with normalization due to consideration of only half the overall distribution.

We have estimated the liquid-liquid thermodynamic limit critical temperatures for different models by using the cumulant intersection method of Binder [46, 54]. The fourth-order Binder cumulant, a dimensionless quantity, is defined as [46, 54]

$$U_L(T) = \frac{\langle (x_A - \frac{1}{2})^2 \rangle^2}{\langle (x_A - \frac{1}{2})^4 \rangle}. \tag{5.16}$$

The limiting values of this quantity are [46, 54] are $U_L(T \to 0) = 1/3$ and $U_L(T \to \infty) = 1$, that are decided by the types of distributions of the order parameter. For finite systems there will be deviations from these values – approaches to 1/3 and 1 occur in opposite directions with the increase of system size. Thus, when we plot $U_L(T)$ versus $T$, for several $L$, different curves intersect at $T_c$, provided that $L$ is big so that the finite-size effects can be ignored. At $T = T_c$ for 3D Ising universality class one has $U_L(T_c) = 0.6236$ [55, 56]. Close to the criticality the cumulant has the behavior $U_L(T) \equiv \tilde{U}(\tau L^{1/\nu})$.

In Fig 5.2 we have shown the plots of the cumulant versus $T$ for different $L$ for Model I. The plots for different system sizes cross at a reasonably unique intersection point, from which we estimate the thermodynamic $T_c$ quite accurately. From this exercise we quote $T_c = 1.628$. The latter is in good agreement with a previous study [50].

At low temperatures, because of high free energy barrier between the coexisting phases the systems may get stuck into one of the phases. This can be overcome by employing a biased simulation technique. Here we have performed a successive umbrella sampling [57] in the semi-grand canonical ensemble. In this method the whole range of particle number is divided into small windows and simulations are performed by appropriately forcing the system into successive windows. This enables us to sample the whole composition space efficiently and estimate probability distributions $P(x_A)$ more accurately as a function of $x_A$.

## 5.4 Facts and Basic Results related to the Umbrella Sampling Technique

The normalized distribution, obtained from the umbrella sampling simulations, is connected to the free energy density as [14, 58–61]

$$f_L(x_A, T) = -\frac{k_B T}{L^3} \ln[P(x_A)/P(x_A^{\rm coex})]. \tag{5.17}$$

The latter we have shown in Fig 5.3(a) for different system sizes $L$. In this figure the minimum on the left corresponds to a bulk B-rich phase. Gradually, as number of A-type particles is increased, an A-rich spherical droplet will appear and in the background of it there will be the B-rich phase. This is manifested as a sharp change in slope in the free energy curve. The size of this droplet keeps increasing as $x_A$ increases until it takes the shape of a cylinder which is energetically more stable at a higher $x_A$, reflected as another sharp change in the slope. Finally, as $x_A$ approaches the critical concentration 1/2, both the coexisting phases achieve slab geometries. The structural changes in the nucleating phase can be visualized more prominently from the sudden jumps in the behavior of chemical potential difference with respect to the bulk coexistence,

$$\frac{\Delta\mu_L(x_A, T)}{k_B T} = \left[\frac{\partial f_L(x_A, T)}{\partial x_A}\right]_T, \tag{5.18}$$

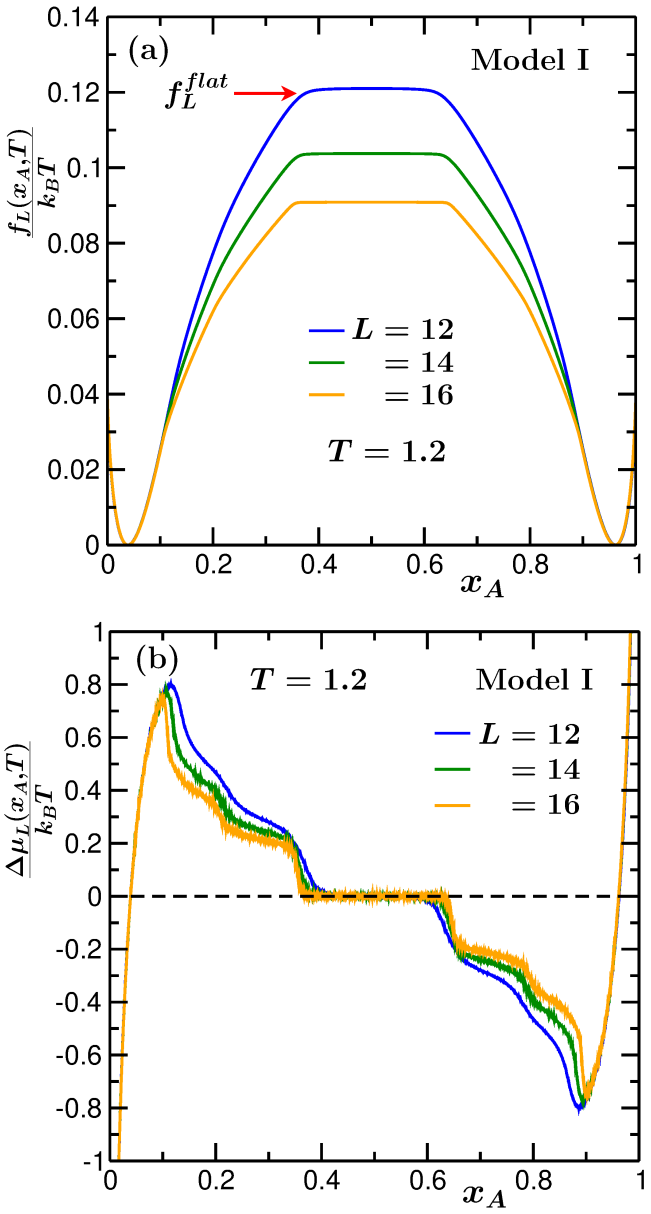


Fig. 5.3 (a) Plots of normalized free energy density, $f_L(x_A, T)/k_BT$, versus the concentration of A particles, $x_A$, at temperature $T = 1.2$, for three different choices of system size $L$. With the increase in $x_A$ the free energy curves show certain sudden changes in the slope which are the consequences of the changes in the shape of the minority phase (A-rich phase): from spherical to cylindrical to slab-like structures. One can obtain $L$-dependent flat interfacial tension $\gamma(L)$ (for $L = \infty$, this is same as $\gamma(\infty)$, as previously introduced in the context of curved interface) from the height of the free energy curve. (b) Plots of $\Delta\mu_L(x_A, T)/k_BT$ vs $x_A$ for the same systems as in (a). Both the figures are for Model I.

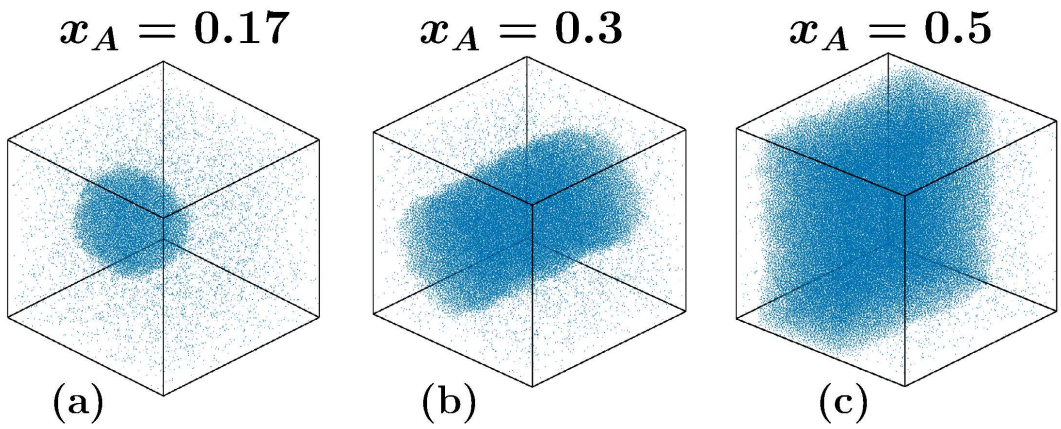


Fig. 5.4 Various geometrical structures obtained for A-rich phase via the umbrella sampling SGMC simulations. B particles are not shown. The values of $x_A$ are mentioned at the top of the frames. These pictures are from temperature $T = 1.2$, with $L = 16$ and $N = 4096$, for Model I.

which we show in Fig. 5.3 (b). With increasing system size the structural changes from sphere to cylinder to slab become more and more prominent.

In Fig 5.4 we have presented a series of snapshots of the nucleating phase obtained during the simulations. The corresponding concentrations have been specified in the figure. Although there are statistical fluctuations in the shapes, to a high degree of accuracy they have spherical or cylindrical symmetry, before taking the slab geometry.

The height of the free energy plot, denoted by $f_L^{flat}$ in Fig. 5.3 (a), is the barrier between the coexisting phases [13, 36, 58] for a system size $L$. One can calculate the corresponding interfacial tension ($\gamma(L)$) as [58]

$$\gamma(L) = \frac{L}{2} f_L^{flat}, \tag{5.19}$$

the factor 1/2 arising due to two similar interfaces in systems having periodic boundaries.

The flat interfacial tension in the $L = \infty$ limit can be calculated from those in finite systems via [58, 62]

$$\gamma(L) = \gamma + \frac{a}{L^2} \ln \frac{b}{L}. \tag{5.20}$$

Here $\gamma$ [$= \gamma(\infty)$] is the thermodynamic limit interfacial tension. We have estimated the finite-size flat interfacial tension for significantly different values of L. This allowed us an accurate estimation of $\gamma$ via the above equation. The exercise is demonstrated in Fig. 5.5.

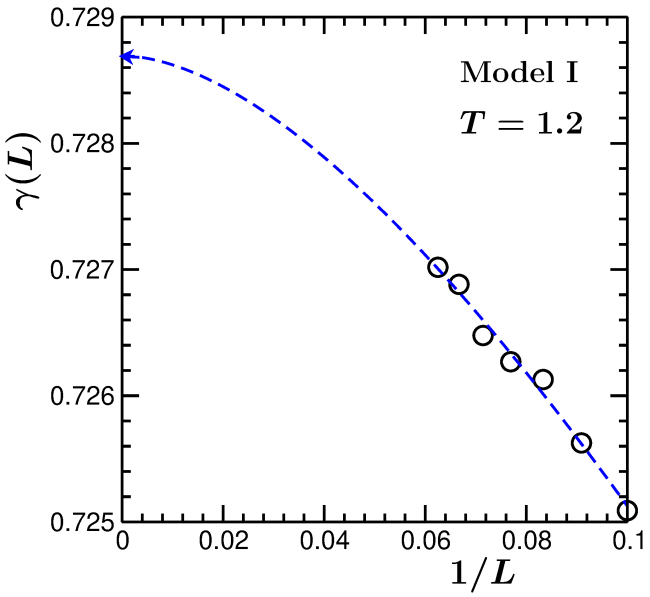


Fig. 5.5 Plot of $\gamma(L)$ versus $1/L$, for Model I and temperature $T = 1.2$. The dashed line is an extrapolation to $L \to \infty$ to estimate $\gamma(\infty)$, by using the form $\gamma(L) = \gamma(\infty) + (a/L^2)\ln(b/L)$, where $a$ and $b$ are constants.

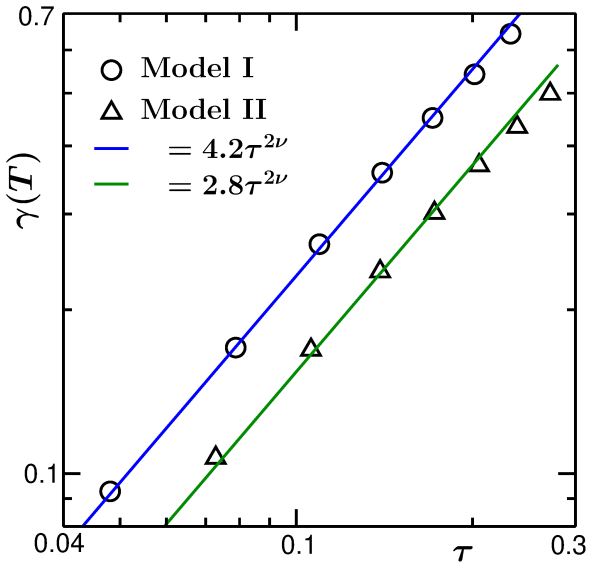


Fig. 5.6 Flat interfacial tensions are plotted against $\tau$ for Models I and II. The continuous lines are fits to $\gamma_0 \tau^{2\nu}$. The values of $\gamma_0$ for Models I and II are 4.2 and 2.8, respectively. Here $\nu$ is fixed at 0.63, which is the 3D Ising value.

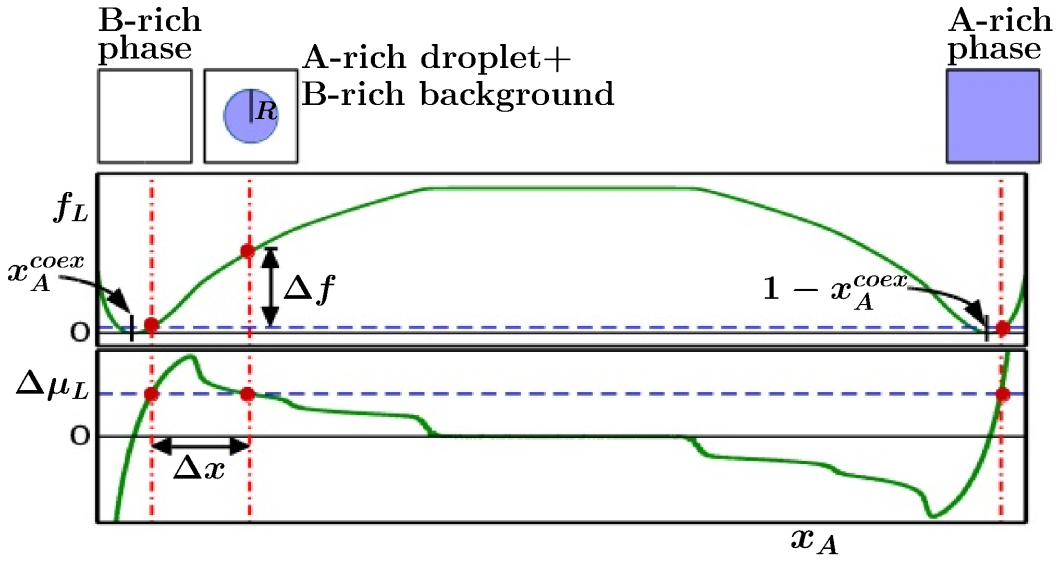


Fig. 5.7 The procedure of estimation of $\Delta x$ and $\Delta f$ from the plots of $f_L$ and $\Delta\mu$ has been shown schematically. See text for details.

To study the critical divergence of thermodynamic limit flat interfacial tension we have plotted $\gamma(T)$ against the reduced temperature $\tau$ in Fig. 5.6. There we have included data from two different models. The behavior is consistent with the expected critical singularity $\tau^{2\nu}$, with $\nu = 0.63$.

To calculate curved interfacial tension ($\gamma(R)$) we have employed a recently proposed thermodynamic method [13] which is based on the principle that the coexisting phases in equilibrium will have equal chemical potential. The method has been illustrated in Fig 5.7. Here we have to choose the regions of $f_L$ where the A-rich droplet is structurally stable and it is coexisting with the B-rich background phase in thermal equilibrium. The protocol is the following. We describe it for spherical droplet which is the focus in this chapter.

(1) First we need to identity the range of $x_A$ within which an A-rich spherical droplet exists inside the B-rich phase.

(2) The bulk contributions of the free energy can be estimated and difference of this from the total free energy will provide the excess part due to the presence of the curvature in interface:

$$V\Delta f = 4\pi R^2\gamma(R). \tag{5.21}$$

See the schematic definition of $\Delta f$ in the figure.
(3) According to a lever rule, one has for the related concentration difference in $x_A$:

$$\Delta x = \frac{4}{3}\pi R^3 \frac{[1 - 2x_A^{\text{coex}}]}{V}. \tag{5.22}$$

From the simulation the quantities $\Delta f$, $V$, $\Delta x$ and $x_A^{\text{coex}}$ can be obtained. Therefore from Eqs. (5.21) and (5.22) one estimates $R$ and $\gamma(R)$. Below we describe structural quantities, which are essential for the calculation of $\xi$ and thus, for the quantification of critical behavior of $\gamma(R)$.

## 5.5 Estimation of Concentration Fluctuation

The standard pairwise radial distribution function is expressed as [63]

$$g_{\alpha\beta}(r) = \frac{N}{\rho N_\alpha N_\beta}\left\langle \sum_{i=1}^{N_\alpha}\sum_{j=1}^{N_\beta}{}' \delta(r - |\vec{r_i} - \vec{r_j}|)\right\rangle, \qquad \alpha, \beta \in [\text{A,B}], \tag{5.23}$$

with the prime restricting $i \neq j$ if $\alpha = \beta$. The partial structure factor, corresponding Fourier transform, has the form

$$S_{\alpha\beta}(q) = x_\alpha \delta_{\alpha\beta} + x_\alpha x_\beta \rho \int_0^\infty g_{\alpha\beta} \frac{\sin(qr)}{qr} 4\pi r^2 dr, \tag{5.24}$$

$q$ being the wave number. Our interest is in the concentration fluctuation near criticality. The concentration-concentration structure factor $S_{cc}(q)$ is written as the combination [64]:

$$S_{cc}(q) = (1 - x_A)^2 S_{AA}(q) + {x_B}^2 S_{BB}(q) - 2x_A(1 - x_A)S_{AB}(q). \tag{5.25}$$

$S_{cc}(q)$ obeys the Ornstein-Zernike form at small $q$ limit [42]:

$$S_{cc}(q) = \frac{k_B T \chi}{1 + \xi^2 q^2}. \tag{5.26}$$

Fig. 5.8 shows the the plots of $S_{cc}(q, T)$ as a function of $q$ for a few temperatures for Model I. In the limit $q \to 0$ more sudden rise in $S_{cc}(q)$, as $T$ approaches $T_c$, reflects the critical enhancement of the concentration fluctuation. The Ornstein-Zernike form is fitted to the data sets in the small $q$ regimes by treating $\xi$ as an adjustable parameter,

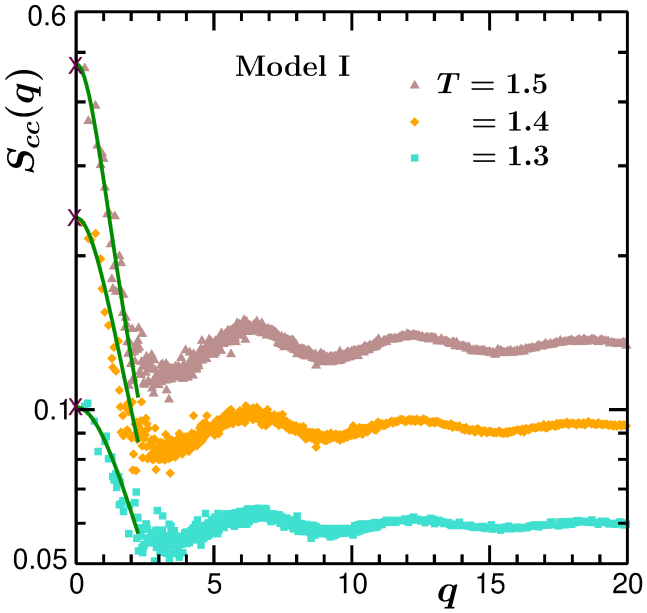


Fig. 5.8 Concentration-concentration structure factors, $S_{cc}(q)$, are shown versus the wave number, $q$, for three different temperatures close to $T_c$ for Model I. The continuous lines are fits to Eq. (5.26) and the crosses denote the values of $S_{cc}(q = 0)$ $(= k_B T\chi)$ as obtained from Eq. (5.15) by using the concentration distribution.

while $\chi$ has already been estimated from the probability distribution via Eq. (5.15). From the best fits $\xi$ have been calculated for different temperatures close to $T_c$.

## 5.6 Results on Curvature Dependent Interfacial Tension and Quantification of Its Critical Behavior

As we are working with symmetric models, it is expected that the Tolman length $\delta$ will be zero [35] and the relation between $\gamma(\infty)$ and $\gamma(R)$ should follow Eq. (5.3).

Hence in Fig. 5.9 we plot $\frac{\gamma(\infty)}{\gamma(R)} - 1$ with the variation of $1/R^2$ for various different system sizes as well as for different temperatures for Model I. As the size of the droplet $(R)$ is constrained by the system size $(L)$, results from several $L$ become useful to avail the behavior of $\gamma$ in a longer range of $R$ [14]. The data sets for different system sizes and different temperatures behave linearly and converge to zero in the $R \to \infty$ limit. This is consistent with the expectation: the leading correction is quadratic for symmetric models [14, 36, 37].

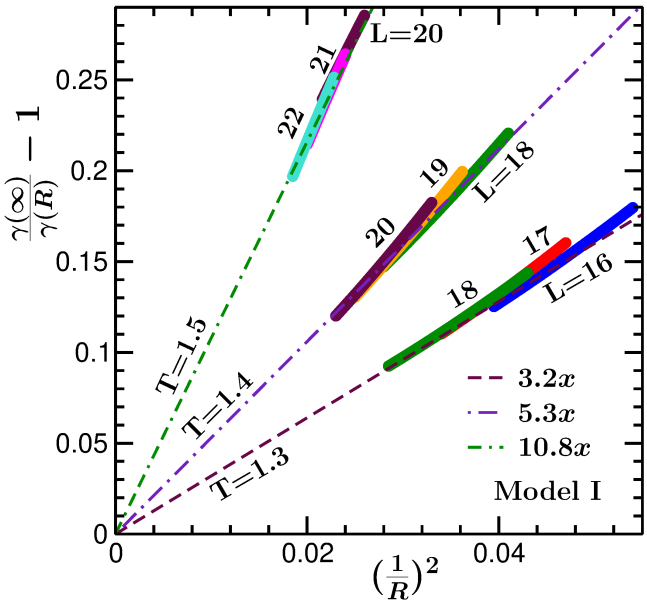


Fig. 5.9 Plots of $\frac{\gamma(\infty)}{\gamma(R)} - 1$ versus $\frac{1}{R^2}$ for spherical droplets at three different temperatures for Model I. For each of the temperatures data from multiple system sizes are included. The broken lines are linear fits to the data sets. The values of $\ell$ have been calculated from the corresponding slopes.

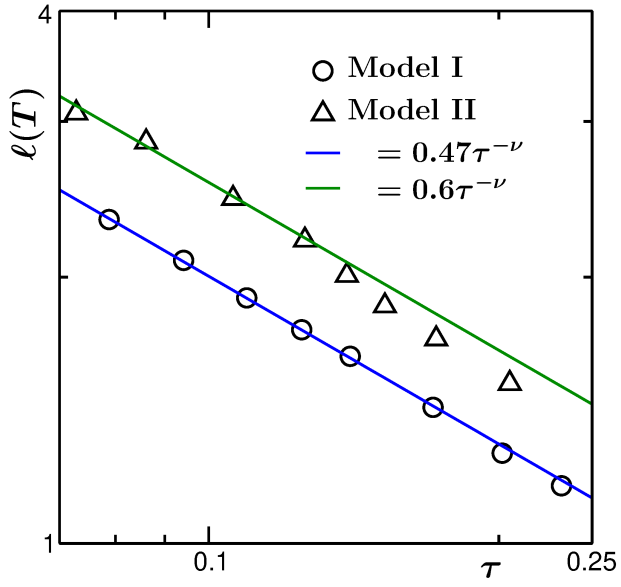


Fig. 5.10 Here we show $\ell(T)$ against $\tau$, on a log-log scale, for two models, viz., Model I and Model II. The continuous lines are fits to the form $\ell_0 \tau^{-0.63}$.

The broken lines of various styles are linear fits to the data sets. The quantity $\ell$ [see Eq. (5.3)] for different temperatures can be estimated from the slopes of these lines. Near $T_c$, we need large enough systems for the reliable estimation of surface tension for flat as well as curved interfaces as the latter becomes more and more fuzzy as $\xi$ increases.

In Fig. 5.10 we have shown the behavior of $\ell$ with the variation of $\tau$ for two different models. The solid lines denote the power-law divergence of the form $\ell_0\tau^{-\nu}$, with $\nu$ having the Ising value 0.63. Close to $T_c$ the data points are following the solid lines more consistently [14, 37], implying the fact that the singularity of $\ell$ is the same as $\xi$ [14, 37]. For direct comparison we need to calculate $\xi$.

Fig. 5.11 (a) shows the plots of $\xi$ versus $\tau$ for two different models, on a log-log scale. Again the data sets follow the 3D Ising critical divergence $\tau^{-\nu}$ with $\nu = 0.63$, represented by the continuous lines. For the sake of completeness, the concentration susceptibility for representative models have also been plotted against $\tau$ on a log-log scale in Fig. 5.11 (b). The data sets are again consistent with the 3D Ising critical divergence $\tau^{-\gamma}$, with $\gamma = 1.239$ that are represented by the solid lines.

In Fig. 5.12 the ratio $\ell/\xi$, for different models, are plotted against temperature (close to $T_c$). For a particular model the ratio is essentially constant for a wide range of temperature. These results again confirm the fact that the critical divergence of $\ell$ is similar to $\xi$ [14, 37]. In table 5.2 we have listed the values of $C_1$ and $C_2$ for different models. Recall that

$$C_2 = 2\left(\frac{\ell}{\xi}\right)^2 = 2\left(\frac{\ell_0}{\xi_0^-}\right)^2. \tag{5.27}$$

There we have also provided the values of $T_c$ for different models. Clearly $C_2$, as already

Table 5.2 List of values of $T_c$, $C_1$ and $C_2$ for different models.

| Model | $T_c$ | $C_1$ | $C_2$ |
|---|---|---|---|
| Model I | 1.628 | 0.0945 | 18.97 |
| Model II | 1.509 | 0.0699 | 24.5 |
| Model III | 1.423 | 0.072 [14, 37] | 32.0 [14, 37] |
| Model IV | 1.326 | 0.0717 | 44.37 |
| Model V | 1.258 | 0.0681 | 54.71 |

appreciated from Fig. 5.12, is nonuniverval. Interestingly, it has a monotonic behavior with the variation of $T_c$. For the sake of convenient visualization we have plotted $C_2$, as a function of $T_c$, in Fig. 5.13. For $C_1$ $(= \gamma_0(\xi_0^-)^2)$, on the other hand, we obtain an

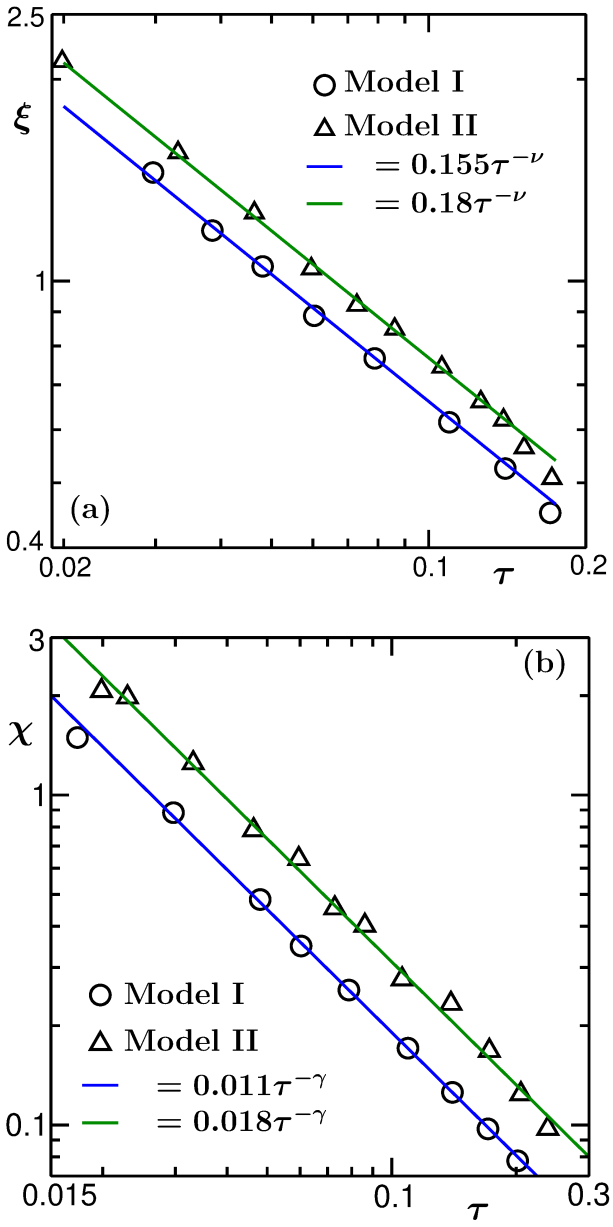


Fig. 5.11 (a) Log-log plots of the correlation length $\xi$ versus the reduced temperature $\tau$, for two different models, with $T < T_c$. The solid lines correspond to the critical divergence with exponent $\nu = 0.63$. The amplitudes are $\xi_0^- = 0.155$ for Model I and $\xi_0^- = 0.18$ for Model II. (b) Plots of concentration susceptibility $\chi$ versus the reduced temperature $\tau$ for $T < T_c$, on a log-log scale. The solid lines correspond to the critical behaviors with the exponent $\gamma = 1.239$.

average value 0.075, without a systematic dependence on $T_c$. The value is close to the theoretically predicted universal number [47, 48] 0.089.

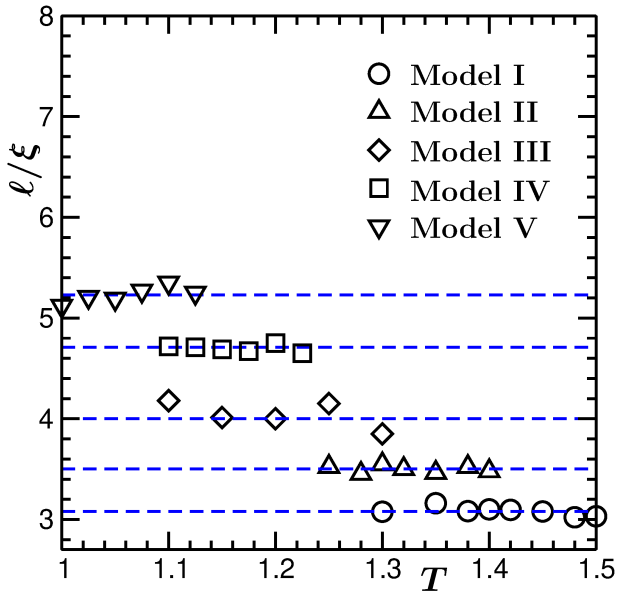


Fig. 5.12 The ratio $\ell/\xi$ is plotted against temperature. Results from different models are presented by choosing the temperatures close to the corresponding critical values. The data set for Model III is taken from [14, 37].

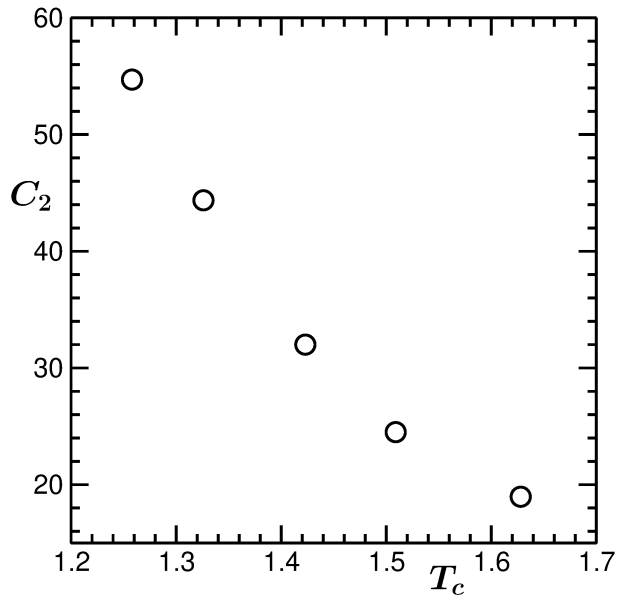


Fig. 5.13 Plot of nonuniversal constant, $C_2$, versus $T_c$, for different models. This is the central result of this work.

## 5.7 Conclusion

We have studied the equilibrium properties of phase coexistence in multiple models, that describe symmetric binary fluids, using successive umbrella sampling [57] Monte Carlo simulations in a semi-grand canonical ensemble [49]. Taking help of a recently developed thermodynamic method [13] surface tensions of curved interfaces have been calculated. It is seen that the leading order curvature correction is quadratic in nature [35] for the studied models.

A universal form, as described via Eq. (5.9) [14, 37], for critical behavior of curvature dependent interfacial tension has been seen to be obeyed by the considered models. The study strengthens the fact that the critical behavior of the quantity $\ell$, as introduced in Eq. (5.3), is similar to that of the correlation length [14, 37] which leads to the above mentioned critical behavior. The form in Eq. (5.9) is argued [14, 37] to be valid for asymmetric models also as the critical divergence of $\ell$ is much stronger than that of $\delta$ [32].

The expression in Eq. (5.9) contains two constants, viz., $C_1$ and $C_2$. Between these, $C_1$ is universal, but a conclusion on the nature of the other constant $C_2$ was not previously drawn via studies of a spectrum of models. We have performed systematic investigations with several different symmetric models and found that $C_2$ is a model dependent constant. Its value varies with the critical temperature of the model in a strong and monotonic fashion. Identification of a mathematical form we leave out for future.

For the above purpose we will perform similar studies for few other models by considering different values of the truncation radius. Also it will be interesting to study asymmetric mixtures and check whether the corresponding critical behavior of curvature dependent interfacial tension follows Eq. (5.9) and if so, then what is the nature of $C_2$. In the latter case it will be challenging to separate out $\delta$ and $\ell$ from the curvature dependent data.

Note that $\delta$ and $\ell$ are related to different measures of interface width. It is already interesting to have different critical singularities for these quantities. Observation of same critical exponent for $\ell$ and $\xi$ is important. However, the amplitude of $\ell$ having quite different model dependence than $\xi$ adds to the puzzle. This is interesting and requires attention.

# References


[1] M. Volmer and A. Weber, Z. Phys. Chem. **119**, 277 (1926).

[2] R. Becker and W. Döring, Ann. Phys. **416**, 719 (1935).

[3] Yu.B. Zeldovitch, Acta Physicochim. URSS **18**, 1 (1943).

[4] J. Frenkel, *Kinetic Theory of Liquids* (Dover, New York, 1955).

[5] F.F. Abraham, *Homogeneous Nucleation Theory* (Academic, New York, 1974).

[6] *Nucleation*, edited by A.C. Zettlemoyer (M. Dekker, New York, 1969).

[7] D. Kashchiev, *Nucleation: Basic Theory with Applications* (Butterworth-Heinemann, Oxford, 2000).

[8] K.F. Kelton and A.L. Greer, *Nucleation* (Pergamon, Oxford, 2009).

[9] K. Binder and M. H. Kalos, J. Stat. Phys. **22**, 363 (1980).

[10] H. Furukawa and K. Binder, Phys. Rev. A **26**, 556 (1982).

[11] K. Binder, Physica A **319**, 99 (2003).

[12] L. G. MacDowell, P. Virnau, M. Müller, and K. Binder, J. Chem. Phys. **120**, 5293 (2004).

[13] M. Schrader, P. Virnau, and K. Binder, Phys. Rev. E **79**, 061104 (2009).

[14] S.K. Das and K. Binder, Phys. Rev. E **84**, 061607 (2011).

[15] A. Statt, P. Virnau, and K. Binder, Phys. Rev. Lett. **114**, 026101 (2015).

[16] A. Tröster, F. Schmitz, P. Virnau, and K. Binder, J. Phys. Chem. B **122**, 3407 (2018).

[17] D. Winter, P. Virnau, and K. Binder, J. Phys.: Condens. Matter **21**, 464118 (2009).

[18] D. Winter, P. Virnau, and K. Binder, Phys. Rev. Lett. **103**, 225703 (2009).

[19] S.K. Das and K. Binder, Europhys. Lett. **92**, 26006 (2011).

[20] S.K. Das and K. Binder, Mol. Phys. **109**, 1043 (2011).

[21] L.D. Gelb, K.E. Gubbins, R. Radhakrishnan, and M Sliwinska-Bartkowiak, Rep. Prog. Phys. **62**, 1573 (1999).

[22] S. Basu, S. Majumder, S. Sutradhar, S.K. Das, and R. Paul, Europhys. Lett. **116**, 56003 (2016).

[23] J.S. Langer, Ann. Phys. **41**, 108 (1967).

[24] J.S. Langer, Ann. Phys. **54**, 254 (1969).

[25] K. Binder and D. Stauffer, Adv. Phys. **25**, 343 (1976).

[26] K. Binder, Phys. Rev. A **29**, 341 (1984).

[27] K. Binder, Rep. Prog. Phys. **50**, 783 (1987).

[28] J. Willard Gibbs, *Collected Works* (Longmans Green and Company, New York, 1928).

[29] R.C. Tolman, J. Chem. Phys. **16**, 758 (1948).

[30] R.C. Tolman, J. Chem. Phys. **17**, 118 (1949).

[31] R.C. Tolman, J. Chem. Phys. **17**, 333 (1949).

[32] M.A. Anisimov, Phys. Rev. Lett. **98**, 035702 (2007).

[33] E.M. Blokhuis and D. Bedeaux, J. Chem. Phys. **97**, 3576 (1992).

[34] M.J. Haye and C. Bruin, J. Chem. Phys. **100**, 556 (1994).

[35] M.P.A. Fisher and M. Wortis, Phys. Rev. B **29**, 652 (1984).

[36] B.J. Block, S.K. Das, M. Oettel, P. Virnau, and K. Binder, J. Chem. Phys. **133**, 154702 (2010).

[37] S.K. Das and K. Binder, Phys. Rev. Lett. **107**, 235702 (2011).

[38] E.M. Blokhuis and D. Dedeaux, Mol. Phys. **80**, 705 (1993).

[39] A.E. van Giessen, E.M. Blokhuis, and D.J. Bukman, J. Chem. Phys. **108**, 1148 (1998).

[40] M.E. Fisher, Rep. Prog. Phys. **30**, 615 (1967).

[41] M.E. Fisher, in *Critical Phenomena*, edited by M.S. Green (Academic, London, 1971).

[42] H.E. Stanley, *Introduction to Phase Transitions and Critical Phenomena* (Clarendon Press, Oxford, 1971).

[43] P.C. Hohenberg and B.I. Halperin, Rev. Mod. Phys. **49**, 435 (1977).

[44] V. Privman, P.C. Hohenberg, and A. Aharony, in *Phase Transitions and Critical Phenomena*, edited by C. Domb and J.L. Lebowitz (Academic Press, New York, 1991).

[45] J. Zinn-Justin, Phys. Rep. **344**, 159 (2001).

[46] K. Binder and E. Luijten, Phys. Rep. **344**, 179 (2001).

[47] M.E. Fisher and H. Wen, Phys. Rev. Lett. **68**, 3654 (1992).

[48] M. Hasenbusch and K. Pinn, Physica (Amsterdam) **192A**, 342 (1993).

[49] D.P. Landau and K. Binder, *A Guide to Mote Carlo Simulations in Statistical Physics* (Cambridge University Press, Cambridge, 2009).

[50] S.K. Das, J. Horbach, and K. Binder, J. Chem. Phys. **119**, 1547 (2003).

[51] S. Roy, S. Dietrich, and F. Höfling, J. Chem. Phys. **145**, 134505 (2016).

[52] M.P. Allen and D.J. Tildesly, *Computer Simulations of Liquids* (Clarendon, Oxford, 1987).

[53] D. Frenkel and B. Smit, *Understanding Molecular Simulations: From Algorithms to Applications* (Academic Press, San Diego, 2002).

[54] K. Binder, Z. Phys. B: Condens. Matter **43**, 119 (1981).

[55] E. Luijten, M.E. Fisher, and A.Z. Panagiotopoulos, Phys. Rev. Lett. **88**, 185701 (2002).

[56] (a) Y.C. Kim, M.E. Fisher, and E. Luijten, Phys. Rev. Lett. **91**, 065701 (2003); (b) Y.C. Kim and M.E. Fisher, Phys. Rev. E **68**, 041506 (2003); (c) Phys. Rev. Lett. **92**, 185703 (2004); (d) Comput. Phys. Commun. **169**, 295 (2005).

[57] P. Virnau and M. Müller, J. Chem. Phys. **120**, 10925 (2004).

[58] K. Binder, Phys. Rev. A **25**, 1699 (1982).

[59] M. Müller, K. Binder, and W. Oed, J. Chem. Soc., Faraday Trans. **91**, 2369 (1995).

[60] J. R. Errington, Phys. Rev. E **67**, 012102 (2003).

[61] P. Virnau, M. Müller, L.G. MacDowell, and K. Binder, J. Chem. Phys. **121**, 2169 (2004).

[62] F. Schmitz, P. Virnau, and K. Binder, Phy. Rev. E **90**, 012128 (2014).

[63] J.-P. Hansen and I.R. McDonald, *Theory of Simple Liquids* (Academic, London, 1986).

[64] A.B. Bhatia and D.E. Thornton, Phys. Rev. B **2**, 3004 (1970).

# Chapter 6

# Dependence of Interfacial Tension on Mean Radius of Curvature

## 6.1 Introduction

In nature the interface in a heterogeneous system can be of complex shape [1–7] where at a given point on the surface one can imagine multiple curvatures. In such a situation how the curvature dependence of thermodynamic quantities can be understood as a function of a single variable? Let us first discuss the necessary mathematical background to characterize an arbitrary surface.

At a point on a surface there are two principal radii of curvature $R_1$ $(= 1/\kappa_1)$ and $R_2$ $(= 1/\kappa_2)$ [8, 9]. At that point one can consider a unit normal vector $\vec{N}$ and a normal plane containing the vector. This plane will contain a tangent to the surface and cut the latter in the shape of a plane curve. The latter will possess varying curvatures with the change of normal planes at a point on the surface. The principal radii of curvature correspond to the largest and lowest values of these curvatures. This has been shown schematically in Fig. 6.1. For convenient illustration of this we will consider two simple cases, i.e., spherical and cylindrical surfaces, as presented in Fig. 6.2 (a) and (b), respectively.

At a particular point P, on the spherical surface, both the radii ($R_1$ and $R_2$) are positive and equal to the radius of the sphere. On the other hand, for the cylindrical case, one of these radii is infinite, i.e., the corresponding curvature is zero. In this case the other radius is equal to the radius of the curved surface. Another important case, which is not shown here, is a saddle-like surface where the principal curvatures have opposite signs. Below we discuss how these principal radii of curvature are typically combined to obtain important measures.

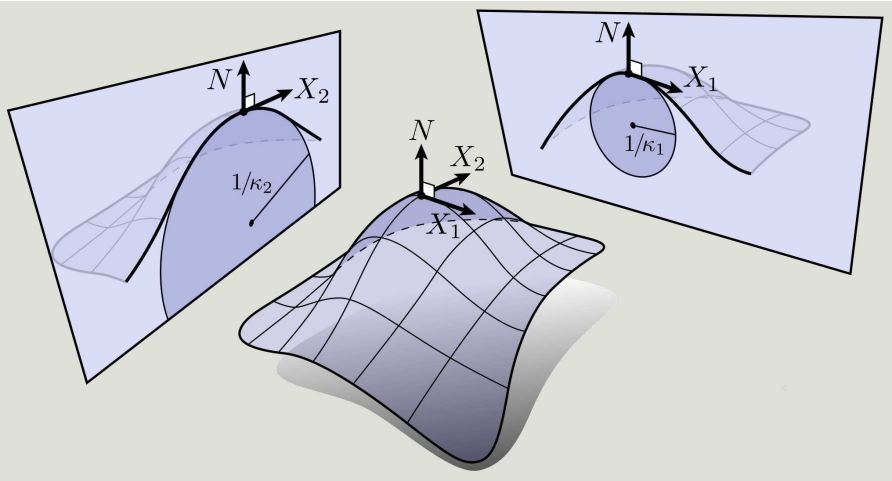


Fig. 6.1 The procedure of calculation of principal curvatures of an arbitrary surface has been illustrated. See text for description. Source: K. Crane, F. De Goes, M. Desbrun and P. Schröder, "Digital geometry processing with discrete exterior calculus" (ACM SIGGRAPH 2013 Courses) pp. 1-20 (2013). Reproduced with permission. ©incollectioncrane2013digital. https://www.cs.cmu.edu/~kmcrane/Projects/DDG/

First, we consider the Gaussian curvature. This is given by $1/R_G = 1/R_1R_2$, which is the product of these two curvatures. For example, the Gaussian curvature of a sphere, saddle and cylinder are positive, negative and zero, respectively. Next we discuss the mean curvature. This is the addition of the curvatures of these two curves, i.e., $1/R_m = 1/R_1 + 1/R_2$. Thus, $R_m$ for a cylinder is finite despite one of the principal radii being infinite. Combining the cases of sphere and cylinder we can write $R_m = aR$, where $a$, a scale factor, depends on the geometry of the surface, e.g., $a_s = 0.5$ (the subscript '$s$' corresponds to sphere) for spherical surface and $a_c = 1$ ('$c$' stands for cylinder) for cylindrical surface.

Let us write down the curvature dependence [10, 11], in the symmetric case [12–15], as discussed in the previous chapter, in terms of mean radius of curvature ($R_m$). We will consider the simple cases, viz., spherical and cylindrical interfaces. The reason behind choosing $R_m$ as the variable is that for both the geometries it has finite values, as discussed above. We can then express the dependence as

$$\gamma(R) = \frac{\gamma(\infty)}{1 + 2(\frac{\ell}{aR})^2}. \tag{6.1}$$

In this chapter we will investigate whether Eq. (6.1) can describe the curvature dependence of interfacial tension, for the values of $a = a_s = 0.5$ and $a = a_c = 1$, in unique

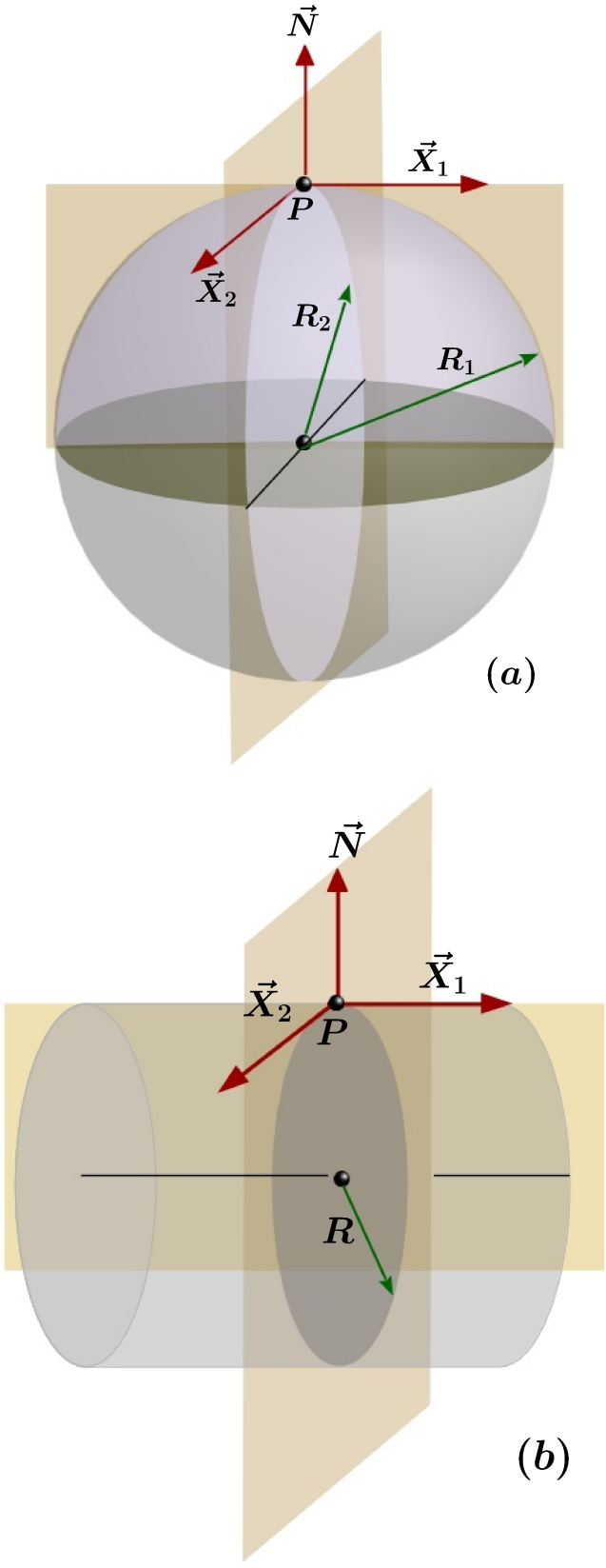


Fig. 6.2 (a) Schematic illustration of curvature related definitions for spherical surface. The planes of principal curvature and the corresponding radii at a point P on the surface are shown. (b) Same as (a) but here we illustrate the cylindrical case.

manner such that $R_m$ decides the value of curvature dependent interfacial tension. For this purpose we will perform simple scaling analyses.

## 6.2 Models

Like in the previous chapter we have used the Lennard-Jones potential [16] for the study in this chapter as well. We have considered both truncated-shifted and truncated-shifted-force-corrected versions [17, 18], with different overall densities. These are listed in table 6.1.

Table 6.1 Details of different models.

| Interaction potential | Overall density ($N/L^3$) | $T_c$ | Name of the model |
|---|---|---|---|
| tsLJ | 1.0 | 1.628 | Model I |
| | 0.7 | 1.509 | Model II |
| tsfLJ | 0.7 | 1.326 | Model III |
| | 0.65 | 1.258 | Model IV |

## 6.3 Methods

Similar to the previous chapter here also we have obtained the equilibrium configurations by simulating the model efficiently via successive umbrella sampling [19] in the semi-grand canonical ensemble [16].

The behavior of $f_L$, as described in the previous chapter, has been shown in the upper panel of Fig. 6.3, amending it in such a way that it appears more relevant for the present chapter. There the presence of kinks are due to the structural changes of the interface with the increase in $x_A$ [13–15, 20–23]. For very small value of $x_A$ the system is in bulk B-rich phase (corresponding to the left hand side minimum). Gradually, as the number of A-type particles is increased, an A-rich spherical droplet will appear in the B-rich background phase, indicated by the first sharp change in slope. The size of this droplet continues to increase as one moves further right until it takes the shape of a cylinder which is energetically more stable at a higher $x_A$, reflected as another sharp change. Finally as $x_A$ reaches close to the critical concentration 1/2, both the coexisting phases acquire slab geometries. The structural changes can be visualized more prominently from the sudden jumps in the behavior of chemical potential difference relative to the bulk coexistence that has been defined in the previous chapter.

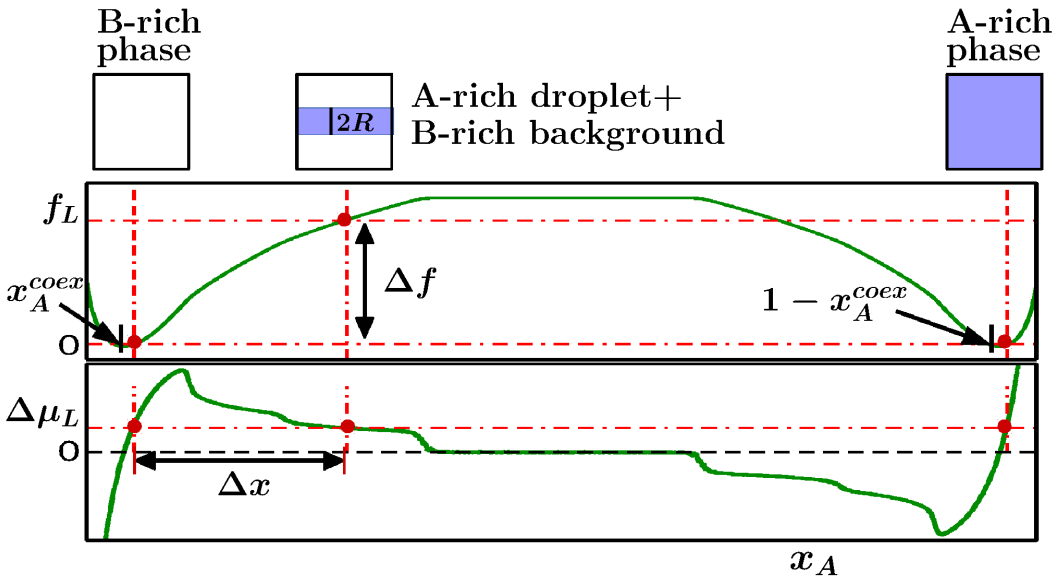


Fig. 6.3 The procedure of estimation of $\Delta x$ and $\Delta f$ from the plots of $f_L$ and $\Delta\mu$ has been shown schematically for the cylindrical interface. For details see text.

The calculation of $\gamma(R)$ has been illustrated in Fig 6.3 for a cylindrical A-rich droplet. Here first we have to identify the range of $x_A$ in $f_L$ plot where the A-rich cylindrical droplet is structurally stable. The bulk contribution can be estimated and subtracted from the total to obtain the excess free energy due to the presence of the curved interface:

$$V\Delta f = 2\pi RL\gamma(R). \tag{6.2}$$

Note that by construction the cylinder has the length same as the linear dimension of the system so that it has volume and surface area as $\pi R^2 L$ and $2\pi RL$, respectively. According to a lever rule [23, 24] the related concentration difference can be written as

$$\Delta x = \pi R^2 L \frac{[1 - 2x_A^{\rm coex}]}{V}. \tag{6.3}$$

From the set-up and simulations the quantities $\Delta f$, $V$, $\Delta x$ and $x_A^{\rm coex}$ are known. Therefore from Eqs. (6.2) and (6.3) one estimates $R$ and $\gamma(R)$.

## 6.4 Results and Discussion

In Fig. 6.4 we have plotted $\frac{\gamma(\infty)}{\gamma(R)} - 1$ versus $1/R^2$ for interfaces corresponding to two different geometrical structures (sphere and cylinder), for various system sizes to explore

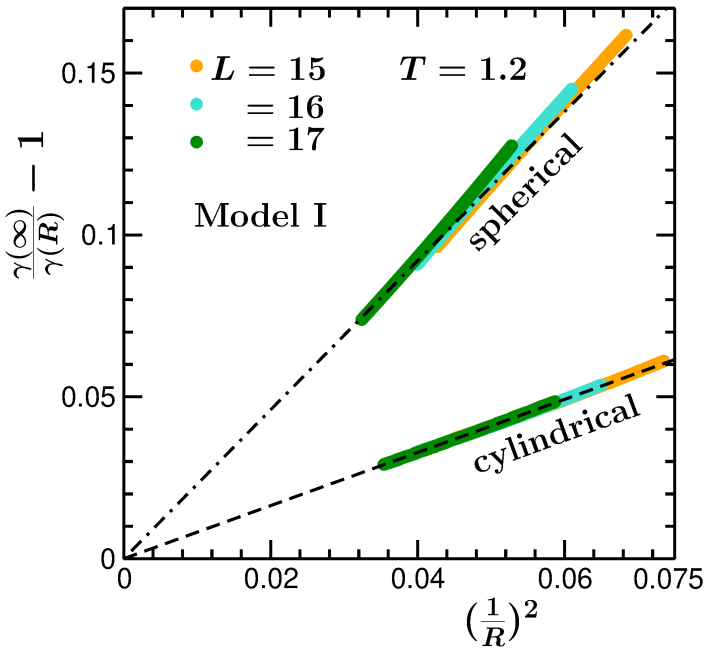


Fig. 6.4 Plots of $\frac{\gamma(\infty)}{\gamma(R)} - 1$ versus $1/R^2$ for two different geometries of the interface at temperature $T = 1.2$ for Model I.

a wide range of $R$, at temperature $T = 1.2$ for Model I. Data for different system sizes superimpose on straight lines, represented by the broken lines. These converge to zero and validate Eq. (5.3), for both the geometries. This is expected for symmetric systems [12–14].

Despite this, there exists difference between the two cases in the slopes. The origin of the difference may lie in $\ell$. It is also possible that the discrepancy will get away if the curvature dependence is described in terms of the mean radius. Below we take the latter route first.

In order to check whether the curvature dependence can be expressed as a function of mean radius ($R_m$), we have performed a simple scaling exercise, as hinted previously. If one multiplies the abscissas of the plots in Fig. 6.4 by $1/a^2$, where the scale factor $a = a_c = 1$ for the cylindrical and $a = a_s = 0.5$ for the spherical interface, then both the scaled plots may fall onto a single straight line. The outcome of this exercise for Model I, at $T = 1.2$, is shown in Fig. 6.5. It is observed that the collapse of the data sets along the same line did not occur.

Next we replace $a_s$ by $b_s$, the reason being described below, and treat it as an adjustable parameter, by keeping $a_c$ fixed at 1. The best collapse has been obtained for

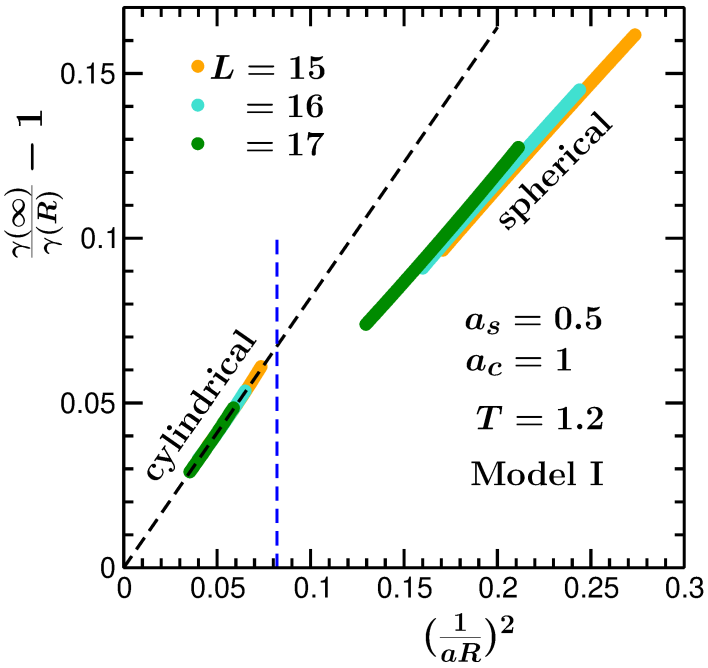


Fig. 6.5 Same as Fig. 6.4. But here the abscissa for the results on spherical curvature has been scaled with factor $1/a^2$ with $a = a_s = 0.5$.

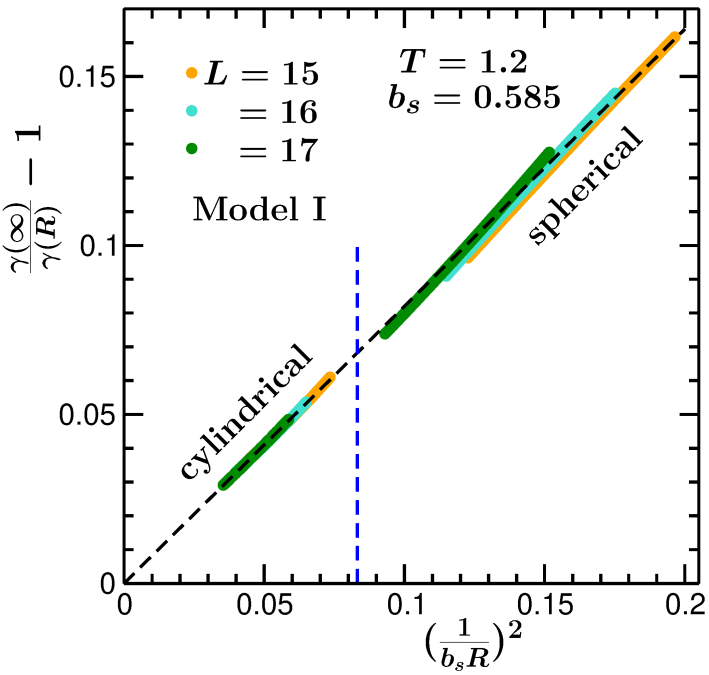


Fig. 6.6 Same as Fig. 6.5 but here we have used $b_s = 0.585$. See text for the definition of $b_s$.

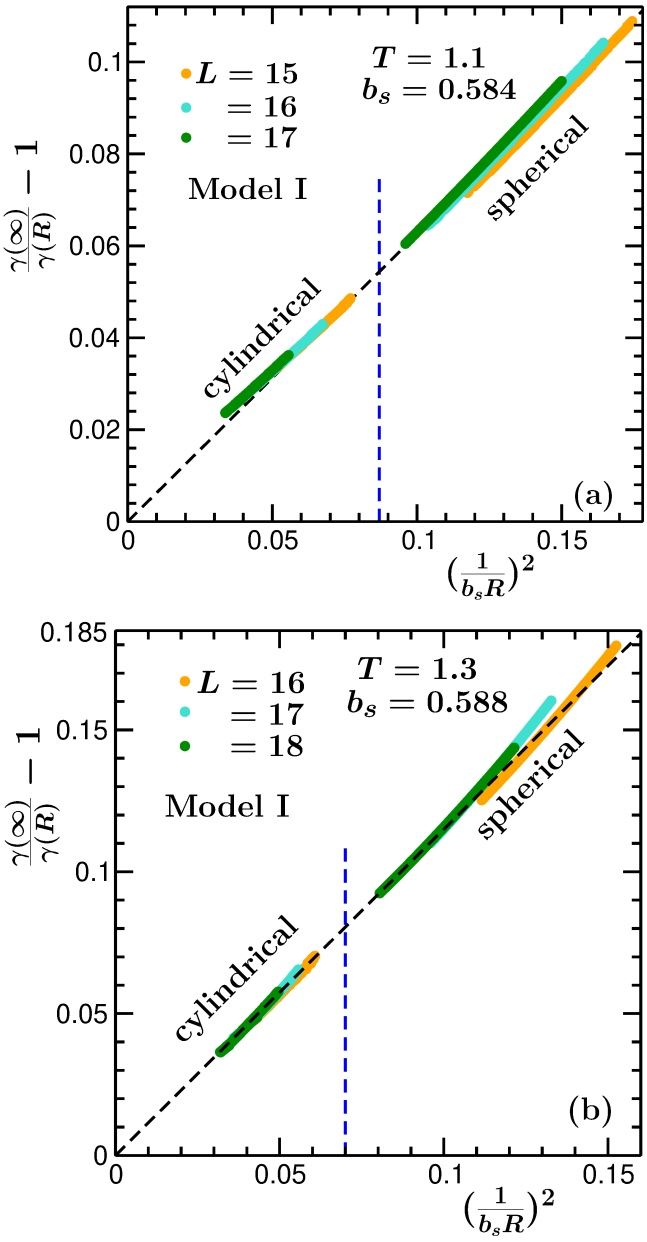


Fig. 6.7 (a) Similar exercises as in Fig. 6.6 have been performed for temperature $T = 1.1$ with $b_s = 0.584$. (b) Same as (a) with $T = 1.3$ and $b_s = 0.588$. Both results are for Model I.

$b_s = 0.588$. This is shown in Fig. 6.6. The value 0.588 is at about 18% deviation from the "expected" value 0.5. If this difference is real one needs to discuss its possible origin.

If the deviation remains same for different models and temperatures, it is likely that it is real. This will also imply that critical exponents for $\ell$ in both the cases, i.e., for spherical and cylindrical geometries, are same but there possibly exists difference in the amplitudes. In that case, by writing $b_s = a_s/\ell_0$, with $a_s = 0.5$, the value by mathematical construction, $b_s = 0.59$ would mean that $\ell_0$, the critical amplitude of $\ell$, is different for the spherical shape of droplets from the cylindrical case. Note that this exercise effectively implies that we have fixed $\ell_0$ for the cylindrical case at 1.

To check for the above we have done the similar exercise for other temperatures, as demonstrated in Fig. 6.7 (a) and (b), again for Model I. In each of these cases $b_s$ remains same and different from the theoretical value of $a_s$. Inspired by this we have performed similar exercise for different models. In table 6.2 we have listed the values of $b_s$ obtained from the best collapse of the data sets, for different models as well as for different temperatures. The deviation is about 20% in each of the cases. Note that, as understood, throughout the study the value of $a_c$ is kept fixed at unity.

Table 6.2 List of the values of $b_s$ for different models.

| | Model I | | | Model II | | | Model III | | | Model IV | | |
|---|---|---|---|---|---|---|---|---|---|---|---|---|
| T | 1.1 | 1.2 | 1.3 | 1.0 | 1.1 | 1.2 | 1.0 | 1.05 | 1.1 | 0.9 | 0.95 | 1.0 |
| $b_s$ | 0.58 | 0.59 | 0.59 | 0.6 | 0.58 | 0.59 | 0.61 | 0.59 | 0.6 | 0.58 | 0.59 | 0.61 |

## 6.5 Conclusion

We have studied the coexistence pictures in different models of symmetric liquid mixtures at temperatures lower than the corresponding $T_c$ values. For this purpose we have performed Monte Carlo simulations in the semi-grand canonical ensemble [16]. To overcome certain free energy barrier successive umbrella sampling [19] technique has been used. We have brought in the gradual structural change of the interface, from spherical to cylindrical to slab-like, between A-rich and B-rich coexisting phases, with the increase in number of A-type particles in the system.

The curvature dependence of interfacial tension has been studied for two different geometries, viz., sphere and cylinder. It is seen that for both the cases, with a difference in the slopes, the leading order correction is quadratic in nature. This validates the

applicability of Eq. (5.3). Now the question is whether one can construct a generic form of $\gamma(R)$ for an arbitrary surface by using mean radius of curvature $R_m$ as a variable.

To check the validity of such a description we have performed simple scaling analyses and found that there exist uniform mismatch of about 20% between the results obtained from the simulation and the expectation. We believe that this is due to a difference in the critical amplitudes between the two geometries.

# References


[1] D. Winter, P. Virnau, and K. Binder, Phys. Rev. Lett. **103**, 225703 (2009).

[2] S.K. Das and K. Binder, Europhys. Lett. **92**, 26006 (2011).

[3] S.K. Das and K. Binder, Mol. Phys. **109**, 1043 (2011).

[4] L.D. Gelb, K.E. Gubbins, R. Radhakrishnan, and M Sliwinska-Bartkowiak, Rep. Prog. Phys. **62**, 1573 (1999).

[5] S. Basu, S. Majumder, S. Sutradhar, S.K. Das, and R. Paul, Europhys. Lett. **116**, 56003 (2016).

[6] R. Shimizu and H. Tanaka, Science Advances **3**, 12 (2017).

[7] M. Wang, Z. Cui, and Y Xue, Langmuir **37**, 14463 (2021).

[8] M.P. do Carmo, *Differential Geometry of Curves and Surfaces* (Dover Publication, Mineola, NY, 2016).

[9] M. Spivak, *A comprehensive introduction to differential geometry* (Volumes 3-4) (3rd ed., Publish or Perish Press, Boston, 1999).

[10] J. Willard Gibbs, *Collected Works* (Longmans Green and Company, New York, 1928).

[11] R.C. Tolman, J. Chem. Phys. **17**, 333 (1949).

[12] M.P.A. Fisher and M. Wortis, Phys. Rev. B **29**, 652 (1984).

[13] B.J. Block, S.K. Das, M. Oettel, P. Virnau, and K. Binder, J. Chem. Phys. **133**, 154702 (2010).

[14] S.K. Das and K. Binder, Phys. Rev. E **84**, 061607 (2011).

[15] S.K. Das and K. Binder, Phys. Rev. Lett. **107**, 235702 (2011).

[16] D.P. Landau and K. Binder, *A Guide to Mote Carlo Simulations in Statistical Physics* (Cambridge University Press, Cambridge, 2009).

[17] M.P. Allen and D.J. Tildesly, *Computer Simulations of Liquids* (Clarendon, Oxford, 1987).

[18] D. Frenkel and B. Smit, *Understanding Molecular Simulations: From Algorithms to Applications* (Academic Press, San Diego, 2002).

[19] P. Virnau and M. Müller, J. Chem. Phys. **120**, 10925 (2004).

[20] K. Binder, Physica A **319**, 99 (2003).

[21] L.G. MacDowell, P. Virnau, M. Müller, and K. Binder, J. Chem. Phys. **120**, 5293 (2004).

[22] L.G. MacDowell, V.K. Shen, and J.R. Errington, J. Chem. Phys. **125**, 034705 (2006).

[23] M. Schrader, P. Virnau, and K. Binder, Phys. Rev. E **79**, 061104 (2009).

[24] M. Schrader, P. Virnau, D. Winter, T. Zykova-Timan and K. Binder, Eur. Phys. J. Spec. Top. **177**, 103 (2009).

# Chapter 7

# Summary of the Thesis

This thesis deals with the investigation of various thermodynamic and dynamic aspects of phase separations in binary (A+B) mixtures. The background related to the problems are provided in Chapter 1.

In Chapter 2 we have studied the influence of long-range initial spatial correlation on aging dynamics during phase separation in solid mixtures in space dimension $d = 2$. For this purpose, we have used the Ising model, with nearest neighbor interaction, on a square lattice and performed Kawasaki exchange Monte Carlo simulations. To achieve the long rage correlation we have prepared systems at starting temperature $T_s =$"$T_c$"and quenched them to the final temperature $T_f = 0.6T_c$. During the coarsening process we have probed the order-parameter autocorrelation function, $C_{\rm ag}(t, t_w)$, which is a key quantity for the study of aging phenomena in nonequilibrium systems. We have found that the decay of $C_{\rm ag}(t, t_w)$, which is quantified by the power-law exponent $\lambda$, was significantly slower than that for the quenches from the random initial configurations. In Fig. 7.1(a) we have plotted $C_{\rm ag}(t, t_w)$ as a function of $\ell/\ell_w$, for quenches from two different $T_s$ values, viz., $T_s = T_c$ and $\infty$. Here $\ell$ and $\ell_w$ correspond to average the domain lengths at observation and waiting times $t$ and $t_w$, respectively. The values of $\lambda$ for both the cases have been mentioned inside the frame. We have studied the structure to explain the appearance of such a small value of aging exponent [1] in the case of quenches from $T_c$.

The above study has been extended in Chapter 3. There the same model has been considered in dimension $d = 3$. In this case also $\lambda$ is found to be much smaller than that for the quench from random initial state. This is depicted in Fig. 7.1(b). These results state that universality in coarsening dynamics can be classified based on the extent of spatial correlation present in the initial configurations [2].

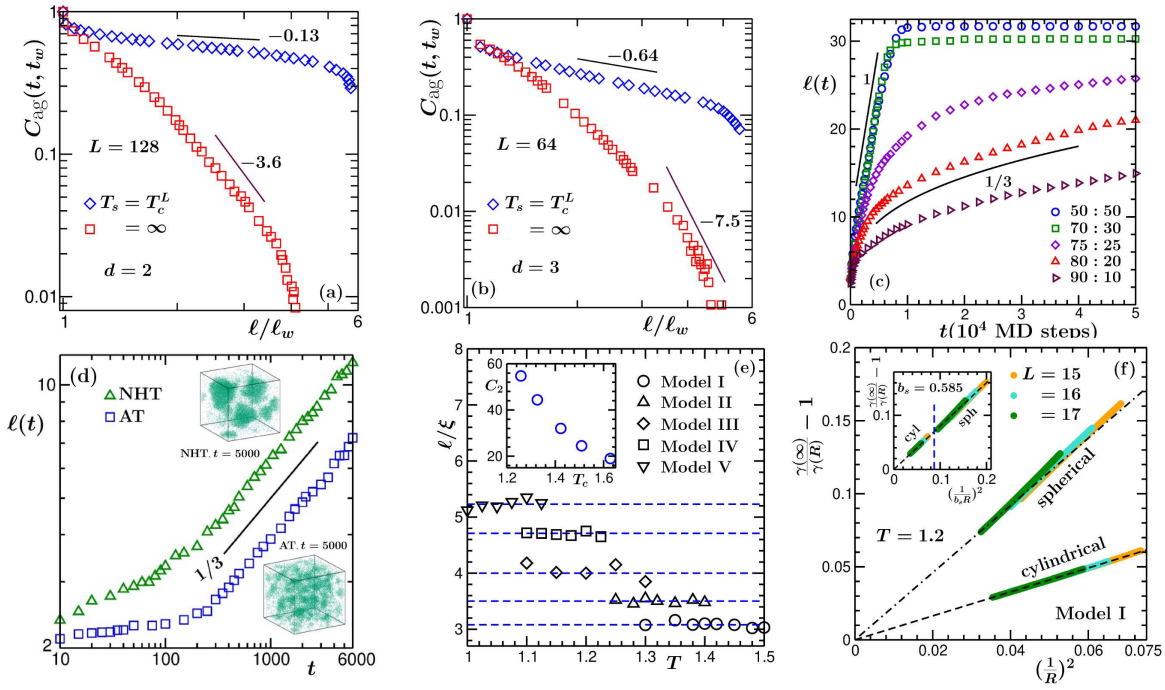


Fig. 7.1 (a) Plots of $C_{\rm ag}(t, t_w)$ versus $\ell/\ell_w$, the ratio of domain lengths at observation and waiting times $t$ and $t_w$, respectively, on a log-log scale, for quenches from $T_s = T_c^L$ and $T_s = \infty$, for Ising system, with size $L = 128$ in dimension $d = 2$, to $T_f = 0.6T_c$. Here $T_c^L$ is the finite-size critical temperature. (b) Same as (a) for system size $L = 64$ in dimension $d = 3$. (c) Average domain lengths, $\ell(t)$, are shown with the variation of time, for quenched binary liquid systems having different compositions of A and B particles, from random configurations. The solid lines represent power-laws with mentioned exponents. These results were obtained via the application of hydrodynamics preserving Nosé-Hoover thermostat (NHT). (d) Plots of $\ell$ versus time, on a log-log scale, for binary liquids. Here we have compared the results obtained via the applications of NHT with those obtained by using Andersen thermostat (AT). These results are for the composition 80 : 20. The solid line is a power-law with exponent 1/3. The evolution snapshots at late time for both the thermostats are shown in small frames. (e) Plots of $\ell/\xi$ versus temperature, for different models of binary liquid mixture. Here $\ell$ is a length corresponding to curvature correction to interfacial tension and $\xi$ is the equilibrium correlation length. In the inset we present the variation of a constant, $C_2$, that appears in the expression of critical behavior of curvature dependent interfacial tension $\gamma(R)$, against $T_c$. (f) Plots of $\gamma(\infty)/\gamma(R) - 1$ versus $1/R^2$ for different system sizes in the cases of spherical and cylindrical droplets, $\gamma(\infty)$ being the flat interfacial tension. Inset shows certain scaled plots for the same.

In Chapter 4 we have studied kinetics of phase separation in a high density symmetric binary fluid model, by varying compositions from critical to extreme off-critical values, via molecular dynamics simulations with hydrodynamics preserving Nose-Hoover thermostat. While around the symmetric composition a bicontinuous domain morphology is observed, with the linear viscous hydrodynamic growth, for compositions close to the branches of the coexistence curve the domain morphology consists of disconnected droplets of the minority phase with the the majority species in the background. In Fig. 7.1(c) we have shown $\ell$ versus $t$ plots for several different compositions. Late time behavior, for compositions far away from the critical value, is consistent with the exponent $\alpha = 1/3$. Our objective was to understand the mechanism for the latter. Via the calculations of mean-squared-displacements of the centres of mass of the droplets, we show that these droplets exhibit diffusive motion. Due to sticky collisions among themselves, the number density of these objects decreases, thereby the characteristic length scale increases [3]. We have found that the number of constituent particles in these droplets remain practically fixed between collisions. Thus, the observed value $\alpha = 1/3$ is due to the diffusive coalescence mechanism. These results were compared with those obtained via the application of a stochastic thermostat which mimics the coarsening in solid binary mixtures. In this case the droplets are practically static and growth occurs via particle diffusion from smaller to larger droplets. Although the exponent remains same in both the cases, as shown in Fig. 7.1(d), the ratio of the growth amplitudes in the two cases suggests that the hydrodynamic growth is faster [3].

Till Chapter 4 we have studied the nonequilibrium aspects of phase separation. In Chapters 5 and 6 we have undertaken the studies of equilibrium properties of liquid-liquid phase coexistence in multiple models of symmetric binary fluids. For this we use a successive umbrella sampling technique in Monte Carlo simulations in semi-grand canonical ensembles.

Using an advanced thermodynamic method, surface tensions of curved interfaces have been calculated from the simulation data. In Chapter 5 we deal with spherical interface. It is seen that the leading order curvature correction is quadratic in nature. The critical behavior of the quantity $\ell$, a length associated with this correction term, is similar to that of the correlation length. This is depicted in the main frame of Fig. 7.1(e). A universal form for critical behavior of curvature dependent interfacial tension has been seen to be obeyed by the results from all considered models. This form contains two constants, viz., $C_1$ and $C_2$. Between these, $C_1$ is universal, but a conclusion on the nature of the other constant $C_2$ was not previously drawn via studies of different models.

Via systematic investigations we conclude that $C_2$ is model dependent. Its value varies with the critical temperature of the model in a strong monotonic fashion [4], as shown in the inset of Fig. 7.1(e).

In Chapter 6 we analyze the results from spherical as well as cylindrical geometries and find that for both the cases curvature correction is quadratic in nature. This is shown in the main frame of Fig. 7.1(f). However, the results for these two cases differ in the slopes. This difference reduces if one expresses the curvature dependence in terms of the mean radius. From such an exercise we observe that there exists about 20% difference between the expectation and results obtained from the simulation. We speculate that this discrepancy is due to the difference in the critical amplitude of the quantity $\ell$ for these two cases [5]. If this fact is true adjusted results for spherical and cylindrical geometries should fall on the same straight line for all models and temperatures for the same value of the corresponding scaling factor – see the inset of Fig. 7.1(f) for a representative example.

In future we would like to obtain a better quantitative understanding of dependence of $C_2$ on $T_c$. We will also investigate why the critical amplitude of $\ell$ in the spherical and cylindrical cases should differ.

# References


[1] S.K. Das, K. Das, N. Vadakkayil, S. Chakraborty, and S. Paul, J. Phys.: Condens. Matter **32**, 184005 (2020).

[2] K. Das, N. Vadakkayil, and S.K. Das, Phys. Rev. E **101**, 062112 (2020).

[3] K. Das and S.K. Das, arXiv:2107.10698 (2021).

[4] K. Das and S.K. Das, Manuscript under preparation.

[5] K. Das and S.K. Das, Manuscript under preparation.

**Zimbra** **koyeldas@jncasr.ac.in**

**Re: seeking permission to reuse the parts of text and figures of our paper**

**From :** Permissions <permissions@ioppublishing.org> Fri, Dec 17, 2021 09:29 PM
**Subject :** Re: seeking permission to reuse the parts of text and figures of our paper
**To :** koyeldas@jncasr.ac.in
**Cc :** das <das@jncasr.ac.in>, nalina <nalina@jncasr.ac.in>, paul <paul@itp.uni-leipzig.de>, chakrabortys@mpip-mainz.mpg.de

Dear Koyel Das,

Thank you for your email and for taking the time to seek this permission.

When you transferred the copyright in your article to IOP, we granted back to you certain rights, including the right to include all or part of the Final Published Version of the article within any thesis or dissertation. Please note you may need to obtain separate permission for any third party content you included within your article.

Please include citation details, "© IOP Publishing. Reproduced with permission. All rights reserved" and for online use, a link to the Version of Record.

The only restriction is that if, at a later date, you wanted your thesis/dissertation to be published commercially, further permission would be required.

I wish you the best of luck with the completion of your thesis/dissertation.

Kind regards,

Sophie

**Copyright & Permissions Team**

Sophie Brittain - Rights & Permissions Assistant
Cameron Wood - Legal & Rights Adviser
Contact Details
E-mail: permissions@ioppublishing.org

For further information about copyright and how to request permission:
https://publishingsupport.iopscience.iop.org/copyright-journals/
See also: https://publishingsupport.iopscience.iop.org/
Please see our Author Rights Policy https://publishingsupport.iopscience.iop.org/author-rights-policies/
**Please note**: We do not provide signed permission forms as a separate attachment. Please print this email and provide it to your publisher as proof of permission. **Please note**: Any statements made by IOP Publishing to the effect that authors do not need to get permission to use any content where IOP Publishing is not the publisher is not

intended to constitute any sort of legal advice. Authors must make their own decisions as to the suitability of the content they are using and whether they require permission for it to be published within their article.

---

**From:** koyeldas@jncasr.ac.in <koyeldas@jncasr.ac.in>
**Sent:** 17 December 2021 07:10
**To:** Permissions <permissions@ioppublishing.org>
**Cc:** das <das@jncasr.ac.in>; nalina <nalina@jncasr.ac.in>; paul <paul@itp.uni-leipzig.de>; chakrabortys@mpip-mainz.mpg.de <chakrabortys@mpip-mainz.mpg.de>
**Subject:** seeking permission to reuse the parts of text and figures of our paper

Respected Madam/Sir,

I am Koyel Das, a Ph. D. student working with Prof. Subir K. Das, from Theoretical Sciences Unit, Jawaharlal Nehru Centre for Advanced Scientific Research, Bangalore, India. I am writing this to seek permission to include parts of the text and figures of a paper that was published in Journal of Physics: Condensed Matter, that I co-authored, in my thesis (titled 'Investigations of Thermodynamics and Dynamics in Phase Separating Mixtures'). The details of the paper are given below:

"Initial correlation dependence of aging in phase separating solid binary mixtures and ordering ferromagnets", Subir K. Das, Koyel Das, Nalina Vadakkayil, Saikat Chakraborty, and Subhajit Paul, J. Phys.: Condens. Matter **32**, 184005 (2020).

This will be used only for academic purposes. So, I request you to kindly give me the permission to reuse the parts of text and figures.

Your sincerely,
Koyel Das

---

December 2017

# APS Copyright Policies and Frequently Asked Questions



## What is copyright? http://www.copyright.gov/ (http://www.copyright.gov/)

Copyright is a form of legal protection for original works of authorship. Copyright covers both published and unpublished works.

## What does copyright protect?

Copyright, a form of intellectual property law, protects original works of authorship including literary, dramatic, musical, and artistic works, such as poetry, novels, movies, songs, computer software, and architecture. Copyright does not protect facts, ideas, systems, or methods of operation, although it may protect the way these things are expressed. See Circular 1, Copyright Basics, section "What Works Are Protected", see http://www.copyright.gov/circs/circ01.pdf (http://www.copyright.gov/circs/circ01.pdf)

## How is a copyright different from a patent or a trademark?

Copyright protects original works of authorship, while a patent protects inventions or discoveries. Ideas and discoveries are not protected by the copyright law, although the way in which they are expressed may be. A trademark protects words, phrases, symbols, or designs identifying the source of the goods or services of one party and distinguishing them from those of others.

## What is the difference between copyright infringement and plagiarism?

Copyright infringement occurs when an author's work is reused or republished without the permission of the copyright owner, whether or not author attribution accompanied the reuse.

Plagiarism occurs when an author's work has been reused or republished in such a manner as to make it appear as someone else's work, e.g., without quotation marks and citation of the original work.

### Why should I transfer copyright to APS?

Like many other scientific publishers, the American Physical Society (APS) requires authors or their employers to provide transfer of copyright prior to publication. This permits APS to publish the article and to defend against improper use (or even theft) of the article. It also permits APS to publish the article online and to use the article in other forms or media, such as PROLA. By the APS transfer agreement, authors and their employers retain substantial rights in the work, as specified in the agreement https://journals.aps.org/authors/transfer-of-copyright-agreement (https://journals.aps.org/authors/transfer-of-copyright-agreement) and discussed in your copyright permission letter.

### Why should I transfer copyright to APS before the article is accepted for publication by an APS journal?

Transferring copyright early in the process avoids the possibility of delaying publication if the transfer has to be obtained later in the process. As stated in the terms of the copyright transfer agreement, transfer does not take effect until the paper is accepted by an APS journal. The author retains the copyright until acceptance, and has the full freedom, for example, to withdraw the paper from consideration by an APS journal and submit it elsewhere.

### Does transferring copyright affect my patent rights?

No. Copyright is separate from any patent rights, and the APS transfer agreement specifically states that patent rights are not affected. However, you should be aware that submitting a manuscript to a journal without first taking steps to protect your patent rights (e.g., filing for a patent) could endanger those rights. Consult your patent attorney.

### As the author of an APS-published article, may I post my article or a portion of my article on my own website?

Yes, the author or the author's employer may use all or part of the APS published article, including the APS-prepared version (e.g., the PDF from the online journal) without revision or modification, on the author's or employer's website as long as a fee is not charged. If a fee is charged, then APS permission must be sought. In all cases, the appropriate bibliographic citation and notice of the APS copyright must be included.

### What happens if the author has posted an APS-published article on a free access e-print server or on the authors' or institutions' web page and subsequently a fee is imposed for access to those sites?

When a fee is imposed, the author must either obtain permission from APS or withdraw the article from the e-print server or Institutional Repository.

### As the author of an APS-published article, may I post my article or a portion of my article on an e-print server?

The author has the right to post and update the article on a free-access e-print server using files prepared and formatted by the author. Any such posting made or updated after acceptance of the article for publication by APS should include a link to the online APS journal article abstract. In all cases, the appropriate bibliographic citation and notice of the APS copyright must be included.

### As the author of an APS-published article, can I post my article or a portion of my article on a web resource like wikipedia or quantiki?

Sites like wikipedia and quantiki are strict about permissions and require that authors hold copyright to articles that they post there. In order to allow authors to comply with this requirement, APS permits authors to hold copyright to a “derived work” based on an article published in an APS journal as long as the work contains at least 10% new material not covered by APS's copyright and does not contain more than 50% of the text (including equations) of the original article. The APS will extend the author of a “derived work” the right to all papers published in APS journals.

### As the author (or the author's employer) of an APS-published article, may I use copies of part or all of my article in the classroom?

Yes, the author or his/her employer may use all or part of the APS-prepared version for educational purposes without requesting permission from the APS as long as the appropriate bibliographic citation is included.

### As the author of an APS-published article, may I use figures, tables, graphs, etc. in future publications?

Yes, as the author you have the right to use figures, tables, graphs, etc. in subsequent publications using files prepared and formatted by you or the APS-prepared versions. The appropriate bibliographic citation must be included.

### As the author of an APS-published article, may I include my article or a portion of my article in my thesis or dissertation?

Yes, the author has the right to use the article or a portion of the article in a thesis or dissertation without requesting permission from APS, provided the bibliographic citation and the APS copyright credit line are given on the appropriate pages.

### As the author of an APS-published article, may I give permission to a colleague or third party to republish all or part of the article in a print publication?

Yes, as the author you may grant permission to third parties to republish print versions of the article provided the APS-published version (e.g., the PDF from the online journal, or a copy of the article from the print journal) is not used for this purpose. The article may not be published in another journal, and the third party may not charge a fee. The appropriate bibliographic citation and notice of the APS copyright must be included.

### As the author of an APS-published article, may I give permission to a colleague or third party to republish all or part of the APS-published version in an online journal, book, database compilation, etc.?

No, an author may not grant permission in this case. To request permission to republish APS-copyrighted material, please refer to the "Reuse & Permissions" link that can be found on each APS article page.

### As the author of an APS-published article, may I provide a PDF of my paper to a colleague or third party?

The author is permitted to provide, for research purposes and as long as a fee is not charged, a PDF copy of his/her article using either the APS-prepared version or the author prepared version.

### As a third party (not an author), may I republish an article or portion of an article published by APS?

Yes, APS will grant permission to republish articles or portions of articles (e.g., tables, graphs, excerpts) published by APS. Depending on the reuse and medium APS has the right to grant permission subject to APS terms and conditions and a fee may be assessed.

### As a third party, may I use articles published by APS for lecture and classroom purposes?

Yes, you may use photocopied articles published by APS for lecture and classroom purposes without asking permission from APS as long as you remain an Authorized User of the APS online research per your institution's site license. Also, there is no limitation on the use of APS articles using links to the material accessible through institutional subscriptions.

### How do I request permission to republish APS-copyrighted material?

APS uses Aptara's SciPris™ platform to manage rights and permission requests. APS will continue to support the STM guidelines for all copyright needs. To request permission to republish APS-copyrighted material, please refer to the "Reuse & Permissions" link that can be found on each APS article page.

Once directed to the SciPris™ platform, the following information is required:

1. The format in which the material will be republished, e.g., print, online, CD-ROM, and/or other format
2. How much of the article you want to republish, e.g., all or portion of article; if a portion describe the specific material, e.g., figure numbers, excerpt
3. How the material will be used, e.g., in a book, journal, proceeding, thesis, etc.
4. The title of the article/thesis/chapter etc., and the name of the publication in which your work will appear
5. The name of the publisher
6. Indicate whether or not a fee will be charged for the publication

Upon submission, a letter of permission will be generated, specifying all guidelines and regulations to follow.

Blanket permissions are not granted. Please note all requests are subject to APS terms and conditions (/info/terms.html) and a fee may be assessed.

If your questions have not been addressed and you need further assistance, please email customercare@aps.org (mailto:customercare@aps.org).

### Further information

For further information about copyright in general, please refer to the Library of Congress FAQ at https://www.copyright.gov/help/faq/ (https://www.copyright.gov/help/faq/)

Journals published by the American Physical Society can be found at https://journals.aps.org/ (https://journals.aps.org/).

FAQ Version: December 12, 2017

APS (https://www.aps.org/) | News & Announcements (/edannounce) | Join APS (https://www.aps.org/membership/join.cfm)
(https://www.facebook.com/apsphysics) (https://twitter.com/APSphysics)

**AUTHORS**

General Information (/authors)
Submit a Manuscript (https://authors.aps.org/Submissions/)
Publication Rights (/pub_rights.html)
Open Access (/open_access.html)
Tips for Authors (/authors/tips-authors-physical-review-physical-review-letters)
Professional Conduct (/authors/professional-conduct-ethics)

**REFEREES**

General Information (/referees)
Submit a Report (http://referees.aps.org/)
Update Your Information (http://referees.aps.org/)
Referee FAQ (/referees/faq.html)
Outstanding Referees (/OutstandingReferees)

**LIBRARIANS**

General Information (https://librarians.aps.org/)
Subscriptions (https://librarians.aps.org/subscriptions)
Online License Agreement (https://librarians.aps.org/sitelicense.pdf)
Usage Statistics (http://counter.aps.org/)
Your Account (https://librarians.aps.org/account)

**STUDENTS**

Physics (https://physics.aps.org)
PhysicsCentral (http://www.physicscentral.com/)
Student Membership (https://www.aps.org/membership/student.cfm)

**APS MEMBERS**

Subscriptions (https://www.aps.org/membership/aps-publications.cfm)
Article Packs (https://journals.aps.org/article-packs)
Membership (https://www.aps.org/membership/index.cfm)
FAQ (https://www.aps.org/membership/faq.cfm)
APS News (https://www.aps.org/publications/apsnews/index.cfm)
Meetings & Events (https://www.aps.org/meetings/index.cfm)

Privacy (https://www.aps.org/about/webpolicies.cfm#privacy) Policies (/policies) Contact Information (/contact.html) Feedback (mailto:feedback@aps.org)

# American Physical Society
# Reuse and Permissions License

04-Dec-2021

This license agreement between the American Physical Society ("APS") and Koyel Das ("You") consists of your license details and the terms and conditions provided by the American Physical Society and SciPris.

## Licensed Content Information

| | |
|---|---|
| **License Number:** | **RNP/21/DEC/047501** |
| **License date:** | 04-Dec-2021 |
| **DOI:** | 10.1103/PhysRevLett.107.235702 |
| **Title:** | Universal Critical Behavior of Curvature-Dependent Interfacial Tension |
| **Author:** | Subir K. Das and Kurt Binder |
| **Publication:** | Physical Review Letters |
| **Publisher:** | American Physical Society |
| **Cost:** | USD $ 0.00 |

## Request Details

**Does your reuse require significant modifications**: No

| | |
|---|---|
| **Specify intended distribution locations:** | Worldwide |
| **Reuse Category:** | Reuse in a thesis/dissertation |
| **Requestor Type:** | Student |
| **Items for Reuse:** | Figures/Tables |
| **Number of Figure/Tables:** | 3 |
| **Figure/Tables Details:** | A plot of $\ell/\xi$ as a function of temperature (inset of Fig 3) |
| **Format for Reuse:** | Electronic |

## Information about New Publication:

| | |
|---|---|
| **University/Publisher:** | Jawaharlal Nehru Centre For Advanced Scientific Research |
| **Title of dissertation/thesis:** | Investigations of Thermodynamics and Dynamics in Phase Separating Mixtures |
| **Author(s):** | Koyel Das |
| **Expected completion date:** | Dec. 2021 |

## License Requestor Information

| | |
|---|---|
| **Name:** | Koyel Das |
| **Affiliation:** | Individual |
| **Email Id:** | koyeldas92@gmail.com |
| **Country:** | India |

# American Physical Society
# Reuse and Permissions License

**TERMS AND CONDITIONS**

The American Physical Society (APS) is pleased to grant the Requestor of this license a non-exclusive, non-transferable permission, limited to Electronic format, provided all criteria outlined below are followed.

1. You must also obtain permission from at least one of the lead authors for each separate work, if you haven't done so already. The author's name and affiliation can be found on the first page of the published Article.

2. For electronic format permissions, Requestor agrees to provide a hyperlink from the reprinted APS material using the source material's DOI on the web page where the work appears. The hyperlink should use the standard DOI resolution URL, http://dx.doi.org/{DOI}. The hyperlink may be embedded in the copyright credit line.

3. For print format permissions, Requestor agrees to print the required copyright credit line on the first page where the material appears: "Reprinted (abstract/excerpt/figure) with permission from [(FULL REFERENCE CITATION) as follows: Author's Names, APS Journal Title, Volume Number, Page Number and Year of Publication.] Copyright (YEAR) by the American Physical Society."

4. Permission granted in this license is for a one-time use and does not include permission for any future editions, updates, databases, formats or other matters. Permission must be sought for any additional use.

5. Use of the material does not and must not imply any endorsement by APS.

6. APS does not imply, purport or intend to grant permission to reuse materials to which it does not hold copyright. It is the requestor's sole responsibility to ensure the licensed material is original to APS and does not contain the copyright of another entity, and that the copyright notice of the figure, photograph, cover or table does not indicate it was reprinted by APS with permission from another source.

7. The permission granted herein is personal to the Requestor for the use specified and is not transferable or assignable without express written permission of APS. This license may not be amended except in writing by APS.

8. You may not alter, edit or modify the material in any manner.

9. You may translate the materials only when translation rights have been granted.

10. APS is not responsible for any errors or omissions due to translation.

11. You may not use the material for promotional, sales, advertising or marketing purposes.

12. The foregoing license shall not take effect unless and until APS or its agent, Aptara, receives payment in full in accordance with Aptara Billing and Payment Terms and Conditions, which are incorporated herein by reference.

13. Should the terms of this license be violated at any time, APS or Aptara may revoke the license with no refund to you and seek relief to the fullest extent of the laws of the USA. Official written notice will be made using the contact information provided with the permission request. Failure to receive such notice will not nullify revocation of the permission.

14. APS reserves all rights not specifically granted herein.

15. This document, including the Aptara Billing and Payment Terms and Conditions, shall be the entire agreement between the parties relating to the subject matter hereof.

**Zimbra** **koyeldas@jncasr.ac.in**

**Re: seeking permission to use a part of figure from your paper**

**From :** Subir K DAS <das@jncasr.ac.in> Sat, Dec 18, 2021 11:28 AM
**Subject :** Re: seeking permission to use a part of figure from your paper 1 attachment
**To :** koyeldas <koyeldas@jncasr.ac.in>

Dear Ms. Das,

I give you the permission to reproduce the results from the below mentioned paper.

Sincerely,

Subir K. Das
Professor
Theoretical Sciences Unit
Jawaharlal Nehru Centre for Advanced Scientific Research
Jakkur P.O., Bangalore 560064, India
Telephone: 0091 80 22082961/2
url: http://www.jncasr.ac.in/das

---

**From:** "koyeldas" <koyeldas@jncasr.ac.in>
**To:** "das" <das@jncasr.ac.in>
**Sent:** Saturday, December 18, 2021 11:09:03 AM
**Subject:** seeking permission to use a part of figure from your paper

Dear Sir,

I am Koyel Das, a Ph. D. student working with Prof. Subir K. Das, from Theoretical Sciences Unit,
Jawaharlal Nehru Centre for Advanced Scientific Research (JNCASR), Bangalore, India. I am writing this to
seek permission to include part (inset) of the Figure 3 from your paper titled **"Universal Critical Behavior
of Curvature-Dependent Interfacial Tension"** published in **Physical Review Letters volume no-107 and first page index- 235702 on 2 December 2011** (the DOI is https://doi.org/10.1103/PhysRevLett.107.235702) in my PhD thesis (titled 'Investigations of Thermodynamics and Dynamics in Phase Separating Mixtures').

This will be used only for academic purposes. May I request you to kindly give me the permission to use the
part of figure 3.

I have already obtained license agreement between the American Physical Society ("APS") and Koyel Das ("me")
which is attached with this mail.

Your sincerely,
Koyel Das
C/O- Prof. Subir K. Das
Jawaharlal Nehru Centre for Advanced Scientific Research (JNCASR)
Jakkur P.O.
Bangalore-560064

---

**RNP_21_DEC_047501.pdf**
47 KB

---

## Re: request for the permission to use a figure

das Koyel <koyeldas@jncasr.ac.in>
Fri 6/10/2022 7:00 PM
To: Keenan Crane <keenanc@andrew.cmu.edu>

Thank you very much Sir. I will surely cite the source.

Get Outlook for Android

---

**From:** Keenan Crane <keenanc@andrew.cmu.edu>
**Sent:** Friday, June 10, 2022 6:56:09 PM
**To:** das Koyel <koyeldas@jncasr.ac.in>
**Cc:** kmcrane@cs.cmu.edu <kmcrane@cs.cmu.edu>
**Subject:** Re: request for the permission to use a figure

Hi Koyel,

Sure—I'd be glad if the figure is useful.  If you do use it, please cite

```
@incollection{crane2013digital,
  title={Digital geometry processing with discrete exterior calculus},
  author={Crane, Keenan and De Goes, Fernando and Desbrun, Mathieu and Schr{\"o}der,
Peter},
  booktitle={ACM SIGGRAPH 2013 Courses},
  pages={1--126},
  year={2013}
}
```

Kind regards,

Keenan

On Fri, Jun 10, 2022 at 8:12 AM das Koyel <koyeldas@jncasr.ac.in> wrote:

> Dear Professor,
>
> I am Koyel Das, a Ph.D student in statistical physics from JNCASR, Bangalore, India. Recently I came
> across TU Berlin Course Blog named Geometry Processing and Applications WS19. There I enjoyed reading
> an article titled "A Quick and Dirty Introduction to the Curvature of Surfaces"
> (http://wordpress.discretization.de/geometryprocessingandapplicationsws19/a-quick-and-dirty-introduction-to-the-curvature-of-surfaces/)
> authored by you.
>
> May I request your permission to use the third figure (from the beginning) of the above-mentioned article
> in one of the chapters of my Ph.D thesis? I intend to use this figure in the context of introduction to interfacial
> curvature. I shall be highly obliged if you permit me to use the figure.
>
> Best regards,
> Koyel Das
> C/O Prof. Subir K. Das
> Theoretical Sciences Unit
> Jawaharlal Nehru Centre for Advanced Scientific Research (JNCASR)
> Jakkur
> Bangalore-560064
> India